Hepatic ceramide synthesis links systemic inflammation to organelle dysfunction in cancer

Ying Liu[1, #, *], Ting Miao[1, #], Alice Wang[2], Ezequiel Dantas[3], Ah-Ram Kim[1], Zhongjie Zhang[1], Xiaomei Sun[1], Richard Binari[1], John M. Asara[4, 5], Yanhui Hu[1], Marcus D. Goncalves[3], Tobias Janowitz[2,6], Norbert Perrimon[1, 7, *]

[1] Department of Genetics, Blavatnik Institute, Harvard Medical School, Boston, MA 02115, USA

[2] Cold Spring Harbor Laboratory, Cold Spring Harbor, New York, NY 11724 USA

[3] Department of Medicine, New York University Grossman School of Medicine, New York, NY 10016, USA

[4] Department of Medicine, Harvard Medical School, Boston, MA, USA

[5] Division of Signal Transduction, Beth Israel Deaconess Medical Center, Boston

[6] Northwell Health Cancer Institute, Northwell Health, New Hyde Park, New York, NY 11042 USA

[7] Howard Hughes Medical Institute, Boston, MA, USA

[#] Authors contribute equally

*Correspondence:

Ying Liu: ying_liu@hms.harvard.edu

Norbert Perrimon: perrimon@genetics.med.harvard.edu

Abstract

Paraneoplastic syndromes arise when tumor-derived cytokines reprogram distant organs. Although mediators such as Interleukin-6 have been implicated, how these signals impair host organ function remains incompletely defined. Here, we identify a cytokine-lipid axis that drives hepatic autophagy dysfunction. Specifically, in *Drosophila*, the gut tumor-derived interleukin-like cytokine Upd3 induces the expression of the triglyceride lipase *CG5966*, which we named "*cancer-associated lipid mobilizer* (*calm*)", and the ceramide synthase *schlank* in the fat body/liver, which rewires fat body lipid metabolism resulting in an autophagic-flux blockade. Genetic reduction of either *CG5966* or *schlank* restores organelle homeostasis and mitigates paraneoplastic phenotypes. This mechanism is conserved in mammals: in mice, IL-6 upregulates the lipoprotein lipase *Lpl* and ceramide synthases which in turn trigger a hepatic autophagy-flux blockade; in humans, hepatic *LPL* and ceramide synthases expression correlates with poorer survival in hepatocellular carcinoma. Our findings position hepatic lipid metabolism rewiring, especially ceramide synthesis as a critical, conserved node coupling systemic inflammation to organelle dysfunction, and suggest this pathway as a possible therapeutic entry point for cancer-associated liver disorders.

Introduction

Paraneoplastic syndromes are systemic disorders in cancer patients caused by tumor-derived factors that disrupt distant organs (Pelosof and Gerber, 2010). Among these factors, cytokines, particularly interleukin-6 (IL-6), are prominent paraneoplastic factors that drive diverse clinical manifestations (Ferrer et al., 2023; Flint et al., 2016; Pelosof and Gerber, 2010; Wu et al., 2017). IL-6 activates the JAK/STAT signaling pathway in remote tissues, rewiring gene expression to induce inflammation, thrombopoiesis, and wasting (Ding et al., 2021; Liu et al., 2025; Stone et al., 2012). One of IL-6's known target is the liver, a central hub of systemic metabolic regulation (Fearon et al., 2012; Liu et al., 2025). In response to chronic inflammatory cues including IL-6, the liver increases gluconeogenesis and acute-phase protein production while promoting adipose lipolysis and skeletal muscle proteolysis, a combination that culminates in cancer cachexia (Ding et al., 2021; Liu et al., 2025). Within hepatocytes, basal autophagy is essential for proteostasis and organelle quality control (Qian et al., 2021). Consistent with this, genetic ablation of core autophagy genes leads to the accumulation of ubiquitinated proteins and p62/SQSTM1-positive inclusions, oxidative stress, hepatomegaly, and hepatic steatosis, underscoring the role of autophagy in maintaining liver function (Komatsu et al., 2007, 2005; Ni et al., 2014). However, whether tumor-derived signals impair hepatic autophagy in a way that contributes to paraneoplastic syndromes remains unknown.

Autophagy is a dynamic membrane-trafficking process that is intrinsically linked to lipid metabolism, making it a highly lipid-demanding pathway. In particular, phospholipids are essential for autophagosome biogenesis, providing the structural components for membrane expansion and remodeling (Harayama and Riezman, 2018; Rowland et al., 2023). Autophagosome formation begins with the nucleation of an isolation membrane (phagophore), which elongates and engulfs cytosolic cargo before sealing into a mature autophagosome (Ryter et al., 2013; Ueno and Komatsu, 2017). This process is tightly regulated by the availability and supply of phospholipids that are synthesized from fatty acyl-CoA and glycerol-3-phosphate. The fatty acyl-CoAs can be produced *de novo* or

liberated from other lipid species through lipolysis, thereby linking autophagic dynamics to fundamental lipid metabolic pathways (Harayama and Riezman, 2018; Rowland et al., 2023). Consistently, recent studies have shown that long-chain acyl-CoA synthetases (ACSLs), which channel fatty acids into *de novo* phospholipid synthesis, relocalize to nascent phagophores, facilitating lipid production required for membrane expansion (Dong et al., 2018; Schütter and Graef, 2020). Autophagosome formation is therefore influenced by membrane delivery to the phagophore, and its expansion also requires the ubiquitin-like protein Atg8/LC3 (Weidberg et al., 2011; Xie et al., 2008). Increasing Atg8 enlarges autophagosomes through membrane elongation and cargo capture, while reducing them yields smaller vesicles (Weidberg et al., 2011; Xie et al., 2008). Thus, in metabolically stressed liver, tumor-induced shifts in lipid supply or Atg8 abundance may influence autophagosome number and/or size, with direct consequences for autophagic capacity (Rowland et al., 2023; Schütter and Graef, 2020; Ueno and Komatsu, 2017).

Dysregulated sphingolipid metabolism exemplifies how lipid imbalances can disrupt autophagy. Ceramides synthesized *de novo* from serine and palmitoyl-CoA by a family of ceramide synthases (CerS1–6), can accumulate in metabolic diseases and some cancers (Hannun and Obeid, 2018; Mullen et al., 2012). While modest ceramide increases can trigger protective autophagy (Taniguchi et al., 2012), chronic or excessive accumulation impairs autophagic flux, often by compromising lysosomal integrity (Gabandé-Rodríguez et al., 2014; Liu et al., 2016). Mechanistically, high ceramide levels destabilize lysosomes, leading to defective hydrolase maturation and leakage of cathepsins into the cytosol, thereby blocking the final stages of autophagic degradation (Gabandé-Rodríguez et al., 2014; Liu et al., 2016; Turk et al., 2001). These findings raise the possibility that tumor-driven alterations in lipid flux, particularly the accumulation of ceramides, could blunt hepatic autophagy and may contribute to hepatic disorders.

98 *Drosophila melanogaster* offers a powerful genetic system for dissecting such cross-organ
99 interactions. Multiple fly tumor models exhibit paraneoplastic-like phenotypes, enabling
100 systematic analysis of underlying tumor-host signaling (Bilder et al., 2021; Cheng et al.,
101 2025; Liu et al., 2022). In the Yorkie (Yki) model, gut tumors induced by overexpressing an
102 active form of the oncoprotein Yki, the fly homolog of YAP (*esg>yki*^{act}; referred to as Yki
103 flies), elicit systemic effects reminiscent of human paraneoplastic syndromes (Kwon et al.,
104 2015). These Yki-driven tumors secrete circulating factors, including PDGF- and VEGF-
105 related factor 1 (Pvf1) and the IL-6-like cytokine Unpaired 3 (Upd3), which acts on distant
106 tissues like muscle and fat body to induce wasting (Ding et al., 2021; Liu et al., 2025; Song
107 et al., 2019). The genetic and physiological tractability of the fly fat body, an organ
108 analogous to the vertebrate liver and adipose tissue, makes it an ideal model to investigate
109 how tumor-derived cytokines reshape hepatic lipid metabolism and autophagy to drive
110 paraneoplastic pathology (Liu et al., 2025). Here, guided by a cross-organ gene expression
111 analysis of paraneoplastic progression, we demonstrate that tumor-derived Upd3 activates
112 JAK–STAT signaling to upregulate the lipase *CG5966* and the ceramide synthase *schlank* in
113 the fat body, disrupting lipid homeostasis and triggering severe autophagy dysfunction.
114 Importantly, this pathogenic axis is conserved in mouse and human, as IL-6 drives
115 expression of lipoprotein lipase (LPL) and ceramide synthases. Further, elevated *LPL* and
116 CERS5/6 expression are significantly associated with reduced survival in hepatocellular
117 carcinoma. Together, these findings suggest that hepatic lipid metabolism, namely
118 ceramide synthesis may be a therapeutic target for cancer-associated hepatic dysfunction.

119

120 **Results**

121 **Identification of CG5966 as a paraneoplastic factor**

122 In cancer patients, the timing of paraneoplastic syndrome onset frequently diverges from
123 tumor growth (Pelosof and Gerber, 2010). Similarly, in the Yki gut-tumor model, peripheral
124 organ dysfunction (renal failure, muscle degeneration, ovary atrophy) emerges with a delay,
125 robust by day 8 following tumor maturation at day 5 (Kwon et al., 2015; Liu et al., 2025;

126 Song et al., 2019; Xu et al., 2024). To distinguish the effects of tumor burden from tumor-
127 driven systemic signals, we leveraged our full-body single-nucleus transcriptomic data
128 generated previously (Liu et al., 2025), which records gene expression dynamics of both gut
129 tumors and host organs at days 5 and 8. By integrating fold-change and significance of
130 gene-expression shifts between these timepoints across cell clusters, we quantified a
131 progression association index of genes (Fig. 1a). Among cell clusters, enterocytes (ECs)
132 exhibited the largest share of genes associated with progression, consistent with continued
133 differentiation of tumor intestinal stem cells (ISCs) into ECs, followed by follicle cells and
134 indirect flight muscle, reflecting ovarian atrophy and muscle decline, respectively (Fig.
135 S1a). Notably, while fat body proportions were relatively stable at both days (Liu et al.,
136 2025), this tissue showed a high fraction of progression-associated genes (Fig. S1). Top
137 genes identified by the progression association index, including *CG14275, Pepck1, IM2,*
138 *CG5966,* and *ScsβA*, were predominantly upregulated in the fat body (Fig. 1a; FigS1b-f). Of
139 these, we previously implicated *Pepck1* and *ScsβA* as causal mediators of hepatic
140 gluconeogenic dysregulation and cachectic decline (Liu et al., 2025). Together, these
141 analyses point to the fat body, a fly tissue with many liver-like functions, as a central driver
142 of paraneoplastic progression.

143

144 Among the top candidates, *CG5966* is an unannotated gene (Fig. 1a). To test whether its
145 induction contributes to pathogenesis rather than simply reflecting end-stage dysfunction,
146 we combined esg-LexA/LexAop to activate Yki in ISCs (*esg-LexA, LexAop-Yki*^{act}) with Lpp-
147 Gal4/UAS to knockdown *CG5966* specifically in the fat body (*Lpp-Gal4, UAS-CG5966-*
148 *RNAi*). Fat-body *CG5966* depletion did not alter GFP-labelled gut tumor size nor phospho-
149 Histone 3 (pH3) signal, a cell mitoses marker, indicating no effect on tumor burden or
150 proliferation (Fig. 1b-d). In contrast, *CG5966* knockdown significantly reduced bloating, as
151 measured by the abdomen-to-head (A/H) ratio and total body fluid, suggesting an
152 attenuation of paraneoplastic progression (Fig. 1b, e-g). Consistent with rescue of systemic
153 decline, climbing ability improved and lifespan was extended in Yki flies upon fat-body
154 *CG5966* knockdown (Fig. 1h, i). Collectively, these data identify *CG5966* as a fat-body-

155 expressed contributor to paraneoplastic pathology in the Yki model, while not impacting
156 gut tumor growth.

157

158 **CG5966 targets a subset of triglycerides and reroutes fatty acids into phospholipids**

159 We next investigated the pathogenic mechanism of CG5966. FlyBase annotates *CG5966* as
160 a putative triglyceride (TG) lipase. As it associates with cancer and is a lipase, we named
161 CG5966 as Cancer-Associated Lipid Mobilizer (calm). Sequence alignment with classical
162 human lipases revealed the signature motif G-x-S-x-G in CG5966, as well as the conserved
163 catalytic triad residues (Ser199-Asp227-His312) required for lipid hydrolysis (Fig. S2a).
164 Complementing this, 3D structural modeling using AlphaFold revealed the closest
165 similarity to human pancreatic lipase (PNLIP) and lipoprotein lipase (LPL) (Fig. 2a, b),
166 supporting a close functional relationship between CG5966 and these lipases. Because Yki
167 flies show reduced total TG levels (Kwon et al., 2015), we initially hypothesized that
168 CG5966 simply drives bulk TG hydrolysis to deplete energy stores. However, fat-body-
169 specific *CG5966* knockdown in Yki flies did not restore total TG levels in the abdomen
170 carcass mainly containing fat body tissue (Fig. S2b), suggesting its selective role in TG
171 hydrolysis. To test substrate preference of CG5966 independent of tumors, we profiled
172 lipids in wild-type flies with or without fat-body *CG5966* overexpression (Fig. S2c).
173 Consistent with the observations in Yki flies, total TG abundance remained unchanged
174 upon *CG5966* overexpression (Fig. 2c). By contrast, species-resolved lipidomics revealed
175 selective depletion of TGs bearing 16:0, 16:1, 18:0, or 18:1 acyl chain upon *CG5966*
176 overexpression (Fig. 2d-g; S2d), suggesting that CG5966 preferentially acts on specific
177 molecular TGs. To further assess the lipase activity of CG5966, we performed molecular
178 docking using TG (16:0/18:1/18:1), one of the most abundant TG species in both fly and
179 mammals that was significantly depleted upon *CG5966* overexpression. The Boltz-2
180 docking model positioned the ester bond of the TG substrate in close proximity to the
181 catalytic triad, with a predicted binding free energy of -8.2 kcal/mol, indicating a highly
182 efficient substrate recognition (Fig. 2h) (Mirdita et al., 2022; Passaro et al., 2025).

Altogether, our data suggest CG5966 preferentially targets TG containing C16 and C18 acyl chains.

As the induction of *CG5966* may not be the leading reason of total TG depletion in our tumor model, we investigated the possible physiological consequences of CG5966-mediated C16/18 TG liberation. Lipidomic profiling indicated that the same acyl chains appear enriched in phospholipids: C18:1 increased in PE/PC/PI/PG (Fig. 2d; Fig. S2e), C18:0 increased in PI (Fig. 2e; Fig. S2f), and C16:1/C16:0 increased in PE/PC/PG (Fig. 2f,g; Fig. S2g,h). In line with these compositional shifts, total phospholipid pools (PC, PG, PI) increased upon *CG5966* overexpression (Fig. S2i-k). Given that phospholipids are major membrane building blocks (Harayama and Riezman, 2018), we hypothesized that CG5966 play a role in supplying membrane-lipid precursors. If so, it would interact with membrane-lipid biogenesis regulators or enzymes. To test this, we used AlphaFold-Multimer (AFM) to screen putative CG5966 protein–protein interfaces with markers of specific compartments (lysosome, ER, Golgi, plasma membrane) and lipid-metabolic enzymes (Fig. S2l) (Evans et al., 2021). We modeled 3,686 proteins (five AF-M models each; 18,430 total predictions) and, using integrated Local Interaction Score (iLIS) (Kim et al., 2024), retained 248 high-confidence interfaces (1.35%), corresponding to 158 candidate interactors (Fig. 2i; Fig. S2l). Clustering of these candidates by interacting sites yielded 13 groups (Fig. 2j). The most enriched group (Cluster 1) contains membrane-lipid biogenesis regulators, and the second enriched group (cluster 8) includes factors acting at multiple steps of autophagy (Fig. 2k). We further checked the interacting interfaces by these top two cluster of proteins, autophagy factors interact CG5966 at out surface, whereas the membrane-lipid biogenesis regulators interact closely to the catalytic triad residues (Ser199-Asp227-His312), suggesting a coordinated procession of lipid (Fig. 2i). Top-scoring partners in the membrane-biogenesis cluster included PGAP5, PIG-H, GPAA1/GAA1 (GPI-anchor synthesis/remodeling) (Kinoshita et al., 2006; Kinoshita, 2020; Tiede et al., 2000), and glycosyltransferases (e.g., α4GT2) implicated in ER/Golgi membrane maturation (Fig. 2k) (Hamel et al., 2010). From the autophagy enriched cluster 8, we recovered autophagy-

212 trafficking factors involved in multiple steps of autophagy process, including Atg12
213 (ubiquitin-like conjugation system required for autophagosome formation) (Mulakkal et al.,
214 2014), Rab26/27/40 (small GTPases coordinating vesicle dynamics) (Gillingham et al.,
215 2014), CG5367 (Cathepsin L4), and GILT1 (a lysosomal thiol-reductase linked to
216 autolysosome function) (Kongton et al., 2014) (Fig. 2k, m-p). Based on these predictions,
217 we investigated whether CG5966 mediated TG hydrolysis regulates autophagy in the fat
218 body. we assayed autophagy *in vivo* with CYTO-ID® Autophagy Detection Reagent that
219 stains pre-autophagosomes, autophagosomes, and autolysosomes. Indeed, fat-body
220 CG5966 overexpression increased the number of autophagic vesicles (pre-
221 autophagosomes, autophagosomes, and autolysosomes), while vesicle sizes were
222 unchanged (Fig. 2q-s). This is consistent with previous report that autophagosome
223 formation depends on the membrane delivery, while size scaling requires other regulators
224 such as ubiquitin-like protein Atg8/LC3 (Weidberg et al., 2011; Xie et al., 2008). Altogether,
225 our results suggest that CG5966 preferentially liberates C16/C18 acyl chains from TG
226 fueling phospholipid synthesis, thereby expanding membrane lipid supply and promoting
227 autophagosome formation.

228

229 **CG5966 promotes autophagosome formation in Yki flies**

230 We next asked whether CG5966 modulates autophagy in the Yki model. Fat-body staining
231 in Yki flies revealed a robust increase in number of autophagic vesicles, mirroring the effect
232 of *CG5966* overexpression in wild-type animals, with an additional enlargement of vesicle
233 sizes unique to the Yki background (Fig. 3a). Both phenotypes (increased vesicle numbers
234 and sizes) were suppressed by fat-body-specific *CG5966* depletion (Fig. 3a-c). Increase in
235 autophagic vesicle numbers suggests elevated autophagosome formation, typically
236 indicative of enhanced initiation of the autophagy process; supporting this, expression of
237 the autophagy-initiating kinase *Atg1* was elevated in the fat body of Yki flies at day 8 (Fig.
238 S3a). To test whether autophagosome formation was increased in Yki flies, we depleted
239 *Atg1* specifically in the fat body of Yki flies. As expected, *Atg1* knockdown blunted
240 autophagic-vesicle staining, reducing both vesicle numbers and sizes (Fig. 3d-f). We then

241 examined whether autophagy initiation contributes to paraneoplastic syndrome in Yki flies.
242 Indeed, fat-body-specific *Atg1* depletion did not alter tumor burden or proliferation (Fig. 3g–
243 i) but significantly reduced bloating and total body fluid (Fig. 3j, k) and improved climbing
244 ability (Fig. 3l). Together, these data suggest that CG5966-mediated autophagosome
245 formation contributes to paraneoplastic syndrome in Yki flies. Notably, while CG5966
246 increases vesicle numbers in both wild-type and Yki contexts, vesicle enlargement is Yki-
247 specific, suggesting altered autophagic flux under tumor conditions and involvement of
248 other players.

249

250 **Autophagic flux is blocked in Yki flies**

251 Although the increased number of autophagic vesicles observed in the fat bodies of Yki
252 flies suggests enhanced autophagy initiation, the enlarged vesicle size raises the possibility
253 that autophagy is either genuinely upregulated or, alternatively, blocked at a later stage of
254 the pathway. Efficient autophagic flux requires lysosomal degradation following
255 autophagosome-lysosome fusion (Galluzzi et al., 2017); we therefore examined lysosomal
256 morphology in the fat body using LysoTracker that stains acidic organelles such as
257 lysosomes and autolysosomes. Similar to autophagic vesicles, both lysosome numbers
258 and sizes were increased in Yki flies, and these morphology alterations were suppressed by
259 fat-body specific *CG5966* depletion (Fig. 4a-c). The parallel enlargement of autophagic
260 vesicles and lysosomes led us to assess autophagosome-lysosome fusion.

261 The co-staining revealed that the enlarged autophagic vesicles and lysosomes largely
262 overlapped, suggesting the expanded vesicles in Yki fat bodies were predominantly
263 autolysosomes (autophagosome-lysosome hybrids) (Fig. 4d,e); the increased average size
264 of autophagic vesicles and lysosomes largely reflect accumulation of enlarged
265 autolysosomes. Consistent with the role of CG5966 in supplying lipids for autophagosome
266 formation, its depletion in Yki flies reduced autolysosome numbers (overlap-positive
267 vesicles), concomitantly decreasing the size of both autophagic vesicles and lysosomes
268 (Fig. 4b,c,f).

The observation that vesicle enlargement is specific to the Yki background suggests that tumor context alters autophagic flux in addition to CG5966-mediated autophagosome formation. To further explore the mechanism, we profiled classical autophagy flux markers in the fat body in Yki flies. In line with increased autophagic vesicle numbers, immunoblotting revealed elevated levels of Atg8-II (LC3-II), the lipidated, membrane-bound form associated with autophagosomes (Fig. S4a) (Xie et al., 2008), as well as increased total Atg8, reflecting transcriptional upregulation (Fig. S4b). Together with the accumulation of enlarged autolysosomes, these data suggest an elevated autophagosome biogenesis and point to a defect in late-stage clearance. Because the anti-p62/Ref(2)P antibody we tested did not perform reliably in the adult fat body, we assessed cathepsin L (Ctsl) maturation as a lysosomal function readout. Ctsl is synthesized as a pro-enzyme that is proteolytically processed into a mature lysosomal form (Turk et al., 2001). Notably, Yki flies displayed elevated levels of pro-Ctsl (Fig. 4g), indicating an impaired lysosomal proteolysis and a late-stage autophagy blockade. Altogether, these findings indicate that vesicle enlargement in Yki flies arises from two coordinated defects: heightened CG5966-mediated autophagosome biogenesis and impaired lysosomal clearance.

Ceramide accumulation underlies lysosomal dysfunction in Yki flies

We further asked what blocks autophagy flux in Yki. Late-stage autophagy can fail for several reasons, including impaired autophagosome-lysosome fusion, defective lysosomal acidification, compromised hydrolase processing, and perturbations in lysosomal membrane lipids that alter enzyme activity (Luzio et al., 2007). We surveyed our Yki datasets (transcriptome, metabolomics, lipidomics) and found that whole-body ceramide levels approximately doubled in Yki flies relative to controls (Fig. 4h). Elevated ceramide has been linked to lysosomal enzyme dysfunction and reduced autophagic flux (Gabandé-Rodríguez et al., 2014; Liu et al., 2016), suggesting a lipid-driven mechanism. In *Drosophila*, ceramide synthesis is catalyzed by the ceramide synthase schlank. To test

297 whether excess ceramide causes the lysosomal defect, we depleted *schlank* in the fat
298 body and assessed CtsL maturation. *schlank* knockdown reduced the accumulation of
299 pro-CtsL in Yki flies, indicating improved lysosomal proteolysis (Fig. 4i). Consistently,
300 *schlank* depletion decreased lysosome numbers and sizes (Fig. 4j-l). Importantly,
301 autolysosome numbers were also reduced (Fig. 4m), and fewer enlarged autolysosomes
302 normalized average autophagic vesicle sizes (Fig. 4n). Notably, *schlank* knockdown did not
303 change autophagic vesicle numbers (Fig. 4o), aligning with our model that autophagosome
304 biogenesis is mediated by CG5966. Functionally, relieving the lysosomal block improved
305 host physiology. Without altering tumor burden or proliferation (Fig. 4p–r), *schlank*
306 depletion reduced bloating and total body fluid (Fig. 4p,s,t), restored climbing ability, and
307 extended survival in Yki flies (Fig. 4u,v). Together, these findings support a model in which
308 ceramide accumulation-induced lysosomal dysfunction blocks autophagic clearance; the
309 consequent accumulation of enlarged, dysfunctional autolysosomes contribute causally
310 to paraneoplastic syndrome pathology in the Yki model.

311

312 **The JAK–STAT pathway drives fat body autophagy dysregulation**

313 We next asked what upstream signal induces fat-body autophagy dysregulation. Many TG
314 lipases (e.g., *brummer/bmm*, fly homolog of *ATGL*) are upregulated when insulin signaling
315 is low to mobilize stored energy (Wang et al., 2011). Although Yki flies exhibit reduced
316 systemic insulin activity due to elevated circulating ImpL2 (an insulin-like peptide
317 antagonist) (Kwon et al., 2015), *CG5966* expression was not suppressed by restoring fat
318 body insulin signaling via overexpression of a constitutively active from of the insulin
319 receptor (*InRca*) (Fig. S5a). Beyond insulin, prior work showed increased Upd3/JAK-STAT
320 and Pvf1/Pvr-RTK signaling in Yki flies (Ding et al., 2021; Liu et al., 2022, 2025; Song et al.,
321 2019); we therefore tested whether these pathways regulate *CG5966*. Among these
322 candidates, *Upd3* overexpression in intestinal stem cells (ISCs) (*esg>Upd3*) led to an
323 upregulation of *CG5966* in the fat body (Fig. 5a). Consistently, fat body expression of
324 constitutively active from of Stat92E (*Lpp>Stat92E^act-HA*) increased *CG5966* expression
325 (Fig. 5b). Strikingly, the ceramide synthase *schlank* showed the same regulatory pattern

(Fig. 5c, d). These results suggest that the Upd3/JAK-STAT pathway induces expression of both *CG5966* and *schlank* in wildtype flies.

To validate this regulatory axis in the tumor context, we used the dual binary systems: GAL4-UAS to express Yki in ISCs and LexA-LexAop to deplete the JAK-STAT pathway components *hop* (JAK) and *Stat92e* (STAT) in the fat body. As expected, inhibition of JAK-STAT pathway reduced *CG5966* and *schlank* expression (Fig. 5e-h). Published Stat92e ChIP-seq dataset (ENCODE, ENCSR290OJD/ENCFF873KIF) revealed STAT-binding motifs and putative Stat92E occupancy within promoter and intronic regions of *CG5966* and *schlank* (Fig. 5i). In agreement, fat body ChIP confirmed Stat92E association at these loci (Fig. 5j). Consistent with the gene expression regulation, inhibiting JAK-STAT signaling in the fat body lowered whole-body ceramide (Fig. 5k), reduced the size and number of autophagic vesicles and lysosomes, decreased autolysosome abundance (Fig. 5i-q), and cleared the accumulation of pro-CtsL (Fig. 5r), indicating restored lysosomal maturation. Together, these data indicate that Upd3/JAK-STAT signaling upregulates two effectors of autophagy in the fat body: *CG5966*, which boosts autophagosome biogenesis; and *schlank*, which elevates ceramide and impairs lysosomal function, together driving autophagy dysregulation in Yki flies.

Conserved pathogenic mechanism in mouse models and humans

We next asked whether this dysregulation axis is conserved in mammals. We used C57BL/6 mice bearing Lewis lung carcinoma (LLC) tumors engineered either to secrete IL-6 (LLC+IL-6) or not (LLC). LLC+IL-6 mice exhibit rapid weight loss, indicating progress of paraneoplastic syndrome (Liu et al., 2025). To examine if mammalian lipases that functionally homologous to CG5966 acts downstream of IL-6 in tumor-bearing mice, we profiled expression of putative mammalian orthologs of *CG5966*, *Pnlip* and *Lpl* in liver as well as adipose tissue, the major TG storage site in mammals. *Pnlip* is predominantly expressed in the pancreas, thus was undetectable in either adipose tissue or liver.

354 Conversely, *Lpl* was induced in both tissues of LLC+IL-6 mice (Fig. 6a, b). Given that
355 triglyceride (TG) stores in mammals reside predominantly in adipose tissue. These data
356 suggest that IL-6 promotes lipolysis in both adipose tissue and liver, aligning with our
357 observation of elevated lipolysis in the fly fat body, which is functionally analogous to
358 mammalian adipose tissue and liver. To map underlying lipid fate, we performed lipidomics
359 on adipose tissue and liver in LLC and LLC+IL-6 mice. In adipose tissue, C16/C18 acyl
360 chains were depleted from TG in LLC+IL-6 mice (Fig. 6c; Fig. S6a), suggesting selective
361 liberation of C16/18 fatty acids. A similar selective TG depletion was evident in the liver
362 (Fig. 6d; Fig. S6b), where phospholipids (PC, PI, PE, PG) with C16/C18 chains were
363 significantly enriched (Fig. 6e-h; Fig. S6c-e), paralleling our fly data. Together, our data
364 reveal a conserved regulation of lipolysis by IL-6 in both fly and mammalian tumor models
365 and suggest that lipolysis provides C16/18 fatty acids for specific phospholipid production.
366 Given that TG substrates for lipolysis are predominantly stored in mammalian adipose
367 tissue, our findings further point to a possible adipose-liver communication mechanism,
368 whereby adipocyte triglyceride hydrolysis fuels hepatic phospholipid biosynthesis in the
369 mouse paraneoplastic syndrome model.

370

371 Mammalian liver preferentially generates C22–C24 ceramide from acyl-CoAs by CerS2
372 (Pewzner-Jung et al., 2010). However, in the LLC+IL-6 mice, C16:0 was depleted from
373 hepatic TG while C16 ceramide was enriched (Fig. 6h), suggesting an elevated hepatic
374 ceramide production from palmitoyl-CoA derived from lipolysis. Motivated by this
375 observation, we examined hepatic ceramide synthesis by measuring the expression of
376 ceramide synthases (CerS1–6) in liver following IL-6 induction. Among them, *CerS4*, *CerS5*,
377 and *CerS6* were upregulated (Fig. 6i-k; Fig. S6f). Given reported substrate preferences of
378 CerS4 (favoring C18 and 20), CerS5 and CerS6 (mostly C16) (Mizutani et al., 2005; Pewzner-
379 Jung et al., 2010; Riebeling et al., 2003), these inductions are consistent with the observed
380 redistribution of C16 acyl chains in TG and ceramide. Next, we asked whether autophagy is
381 blocked similarly as observed in our fly model. Indeed, immunoblot markers of autophagic
382 flux indicated a late-stage block at the autolysosome in livers of LLC+IL-6 mice (Fig. 6l),

383 evidenced by: accumulation of pro-CtsL, indicating impaired lysosomal maturation;
384 elevated SQSTM1/p62, indicating defective cargo degradation; incompletely glycosylated
385 LAMP2, consistent with lysosomal biogenesis/maturation defects; and increased LC3-II,
386 which, in the context of rising p62, supports impaired flux downstream of autophagosome
387 formation (Klionsky et al., 2021). Together, these findings mirror the phenotype of blocked
388 autophagic clearance in Yki flies. To assess consequences of dysregulations of autophagy
389 in mammalian tumor model, we turned to an inducible lung-cancer model (*Kras*$^{LSL\text{-}G12D}$*/+;*
390 *Lkb*$^{\hat{}flox/flox}$; "KL" mice), in which tumors were initiated by intranasal Ad-Cre. In this model,
391 ~70% of mice display cachexia (>15% body-weight loss) 5-6 weeks following the tumor
392 induction (Goncalves et al., 2018). We assessed the expression correlation of *CerS* and
393 their weight loss in cachectic and non-cachectic groups, and found that expression of
394 *CerS4* and *CerS5*, two CerS with substrate preference for C16 and C18-20 fatty acids,
395 positively correlated with weight loss (Fig. 6m, n), reinforcing their link to paraneoplastic
396 syndrome progression.

397

398 Extending these findings to humans, we analyzed non-diseased liver from GTEx project
399 (226 participants). Because IL-6 activates STAT3, we asked whether hepatic *CERS4/5/6*
400 expression corresponds with STAT3 activity. Expression of *CERS5* and *CERS6* positively
401 correlated with canonical IL-6/STAT3 targets (*CRP*, *HIF1A*, *TIMP1*) and with *STAT3* itself (Fig.
402 6o-r; Fig. S6g-j) (Castell et al., 1990; Dien et al., 2006; Johnson et al., 2018; Yu et al., 2007),
403 suggesting IL-6 driven regulation of *CERS5* and *CERS6* in the human liver. To explore the
404 clinical relevance of hepatic lipolysis and ceramide synthesis, we analyzed transcriptomic
405 data from the TCGA Pan-Cancer Hepatocellular Carcinoma cohort (372 participants)
406 (Hoadley et al., 2018; Liu et al., 2018). In alignment with our fly and mouse model findings,
407 higher hepatic *LPL* expression associated with worse survival (Fig. 6t). We then examined
408 genes in human *de novo* ceramide synthesis pathway (Fig. 6s): *CERS5* and *CERS6* were
409 significantly associated with worse survival (Fig. 6u,v; Fig. S6k-n). We also assessed
410 *DEGS1*, which catalyzes the desaturation of dihydroceramide to ceramide (Fig. 6s); higher
411 *DEGS1* aligned with adverse outcomes. By contrast, *DEGS2*, a bifunctional C4-

hydroxylase/desaturase with tissue-restricted roles (Ota et al., 2023; UniProt DEGS2 entry, 2025; Jojima et al., 2023), showed no such association, consistent with its lower hepatic relevance (Fig. S6o). Collectively, these cross-species data support a conserved mechanism: Upd3/IL-6/JAK-STAT signaling induces *LPL* and *CerS* expression (notably CerS5/6), driving a late-stage autophagy block, and contributing to paraneoplastic syndrome.

Discussion

Interleukin-6 (IL-6) is a central cytokine in the metabolic crosstalk between tumors and the host, coordinating systemic inflammation and altered fuel handling that drive paraneoplastic syndromes (Barton, 2001; Johnson et al., 2018). Our work builds upon this understanding by identifying a novel, cytokine-driven lipid axis that causes paraneoplastic hepatic dysfunction. We demonstrate that the *Drosophila* IL-6 ortholog, Upd3, activates the JAK-STAT pathway in the fat body, a liver-like tissue, to simultaneously upregulate two key effectors: the triglyceride lipase *CG5966* (putative ortholog of human *LPL*) and the ceramide synthase *schlank* (ortholog of human *CERS*). This coordinated upregulation diverts liberated fatty acids into both phospholipids and ceramides. While the increase in phospholipids promotes the formation of new autophagosomes, the concurrent accumulation of ceramides impairs lysosomal function, blocking autophagic clearance at a late stage. This dual-pronged mechanism, initiating autophagy while simultaneously blocking its completion, leads to a severe buildup of dysfunctional autolysosomes that contributes to hepatic pathology. Importantly, we show that this pathogenic axis is conserved in mouse models of cancer cachexia and that elevated hepatic CERS expression correlates with poor survival in human hepatocellular carcinoma, suggesting this pathway as a potential therapeutic target.

IL-6 orchestrates a systemic mobilization of energy storage through its coordinated actions on adipose tissue and the liver, though upregulating *LPL* and other lipases, to stimulate

triglyceride hydrolysis, increasing the circulation of free fatty acids (Agca and Kir, 2024). As we have previously shown, IL-6/JAK-STAT3 signaling in the liver also induces gluconeogenic programs and elevates *PDK3*, which inhibits pyruvate dehydrogenase and shunts carbon away from mitochondrial oxidation (Liu et al., 2025). This rerouting creates an uncommon metabolic mismatch: the liver is flooded with fatty acids from adipose tissue while its capacity for complete fatty acid oxidation is constrained. Faced with this chronic fatty acid overload, hepatocytes may buffer the excess by channeling them into alternative pathways, including the synthesis of phospholipids and ceramides. As such, we propose that IL-6's normally adaptive role in substrate mobilization becomes maladaptive when sustained in a cancer context. The liberated fatty acids, unable to be efficiently oxidized, are progressively redirected into membrane lipids and bioactive sphingolipids, setting the stage for lipid-driven organelle dysfunction.

This prolonged fatty acid oversupply directly perturbs membrane biogenesis and autophagy. Autophagosome formation requires a continuous supply of membrane lipids (Harayama and Riezman, 2018), supporting this, studies have shown that phospholipids fueled by *de novo* lipogenesis are essential for efficient autophagic flux (Rowland et al., 2023). However, we show that ceramide accumulation rewires autophagy in a context-dependent manner. Sustained elevation of ceramide compromises lysosomal function by causing membrane permeabilization, altering cathepsin processing, and ultimately blocking late-stage autophagic clearance (Gabandé-Rodríguez et al., 2014; Liu et al., 2016). Our observation that IL-6 signaling leads to the accumulation of enlarged autolysosomes and defective lysosomal maturation is consistent with a model where fatty acid redirection into phospholipids drives autophagy initiation, but the concurrent synthesis of ceramides perturb flux at the lysosome.

Ceramide synthases are sophisticatedly regulated, integrating hormonal, stress, and kinase signals. For instance, their transcription is controlled by factors like 17β-estradiol,

468 GPER1, and FOXP3 (Qi et al., 2021; Wegner et al., 2014), and their activity is modulated
469 post-translationally by phosphorylation via kinases such as CK2 and PKC (Fresques et al.,
470 2015; Mullen et al., 2012). Our data place IL-6 and the JAK-STAT pathway as a novel
471 upstream regulator of hepatic *CerS4/5/6*, adding a critical inflammatory dimension to this
472 complex regulatory landscape. Importantly, *CerS5* and *CerS6* emerge as particularly
473 actionable effectors of IL-6-associated hepatic dysfunction. These isoforms preferentially
474 generate C16-ceramide, a lipid species implicated in hepatic insulin resistance, steatosis,
475 and inflammation (Chavez and Summers, 2012; Pewzner-Jung et al., 2010). Our finding that
476 IL-6 induces *CerS5/6* suggests a pernicious feed-forward loop where cytokine-driven
477 ceramide accumulation sustains insulin resistance, organelle stress, and lysosome-limited
478 autophagy. Supporting this, higher *CerS5/6* expression is significantly associated with
479 reduced survival in hepatocellular carcinoma. This data suggests that targeting this axis,
480 especially by selectively inhibiting CerS5/6, could represent a promising strategy to
481 mitigate lipotoxic stress and restore autophagy-lysosome competence in cancer-
482 associated hepatic dysfunction. In conclusion, we offer insights into a mechanistic link
483 from chronic inflammation to a failure of lipid homeostasis and lysosome-limited
484 autophagy, nominating the IL-6/CerS axis as a key driver of cancer-associated hepatic
485 dysfunction.

Acknowledgments

We thank Mujeeb Qadiri, Baolong Xia, Christians Villalta, Stephanie Mohr, Jonathan Zirin, Luping Liu, Litz Brown, and all members of the Perrimon Lab for their critical suggestions and help on this research. We thank Paula Montero Llopis and Microscopy Resources on the North Quad (MicRoN) core facility at Harvard Medical School for advice and help on confocal imaging. Young Yon Kwon, Yanshan Liang and Sheng Hui Lab for advice and help on lipidomics, and the *Drosophila* RNAi Screening Center (DRSC) and Bloomington Drosophila Stock Center (BDSC) for providing fly stocks used in this study. We thank Erika Bach (NYU School of Medicine) for the generous gift of Stat92E fly stocks. This work is funded in part by R01 DK136945, R01 AR057352, the Cancer Grand Challenges partnership funded by Cancer Research UK (CGCATF-2021/100022), and the National Cancer Institute (1 OT2 CA278685-01). Y.L. is supported by Charles A. King Trust. T. M. is supported by the Cystinosis Research Foundation and the Glenn Foundation for Medical Research Postdoctoral Fellowship in Aging Research. N.P. is an investigator of the Howard Hughes Medical Institute.

This article is subject to HHMI's Immediate Access to Research policy, which requires that this article be made publicly available as initial and revised preprints deposited on a designated preprint server under a CC BY 4.0 license.

Author Contributions

Y.L., T.M, and N.P. conceived the study and designed the experiments. Y.L. and T.M. conducted the majority of the experiments and the data analysis. Y.L. and A.W. carried out the mouse experiments. A.H.K performed AFM analysis. Y.L., T.M. and Y.H. were responsible for the bioinformatics analysis. J. M. A. helped for the lipidomics analysis. R.B generated the transgenic fly strains. Z.J.Z and X.M.S. helped for western blotting and

plasmid construction. Y.L., T.M. and N.P. interpreted the results and wrote the manuscript with contributions and feedback from all authors. All authors reviewed and approved the final manuscript.

Materials and Methods

Drosophila strains

All flies were maintained on standard cornmeal fly food containing yeast and agar. Crosses were reared at 18°C to inactivate Gal4 and LexA. Adult offspring flies were collected within 2 days after emerging, kept at 18°C for an additional day and subsequently shifted to 29°C for indicated days to induce transgene and/or RNAi expression. Fly food was changed every 2 days. Stocks used in this study include *esg-LexA::GAD* (BDSC 66632), *tub-Gal80ts, Lpp-Gal4* (Song et al., 2017), *LexAop-Yki3SA-GFP* (Saavedra et al., 2021), *UAS-CG5966-RNAi* (RNAi #1: VDRC 13163, RNAi #2: VDRC 13164), *UAS-hop-RNAi* (BDSC 32966), *UAS-Stat92e-RNAi* (BDSC 33637), *UAS-schank-RNAi* (BDSC 29340), *UAS-Atg1-RNAi* (BDSC 26731), *UAS-HA-Stat92E* dominant-active form (Ekas et al., 2010), *UAS-Upd3* (Woodcock et al., 2015), and *UAS-Pvf1*(Xu et al., 2022). *w1118* was used as control. Female flies are used in all experiments as they showed a more significant and consistent bloating phenotype.

Plasmid and transgenic *Drosophila* strains

The full-length cDNA of *CG5966* (FlyBase ID: FBcl0163613) was obtained from DGRC (Stock 1514588). The insert was first cloned into pENTR-TOPO (Thermo Fisher) following the manufacturer's protocol, then transferred into the *pWALIUM10-moe UAS* destination vector by Gateway LR recombination to generate *UAS-CG5966*. Positive clones were verified by colony PCR and complete Sanger sequencing. Endotoxin-reduced plasmid DNA

538 was prepared by EndoFree midiprep for embryo injections. ΦC31 integrase–mediated
539 transgenesis was used to integrate *UAS-CG5966* into standard attP docking sites: attP40
540 on chromosome 2L (25C7) or attP2 on chromosome 3L (68A4). Plasmid DNA was injected
541 into pre-blastoderm embryos by in-house microinjection. Surviving G_0 adults were crossed
542 individually to balancer stocks, and transformants were identified in the G_1 by *mini-white*
543 marker selection. GAL4-dependent overexpression of *CG5966* was verified in the fat body
544 by RT-qPCR.

545

546 **Lipidomics**

547 Lipidomics and metabolomics of fly samples were performed following the classic Folch
548 method (Folch et al., 1957). 15 adult flies or 40 abdomens were used for lipidomics and
549 metabolomics. Solid samples were homogenized in a 1 mL Dounce homogenizer (TIGHT)
550 on ice with 0.6 mL chloroform and 0.3 mL methanol (2:1 chloroform-methanol mixture).
551 Homogenized samples were transferred to a 15 mL glass tube with a Teflon cap, and an
552 additional 0.6 mL chloroform and 0.3 mL methanol were added to make the final volume
553 approximately 1.8 mL. Samples were vortexed briefly and incubated at room temperature
554 on a rotator for 30–45 minutes. Following incubation, 0.2 volumes (0.36 mL) of HPLC-grade
555 deionized water (HPLC dH2O) were added. The mixture was vortexed three times (5
556 seconds each), followed by centrifugation at 1000 × g for 10 minutes at 4°C. The lower
557 phase, containing non-polar lipids, was transferred to a clean 1.85 mL glass test tube using
558 a glass pipette. The phase was dried under nitrogen gas for approximately 30 minutes, and
559 the dried lipids were stored at -80°C to prevent oxidation. The non-polar lipids were
560 resuspended in 35 µL of HPLC-grade 50% methanol/50% isopropyl alcohol (IPA) and then
561 injected and analyzed using untargeted LC-MS/MS on a Thermo QExactive Plus Orbitrap
562 mass spectrometer. Lipid molecules were identified using LipidSearch version 4.2 (Thermo
563 Scientific). Ion intensity was quantified by measuring the area size of identified peaks.

564

565 **Protein lysate preparation and Western blot**

566 30 abdomens with gonads and guts removed were dissected and lysed in RIPA lysis buffer
567 (50 mM Tris, pH = 8.0, 150 mM NaCl, 0.1% SDS, 0.5% sodium deoxycholate, 1% Triton X-
568 100, 1× complete ULTRA Mini EDTA-free protease inhibitor (Roche), and 1 mM PMSF).
569 Dissected tissues in RIPA buffer were mixed with zirconium oxide beads (NextAdvance) and
570 homogenized using a TissueLyser II (Qiagen). Homogenates were incubated on ice for 15
571 min and centrifuged for 15 min at 16,000 × g at 4 °C. Supernatants were transferred to new
572 tubes, and protein concentrations were determined using the BCA Protein Assay Kit
573 (Pierce) according to the manufacturer's instructions. Samples were diluted to equal
574 protein concentrations with RIPA buffer and stored at –80 °C. Equal amounts of total
575 protein were mixed with 4× Laemmli sample buffer (Bio-Rad) containing 10% β-
576 mercaptoethanol to a final 1× concentration, boiled at 95 °C for 5 min, and centrifuged at
577 16,000× g for 15 min at 4 °C. Supernatants were transferred to new tubes. Equal amounts
578 of sample were loaded to a Mini-PROTEAN TGX Stain-Free Precast Gels (Bio-Rad) and ran
579 using 1× Tris/Tricine/SDS Running Buffer (Bio-Rad) according to the manufacturer's
580 instructions. Spectra Multicolor Broad Range Protein Ladder (ThermoFish) was used as a
581 molecular weight marker. The samples on the gel were transferred to a FL PVDF membrane
582 using Tris/Glycine Buffer (Millipore) for 16 min, according to the manufacturer's
583 instructions. The membrane was then blocked with 1% Casein in 1× Tris Buffered Saline
584 (TBS) (Bio-Rad) for 1 hour at room temperature. Next, the membrane was incubated in a
585 primary antibody dilution in 1% Casein in 1× TBS overnight at 4 °C with gentle shaking.
586 Primary antibodies were used at the following concentrations: 1:1000 mouse anti-Ctsl
587 (R&D Systems, MAB22591, 1:2000 rabbit anti-Atg8 (Abcam, ab109364). Next, the
588 membrane was washed three times quickly in TBST, followed by three 10-min washes in
589 TBST with gentle shaking. The membrane was then incubated with fluorescently labeled
590 secondary antibody in 1% Casein in 1× TBS for 1 h at room temperature with gentle
591 shaking. The dilution of the fluorescently labeled secondary antibody was used as follow:
592 1:2500 hFAB™ Rhodamine; 1:2500 Goat anti-Rabbit IgG (H+L) Secondary Antibody,
593 DyLight™ 800 4X PEG; 1:2500 IRDye 680RD Goat anti-Mouse IgG Secondary Antibody. After
594 incubation, the membrane was washed three times quickly in TBST, followed by three 10-

min washes in TBST with gentle shaking. Then, the membranes were imaged using a Biorad Chemidoc MP imager.

Quantitative RT-PCR of fly samples

For fly samples, Nucleospin RNA kit (Macherey-Nagel) was used to extract RNA. cDNA was synthesized using iScript™ cDNA Synthesis Kit (Bio-Rad, 1708890) according to the manufacturer's protocol. qPCR was performed with Thermal Cycler CFX 96 Real-Time System qPCR machine using iQ™ SYBR® Green Supermix (Bio-Rad). *RP49* and *CG13220* were used as housekeeping genes. Primers used are listed in the supplemental file.

Body fluid measurements

Body fluid measurement was described previously (Xu et al., 2024). Briefly, flies were weighted, then dried at 65 °C for 5 hours, and weighted again. Body fluid is calculated by subtracting the second read from the first one.

Climbing index and survival curve of flies

To assess the climbing ability, flies were transferred to a new vial and then tapped down to the bottom. Vials were imaged after 4 seconds. Percentages of flies in the upper 2/3 of the vial were recorded. 4 independent vials for each genotype were tested to generate the climbing index. Survival of flies was analyzed by calculating the percentage of flies alive in each vial incubated at 29 °C. 3 vials of 10-16 flies from each genotype were tested and flies were flipped to vials with fresh food daily.

Gut and fly imaging

619 Adult fly guts were dissected in cold 1X PBS and fixed for 30 minutes in 1X PBS with 4%
620 formaldehyde. Samples were washed three times in 1X PBS with 0.3% Triton X-100 (PBT)
621 and then mounted in Vectashield with DAPI (Vector Laboratories, H-1200). For pH3
622 staining, washed guts were incubated with blocking buffer (5% NDS in PBT) for 1 hour at
623 room temperature. Primary antibodies and rabbit anti-pH3 (1:500, CST 9701S) were
624 incubated overnight at 4°C. Guts were washed three times in PBT before incubating with
625 secondary antibody, donkey anti-rabbit 565 (1:2000, Molecular Probes A31572), for 1 hour.
626 After three washes in PBT, guts were mounted in Vectashield with DAPI (Vector
627 Laboratories, H-1200). Confocal images were taken with Nikon Ti and Ti2 Spinning Disk at
628 the Microscopy Resources on the North Quad (MicRoN) core facility at Harvard Medical
629 School with Nikon Elements Acquisition Software AR (v5.02). Tumors were quantified by
630 measuring the average GFP signaling strength of gut tumors from individual flies using Fiji-
631 imageJ. Adult fly phenotypes were imaged using a ZEISS Axiozoom V16 fluorescence
632 microscope. Bloating was quantified by the ratio between abdomen and head
633 compartment size using Fiji-imageJ.

634

635 **Live imaging of autophagic vesicle and lysosome**

636 For live imaging of autophagy and lysosomes, abdominal cuticles were dissected in cold
637 Schneider's insect medium. Samples were then incubated for 10 minutes at room
638 temperature in a staining buffer composed of Schneider's medium, CYTO-ID® Autophagy
639 Detection Reagent (1:1000, Enzo Life Sciences ENZ-KIT175), Hoechst nuclear stain
640 (1:1000), and LysoTracker™ Deep Red (500 nM, Thermo Fisher Scientific L12492). Following
641 incubation, the samples were rinsed once with fresh Schneider's medium and then twice
642 with phosphate-buffered saline (PBS). Finally, the stained cuticles were transferred to a
643 glass slide with mounting medium, coverslipped, and immediately visualized using a Nikon
644 Ti2 Spinning Disk confocal microscope.

645

646 **Chromatin Immunoprecipitation**

647 ChIP assay was performed using SimpleChIP® Plus Enzymatic Chromatin IP Kit (Cell
648 Signaling, 9005). For each immunoprecipitation, fat bodies from 50 adult flies with HA-
649 tagged dominant-active Stat92e fat body expression were dissected and flash-frozen in
650 liquid nitrogen. Samples were cross-linked with 1.5% formaldehyde for 20 minutes at room
651 temperature (RT). After stopping cross-linking by adding glycine solution for 5 minutes at
652 RT, samples were washed twice with 1 ml 1X PBS containing 1X Protease Inhibitor Cocktail
653 (PIC) and disaggregated using 1 ml dounce homogenizer. Nuclei were prepared according
654 to the manufacturer's protocol and were lysed with Diagenode Bioruptor sonicator to
655 release the cross-linked chromatin. Chromatins were diluted in 1X ChIP buffer and
656 incubated with 10 ul HA-Tag (C29F4) Rabbit mAb (Cell Signaling, 3724) or Normal Rabbit
657 IgG (Cell Signaling, 2729) overnight at 4°C with rotation. 30 ul ChIP-Grade Protein G
658 Magnetic Beads (Cell Signaling, 9006) were incubated with each immunoprecipitation for 2
659 hours at 4 °C with rotation. Beads were washed and incubated in 150 µl 1X ChIP Elution
660 Buffer at 65 °C for 30 minutes with vortexing (1200 rpm) to elute the chromatin. Reversing
661 cross-links was done by adding 6 µl 5M NaCl and 2 µl Proteinase K to the eluted chromatin
662 supernatant and incubating 2 hours at 65°C. DNA was purified from each sample using
663 Spin Columns provided by the kit. 1 ul DNA sample was used as template for qPCR to
664 detect enrichments of certain DNA regions. qPCR of a fragment in the Sam-S gene region
665 was used as the negative control. Primers used are listed in the supplemental file.

666

667 **Mouse models**

668 The *Kras*$^{G12D/+}$; *Lkb1*$^{f/f}$ mice have been described before (Ji et al., 2007), and were further
669 backcrossed to FVB mice. Tumor induction in adult FVB mice (12- to 20-week-old) was
670 achieved by intranasal administration of 75 µL of PBS containing 2.5 × 10^7 pfu of
671 Adenovirus CMV-Cre (Ad5CMV-Cre) obtained from the University of Iowa Gene Transfer
672 Vector Core (Iowa City, IA) and 1 mM $CaCl_2$. We had previously defined mice as CACS if
673 they lost more than 15% of body weight from their peak weight over the course of the
674 experiment, otherwise they were classified as NCACS (Goncalves et al., 2018; Queiroz et

675 al., 2022). Male mice were used for liver RNAseq, both male and female mice were used in
676 all other experiments. The *Kras*$^{G12D/+}$; *Lkb1*$^{f/f}$ mice experiments were approved by the
677 Institutional Animal Care and Use Committee (IACUC) of Weill Cornell Medical College and
678 maintained as approved by the Institutional Animal Care and Use Committee (IACUC) at
679 Weill Cornell Medicine (NYC).

680 C57BL/6J mice were obtained from the Jackson Laboratory (Strain #000664). After a week
681 of acclimation, 2 x 10^6 Lewis Lung Carcinoma (LLC) cells or LLC cells edited to produce IL-6
682 (LLC-IL6) were subcutaneously inoculated into their right flank. Mice were kept in
683 pathogen-free conditions on a 24 hour 12:12 light-dark cycle. Male C57BL/6J mice were
684 used in the experiments. C57BL/6J mice experiments were approved by the Institutional
685 Animal Care and Use Committee (IACUC) at Cold Spring Harbor Laboratory (CSHL) and
686 were conducted in accordance with the National Institutes of Health Guide for the Care
687 and Use of Laboratory Animals. Body weights and clinical signs of cachexia were
688 monitored daily. Handling was kept to a minimum. Mice were sacrificed when tumor size
689 exceeded 2 cm length, when weight loss exceeded 15% from peak weight, or when showing
690 clinical signs of discomfort indicative of cachectic endpoint as stated by the Animal
691 Cachexia Score (ACASCO): piloerection, diarrhea or constipation, hunched posture,
692 tremors, and closed eyes. Death was confirmed by cervical dislocation. Mice injected with
693 LLC-IL6 cells reached >15% bodyweight loss endpoint. Mice in the LLC group were
694 sacrificed 22-24 days after injection of the LLC cell line, when tumors reached 2 cm in
695 length. LLC group mice did not reach cachectic endpoint but did exhibit a mild cachectic
696 phenotype, characterized by reduced adipose and muscle tissue mass, and splenomegaly
697 compared to non-tumor bearing control group mice.

698

699 **Plasma measurements from C57BL/6J mice**

700 Tail vein bleeds were performed using a scalpel via tail venesection without restraint.
701 Plasma samples were collected using heparin-coated hematocrit capillary tubes to avoid
702 coagulation and were processed as follows: centrifuge spin at 14,000 rpm for 5 min at 4°C,

703 snap frozen in liquid nitrogen and stored at -80°C. IL-6 levels were measured from plasma
704 using the mouse IL-6 Quantikine ELISA Kit (#M6000B; R&D Systems).

705

706 **Lewis Lung Carcinoma (LLC) cell line**

707 LLC cells were purchased from American Type Culture Collection (ATCC) and cultured in
708 complete growth medium consisting of Dulbecco's Modified Eagle Medium (DMEM)
709 (#10027CV; Corning) containing 10% of Heat-Inactivated Fetal Bovine Serum (FBS) (#10-
710 438-026; Thermo Fisher) and 1x Penicillin-Streptomycin solution (#15-140-122; Thermo
711 Fisher) under sterile conditions. 1x Trypsin-EDTA (#15400054; Thermo Fisher) was used for
712 cell dissociation. Cells were resuspended in FBS-free DMEM and viable cells were counted
713 using a Vi-Cell counter prior to subcutaneous injection of $2x10^6$ viable cells diluted in
714 100µL DMEM into the right flank of each C57BL/6J mouse.

715

716 LLC cells were edited to constitutively produce interleukin-6 (IL-6). LLC cells were seeded
717 into 24-well plates with 50,000 cells per well. After 24 hours, they were transfected with a
718 total of 500ng of plasmid (comprising 2.5:1 PB-IL6 plasmid and PBase plasmids) using
719 Lipofectamine 3000 (Thermo Fisher) according to the manufacturer's protocol. PBase
720 plasmid was obtained from System Biosciences (#PB210PA-1) and PB-IL6 was obtained
721 from VectorBuilding comprising mouse Il6 cDNA driven by EF1a promoter and flanked by
722 piggyBac elements. After 48 hours, the media was changed and replaced with DMEM
723 media supplemented with 3 µg/ml puromycin. After 14 days of antibiotic selection, the
724 media was replaced with DMEM media for 24 hours, followed by isolation of monoclonal
725 populations by serial dilutions in a 96-well plate. To identify clones with constitutive IL-6
726 expression, we measured IL-6 in the cell supernatant for each clone using the Mouse IL-6
727 ELISA Kit (#ab222503; Abcam).

728

729 **Lipid extraction and profiling in mice**

730 Lipid extracts were analyzed using a Dionex Ultimate 3000 RSLC system (Thermo Scientific)
731 coupled with a QExactive mass spectrometer (Thermo Scientific, Waltham, MA, USA) mass
732 spectrometer. Chromatographic separation was achieved on an ACQUITY UPLC CSH C18
733 column (130Å, 1.7 μm, 2.1 mm × 100 mm) with an ACQUITY UPLC CSH C18 VanGuard pre-
734 column (130Å, 1.7 μm, 2.1 mm × 5 mm) (Waters, Milford, MA) with column temperature at
735 50 ˚C. For the gradient, mobile phase A consisted of an acetonitrile-water mixture (6:4), and
736 mobile phase B was a 2-propanol-acetonitrile mixture (9:1), both phases containing 10 mM
737 ammonium formate and 0.1% formic acid. The linear elution gradient was: 0-3 min, 20% B;
738 3- 7 min, 20-55% B; 7-15 min, 55-65% B; 15-21 min, 65-70% B; 21-24 min, 70-100% B; and
739 24-26 min, 100% B, 26-28 min, 100-20% B, 28-30 min, 20% B, with a flow rate of 0.35 mL/
740 min. The autosampler was at 4˚C. The injection volume was 5 μL. Needle wash was applied
741 between samples using a mixture of dichloromethane-isopropanol-acetonitrile (1:1:1).

742

743 ESI-MS analysis was performed in positive and negative ionization polarities using a
744 combined full mass scan and data-dependent MS/MS (Top 10) (Full MS/dd-MS^2) approach.
745 The experimental conditions for full scanning were as follows: resolving power, 70,000;
746 automatic gain control (AGC) target, 1×10^6; and maximum injection time (IT), 100 ms. The
747 scan range of the instrument was set to m/z 100-1200 in both positive and negative ion
748 modes. The experimental conditions for the data-dependent product ion scanning were as
749 follows: resolving power, 17,500; AGC target, 5×10^4; and maximum IT, 50 ms. The isolation
750 width and stepped normalized collision energy (NCE) were set to 1.0 m/z, and 10, 20, and 40
751 eV. The intensity threshold of precursor ions for dd-MS2 analysis and the dynamic exclusion
752 were set to 1.6×10^5 and 10 s. The ionization conditions in the positive mode were as follows:
753 sheath gas flow rate, 50 arb; auxiliary (AUX) gas flow rate, 15 arb; sweep gas flow rate, 1 arb;
754 ion spray voltage, 3.5 kV; AUX gas heater temperature, 325 ˚C; capillary temperature, 350 ˚C;
755 and S-lens RF level, 55. The ionization conditions in the negative mode were as follows:
756 sheath gas flow rate, 45 arb; auxiliary (AUX) gas flow rate, 10 arb; sweep gas flow rate, 1 arb;
757 ion spray voltage, 2.5 kV; AUX gas heater temperature, 320 ˚C; capillary temperature, 320 ˚C;
758 and S-lens RF level, 55.

759 Thermo Scientific™ LipidSearch™ software version 5.0 was used for lipid identification and
760 quantitation. First, the product search mode was used during which lipids were identified
761 based on the exact mass of the precursor ions and the mass spectra resulting from product
762 ion scanning. The precursor and product tolerances were set to 10 and 10 ppm mass
763 windows. The absolute intensity threshold of precursor ions and the relative intensity
764 threshold of product ions were set to 30000 and 1%. Next, the search results from the
765 individual positive or negative ion files from each sample were aligned within a retention time
766 window (±0.25 min) and then all the data were merged for each annotated lipid with a
767 retention time correction tolerance of 0.5 min. The annotated lipids were then filtered to
768 reduce false positives by only including a total grade of A or B or C for PC and SM; otherwise
769 only including grade A or B.

770

771 **Bulk RNA-Sequencing from KL livers**

772 Total RNA was extracted from the liver using TRIzol (Thermo Fisher), followed by a clean-up
773 step using RNeasy kit (Qiagen). One microgram of total RNA from each sample was
774 submitted to the WCM Genomics Resources Core Facility. Raw sequenced reads were
775 aligned to the mouse reference GRCm38 using STAR (v2.4.1d, 2-pass mode) aligner, and
776 raw counts were obtained using HTSeq (v0.6.1). Differential expression analysis, batch
777 correction and principal component analysis (PCA) were performed using R Studio Version
778 4.2.2 and DESeq2 (v.1.38.3). Gene set enrichment analysis (GSEA) analysis was performed
779 with the R package fGSEA (10.18129/B9.bioc.fgsea), using the Reactome pathway
780 database contained in the 2022 release of Mouse Molecular Signatures Database from the
781 Broad Institute (https://www.gsea-msigdb.org/gsea/msigdb/mouse/collections.jsp).

782

783 **Quantitative RT-PCR of mouse samples**

784 For LLC and IL6-secreting LLC mouse samples, 100 mg of liver tissue was lysed in 1 mL of
785 qiazol, using Qiagen TissueLyser II, at 20 Hz for 4 minutes. Samples were centrifuged at

786 12,000 g at 4 degrees C for 12 minutes to separate aqueous layer from organic layer and
787 any debris. Approximately 600 microliters of RNA containing aqueous layer was collected
788 and processed using Qiagen RNeasy lipid RNA extraction kit and QiaCube machine to
789 isolate RNA in 50 microliter elution volumes. RNA concentrations of all samples were
790 quantified, and samples were further diluted using ddH20 to reach a standard
791 concentration of 100 ng/uL for each sample. cDNA was synthesized using iScript™ cDNA
792 Synthesis Kit (Bio-Rad, 1708890) according to the manufacturer's protocol. qPCR was
793 performed with Thermal Cycler CFX 96 Real-Time System qPCR machine using iQ™ SYBR®
794 Green Supermix (Bio-Rad). RN18 was used as housekeeping gene. Primers used are listed
795 in the supplemental file.

796

797 **Public datasets, Software, Quantification and Statistical Analyses**

798 Transcriptomic data from non-diseased liver samples of 226 individuals were obtained
799 from the Genotype-Tissue Expression (GTEx) Project. Additionally, transcriptomic data and
800 corresponding survival records were obtained from the Hepatocellular Carcinoma (LIHC)
801 cohort of 372 patients in the PanCancer Atlas of The Cancer Genome Atlas (TCGA) Program
802 (Hoadley et al., 2018; Liu et al., 2018). Sex and gender were not considered in the design of
803 present research, and related information was not collected for the analysis. Kaplan-Meier
804 survival curves were generated using the R packages survival and survminer. We used
805 Biorender and PyMOL for a subset of figures, and ChatGPT to proofread parts of the text.
806 After using ChatGPT, the authors reviewed and edited the content as needed and take full
807 responsibility for the content of the publication. GraphPad Prism was used for statistical
808 analysis, gene expression correlation analysis, and generation of figures. Data distribution
809 was assumed to be normal, but this was not formally tested. Animals and samples were
810 randomly assigned to experimental groups, and the data collection was randomized. Data
811 collection and analysis were not performed blind to the conditions of the experiments.
812 Statistical analysis was done with student's t test (two experimental groups) or ordinary
813 one-way ANOVA (three or more experimental groups) by the default settings of GraphPad

814 Prism (ns indicates not significant, * indicates $p<0.05$, ** indicates $p<0.01$, *** indicates
815 $p<0.001$, **** indicates $p<0.0001$). Gene expression levels (qPCR) were normalized to the
816 mean of control samples. Error bars indicate the standard deviations with the mean as the
817 center. n indicates the number of biological replicates in each experiment, for fly
818 experiments, each biological replicates contains 10-16 flies otherwise noted; for mouse
819 experiment, each biological replicates is one mouse.

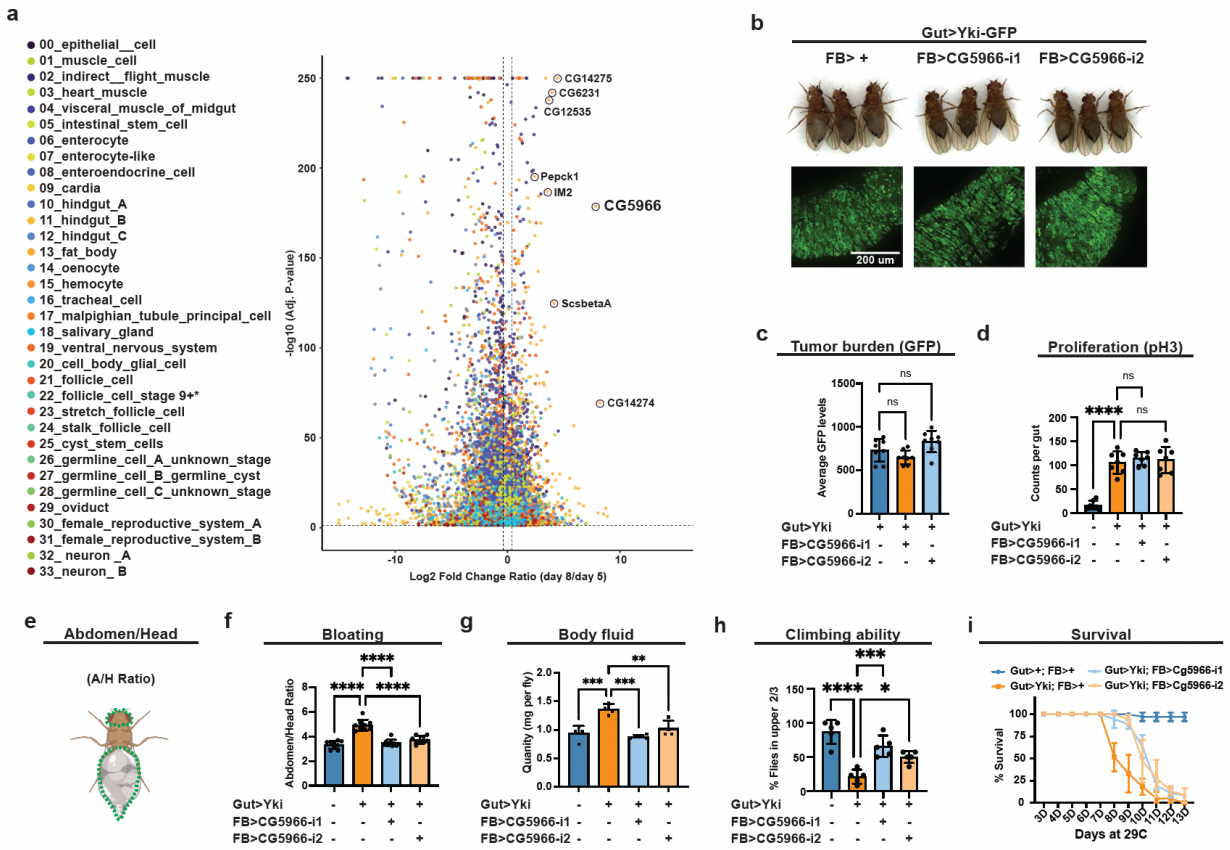
a
00_epithelial__cell
01_muscle_cell
02_indirect__flight_muscle
03_heart_muscle
04_visceral_muscle_of_midgut
05_intestinal_stem_cell
06_enterocyte
07_enterocyte-like
08_enteroendocrine_cell
09_cardia
10_hindgut_A
11_hindgut_B
12_hindgut_C
13_fat_body
14_oenocyte
15_hemocyte
16_tracheal_cell
17_malpighian_tubule_principal_cell
18_salivary_gland
19_ventral_nervous_system
20_cell_body_glial_cell
21_follicle_cell
22_follicle_cell_stage 9+*
23_stretch_follicle_cell
24_stalk_follicle_cell
25_cyst_stem_cells
26_germline_cell_A_unknown_stage
27_germline_cell_B_germline_cyst
28_germline_cell_C_unknown_stage
29_oviduct
30_female_reproductive_system_A
31_female_reproductive_system_B
32_ neuron _A
33_neuron_ B
CG14275
CG6231
CG12535
Pepck1
IM2
CG5966
ScsbetaA
CG14274
-log10 (Adj. P-value)
Log2 Fold Change Ratio (day 8/day 5)
b
Gut>Yki-GFP
FB> +
FB>CG5966-i1
FB>CG5966-i2
200 um
c
Tumor burden (GFP)
Average GFP levels
ns
Gut>Yki
FB>CG5966-i1
FB>CG5966-i2
d
Proliferation (pH3)
Counts per gut
****
e
Abdomen/Head
(A/H Ratio)
f
Bloating
Abdomen/Head Ratio
g
Body fluid
Quanity (mg per fly)
h
Climbing ability
% Flies in upper 2/3
i
Survival
Gut>+; FB>+
Gut>Yki; FB>+
Gut>Yki; FB>Cg5966-i1
Gut>Yki; FB>Cg5966-i2
% Survival
Days at 29C

820

821 **Figure 1. Identification of CG5966 as a paraneoplastic factor**

822 **a**, Progression association index of differential expressed genes across cell clusters. **b**,
823 Images of gut tumors and phenotypes of Yki flies with or without fat-body *CG5966*
824 depletion at day 6. **c**, Quantification of gut tumors (GFP signal, arbitrary units) of Yki flies
825 with or without fat-body *CG5966* depletion at day 6 (n = 8). **d**, Total pH3 counts per gut of
826 control flies and Yki flies with or without fat-body *CG5966* depletion at day 6 (n = 8). **e**, The
827 bloating quantification by abdomen/head (A/H) size ratio. **f**, Quantification of bloating
828 phenotypes of control flies and Yki flies with or without fat-body *CG5966* depletion at day 6
829 (A/H ratio, n=9). **g**, Body-fluid levels of Yki flies with or without fat-body *CG5966* depletion
830 at day 6 (n = 4). **h**,**i**, The climbing ability at day 6 (**h**) (n = 4) and survival curve (**i**) (n = 3) of
831 control flies, Yki flies, and Yki flies with fat-body *CG5966* depletion. *$p < 0.05$, **$p < 0.01$,
832 ***$p < 0.001$, ****$p < 0.0001$, ns indicates not significant. Error bars indicate SDs. n
833 indicates the number of biological replicates in each experiment.

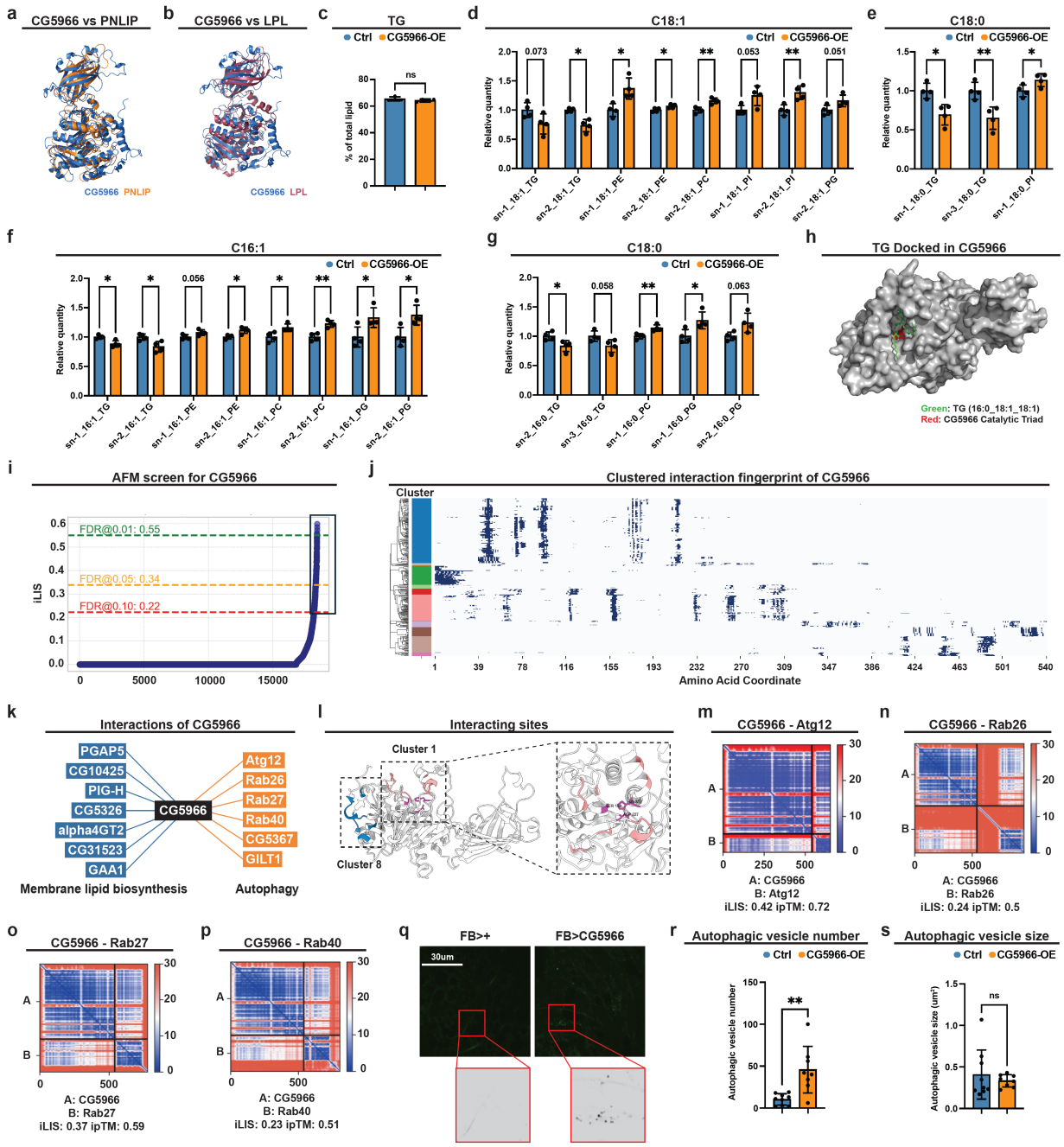
a
CG5966 vs PNLIP
CG5966 PNLIP
b
CG5966 vs LPL
CG5966 LPL
c
TG
Ctrl CG5966-OE
ns
% of total lipid
d
C18:1
Ctrl CG5966-OE
Relative quantity
sn-1_18:1_TG
sn-2_18:1_TG
sn-1_18:1_PE
sn-2_18:1_PE
sn-2_18:1_PC
sn-1_18:1_PI
sn-2_18:1_PI
sn-2_18:1_PG
e
C18:0
Ctrl CG5966-OE
Relative quantity
sn-1_18:0_TG
sn-3_18:0_TG
sn-1_18:0_PI
f
C16:1
Ctrl CG5966-OE
Relative quantity
sn-1_16:1_TG
sn-2_16:1_TG
sn-1_16:1_PE
sn-2_16:1_PE
sn-1_16:1_PC
sn-2_16:1_PC
sn-1_16:1_PG
sn-2_16:1_PG
g
C18:0
Ctrl CG5966-OE
Relative quantity
sn-2_16:0_TG
sn-3_16:0_TG
sn-1_16:0_PC
sn-1_16:0_PG
sn-2_16:0_PG
h
TG Docked in CG5966
Green: TG (16:0_18:1_18:1)
Red: CG5966 Catalytic Triad
i
AFM screen for CG5966
FDR@0.01: 0.55
FDR@0.05: 0.34
FDR@0.10: 0.22
iLIS
j
Clustered interaction fingerprint of CG5966
Cluster
Amino Acid Coordinate
k
Interactions of CG5966
PGAP5
CG10425
PIG-H
CG5326
alpha4GT2
CG31523
GAA1
CG5966
Atg12
Rab26
Rab27
Rab40
CG5367
GILT1
Membrane lipid biosynthesis
Autophagy
l
Interacting sites
Cluster 1
Cluster 8
m
CG5966 - Atg12
A: CG5966
B: Atg12
iLIS: 0.42 ipTM: 0.72
n
CG5966 - Rab26
A: CG5966
B: Rab26
iLIS: 0.24 ipTM: 0.5
o
CG5966 - Rab27
A: CG5966
B: Rab27
iLIS: 0.37 ipTM: 0.59
p
CG5966 - Rab40
A: CG5966
B: Rab40
iLIS: 0.23 ipTM: 0.51
q
FB>+
FB>CG5966
30um
r
Autophagic vesicle number
Ctrl CG5966-OE
Autophagic vesicle number
s
Autophagic vesicle size
Ctrl CG5966-OE
ns
Autophagic vesicle size (um²)

835 **Figure 2. CG5966 is a triglyceride lipase that promotes autophagosome formation.**

836 **a**,**b**, 3D structural modeling using AlphaFold demonstrating similarity of human PNLIP (**a**)
837 and LPL (**b**) to CG5966. **c**, Relative levels of Abdomen TG levels of flies with or without fat-
838 body *CG5966* overexpression (n=4). **d**-**g**, Relative levels of Abdomen C18:1 (**d**), C18:0 (**e**),
839 C16:1 (**f**), and C16:0 (**g**) acyl chains levels of flies with or without fat-body *CG5966*
840 overexpression (n=4), data were retrieved from lipidomics analysis. **h**, Molecular docking of
841 TG (16:0/18:1/18:1) to CG5966 by the Boltz-2 docking model. **i**, AFM prediction of
842 interacting partners of CG5966. **j**, Cluster of predicted interacting partners of CG5966
843 based on interacting sites. Y-axis present grouping of interacting patterners and X-axis
844 indicate the interacting sites of CG5966. **k**, Predicted interactions between CG5966 with
845 membrane lipid biosynthesis and autophagy regulators by AFM. **l**, Predicted interacting
846 pocket of CG5966. **m**-**p**, AFM prediction of interaction between CG5966 and Atg12 (**m**),
847 Rab26 (**n**), Rab27 (**o**), Rab40 (**p**). **q**, Live imaging of fat bodies with autophagic vesicle
848 staining dye in flies with or without fat-body *CG5966* overexpression at day 7. **r**, **s**,
849 Quantification of autophagic vesicle numbers (**r**) and sizes (**s**) in **r**. *$p < 0.05$, **$p < 0.01$,
850 ***$p < 0.001$, ****$p < 0.0001$, ns indicates not significant. Error bars indicate SDs. n
851 indicates the number of biological replicates in each experiment.

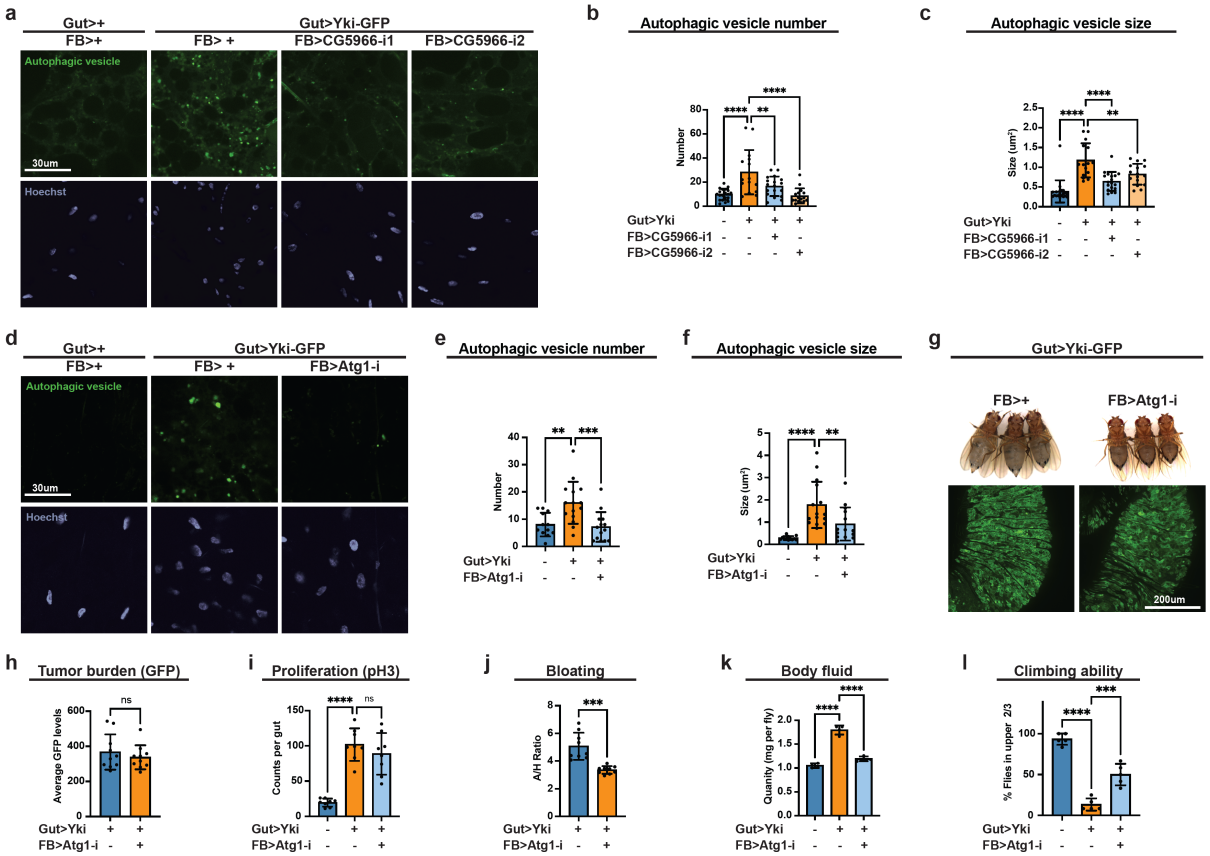
a
Gut>+
FB>+
Gut>Yki-GFP
FB> +
FB>CG5966-i1
FB>CG5966-i2
Autophagic vesicle
30um
Hoechst
b
Autophagic vesicle number
Number
Gut>Yki
FB>CG5966-i1
FB>CG5966-i2
c
Autophagic vesicle size
Size (um²)
d
Gut>+
FB>+
Gut>Yki-GFP
FB> +
FB>Atg1-i
e
Autophagic vesicle number
f
Autophagic vesicle size
g
Gut>Yki-GFP
FB>+
FB>Atg1-i
200um
h
Tumor burden (GFP)
Average GFP levels
i
Proliferation (pH3)
Counts per gut
j
Bloating
A/H Ratio
k
Body fluid
Quanity (mg per fly)
l
Climbing ability
% Flies in upper 2/3

852

853 **Figure 3. CG5966 promotes autophagosome formation in the fat body of Yki flies.**

854 **a**, Live imaging of fat bodies with autophagic vesicle staining dye in Yki flies with or without
855 fat-body *CG5966* depletion at day 7. **b**, **c**, Quantification of autophagic vesicle numbers (**b**)
856 and sizes (**c**) in **a**. **d**, Live imaging of fat bodies with autophagic vesicle staining dye in Yki
857 flies with or without fat-body *Atg1* depletion at day 7. **e**, **f**, Quantification of autophagic
858 vesicle numbers (**e**) and sizes (**f**) in **d**. **g**, Images of gut tumors and phenotypes of Yki flies
859 with or without fat-body *Atg1* depletion at day 6. **h**, Quantification of gut tumors (GFP
860 signal, arbitrary units) of Yki flies with or without fat-body *Atg1* depletion at day 6 (n = 8). **i**,
861 Total pH3 counts per gut of control flies and Yki flies with or without fat-body Atg1 depletion
862 at day 6 (n = 8). **j**, Quantification of bloating phenotypes of control flies and Yki flies with or
863 without fat-body Atg1 depletion at day 6 (A/H ratio, n=9). **k**, Body-fluid levels of Yki flies with
864 or without fat-body *Atg1* depletion at day 6 (n = 4). **l**, The climbing ability at day 6 (n = 4) of
865 control flies, Yki flies, and Yki flies with fat-body *Atg1* depletion. *$p < 0.05$, **$p < 0.01$, ***$p <$
866 0.001, ****$p < 0.0001$, ns indicates not significant. Error bars indicate SDs. n indicates the
867 number of biological replicates in each experiment.

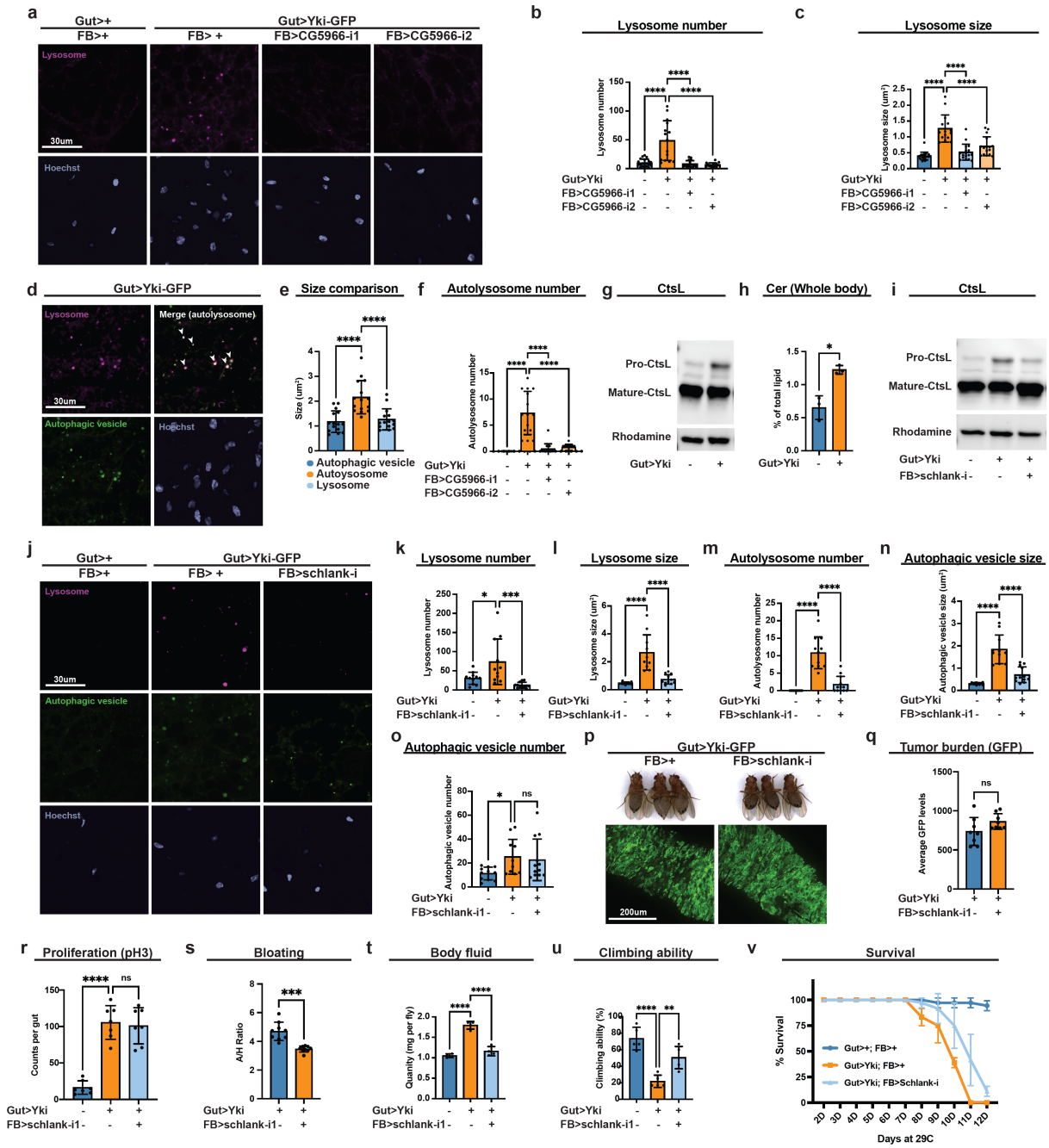
a
Gut>+
FB>+
Gut>Yki-GFP
FB> +
FB>CG5966-i1
FB>CG5966-i2
Lysosome
Hoechst
30um
b
Lysosome number
Lysosome number
Gut>Yki
FB>CG5966-i1
FB>CG5966-i2
c
Lysosome size
Lysosome size (um²)
d
Gut>Yki-GFP
Lysosome
Merge (autolysosome)
Autophagic vesicle
Hoechst
e
Size comparison
Size (um²)
Autophagic vesicle
Autoysosome
Lysosome
f
Autolysosome number
Autolysosome number
g
CtsL
Pro-CtsL
Mature-CtsL
Rhodamine
h
Cer (Whole body)
% of total lipid
i
CtsL
FB>schlank-i
j
Gut>+
FB>+
Gut>Yki-GFP
FB>schlank-i
k
Lysosome number
l
Lysosome size
m
Autolysosome number
n
Autophagic vesicle size
Autophagic vesicle size (um²)
o
Autophagic vesicle number
p
Gut>Yki-GFP
FB>+
FB>schlank-i
200um
q
Tumor burden (GFP)
Average GFP levels
r
Proliferation (pH3)
Counts per gut
s
Bloating
A/H Ratio
t
Body fluid
Quanity (mg per fly)
u
Climbing ability
Climbing ability (%)
v
Survival
% Survival
Gut>+; FB>+
Gut>Yki; FB>+
Gut>Yki; FB>Schlank-i
Days at 29C

868

Figure 4. Autophagic flux is blocked in Yki flies.

a, Live imaging of lysosomes in Yki flies with or without fat-body *CG5966* depletion at day 7. **b**, **c**, Quantification of lysosome numbers (**b**) and sizes (**c**) in **a**. **d**, Live imaging of lysosome and autophagic vesicles in Yki flies at day 7. **e**, Quantification of sizes of autophagic vesicles, autolysosome and lysosome in Yki flies. **f**, Quantification of autolysosome numbers in Yki flies with or without fat-body *CG5966* depletion at day 7. **g**, Western blot showing pro and matured forms of CtsL in Yki and control flies. Rhodamine was used as loading control. **h**, Relative levels of whole-body ceramide levels of Yki and control flies (n=3), data were retrieved from lipidomics analysis. **i**, Western blot showing pro and matured forms of CtsL in control flies, Yki flies with or without fat-body *schlank* depletion at day 7. Rhodamine was used as loading control. **j**, Live imaging of lysosomes and autophagic vesicles in Yki flies with or without fat-body *schlank* depletion at day 7. **k**-**n**, Quantification of lysosome numbers (**k**) and sizes (**l**), autophagic vesicle numbers (**m**) and sizes (**n**), autolysosome numbers (**o**) in **j**. **p**, Images of gut tumors and phenotypes of Yki flies with or without fat-body *schlank* depletion at day 6. **q**, Quantification of gut tumors (GFP signal, arbitrary units) of Yki flies with or without fat-body *schlank* depletion at day 6 (n = 8). **r**, Total pH3 counts per gut of control flies and Yki flies with or without fat-body *schlank* depletion at day 6 (n = 8). **s**, Quantification of bloating phenotypes of control flies and Yki flies with or without fat-body *schlank* depletion at day 6 (A/H ratio, n=9). **t**, Body-fluid levels of Yki flies with or without fat-body *schlank* depletion at day 6 (n = 4). **u**, **v**, The climbing ability at day 6 (**u**) (n = 4) and survival curve (**v**) (n = 3) of control flies, Yki flies, and Yki flies with fat-body *schlank* depletion. *$p < 0.05$, **$p < 0.01$, ***$p < 0.001$, ****$p < 0.0001$, ns indicates not significant. Error bars indicate SDs. n indicates the number of biological replicates in each experiment.

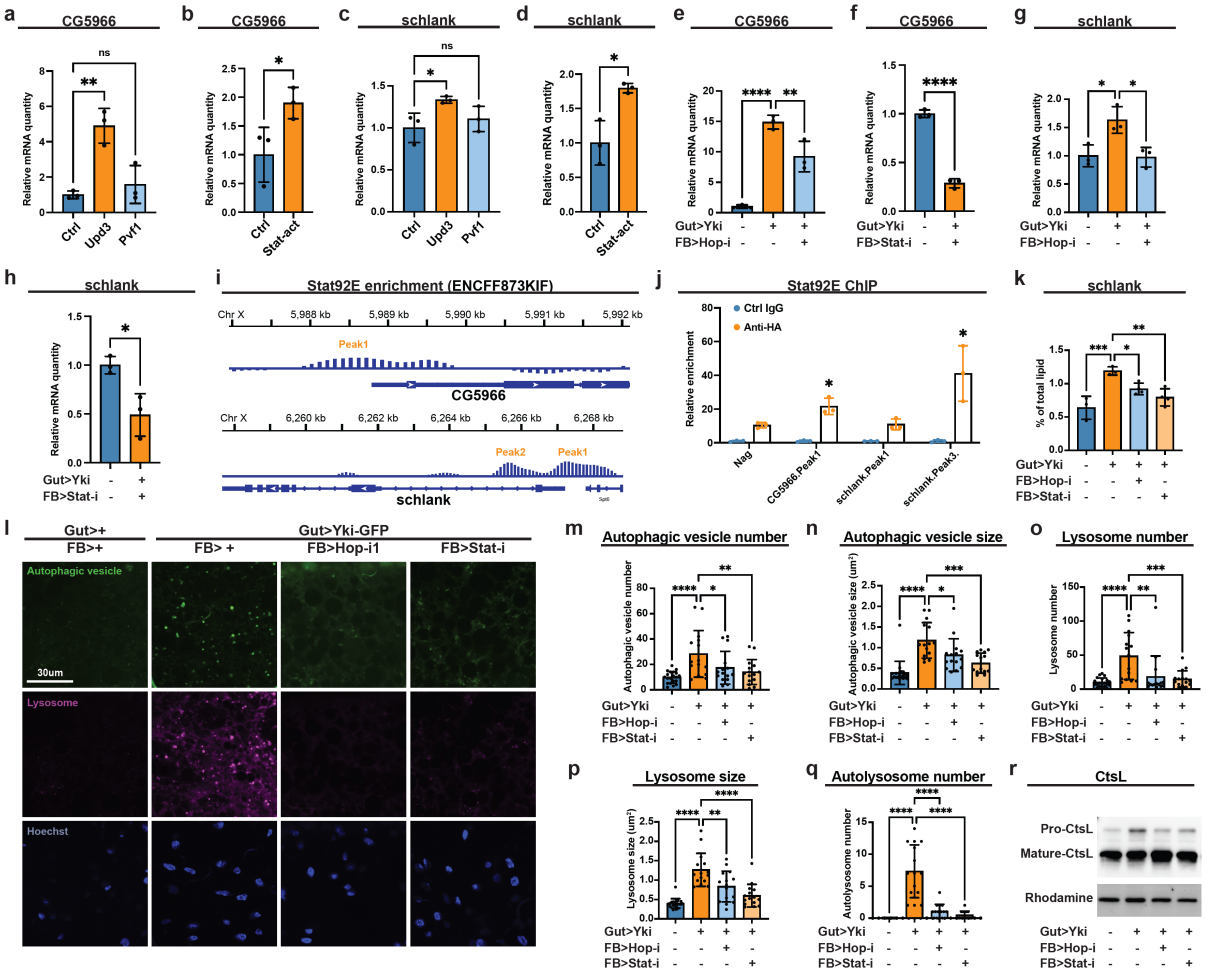
a
CG5966
Relative mRNA quantity
ns
**
Ctrl
Upd3
Pvr1
b
CG5966
*
Ctrl
Stat-act
c
schlank
ns
*
Ctrl
Upd3
Pvr1
d
schlank
*
Ctrl
Stat-act
e
CG5966
****
**
Gut>Yki
FB>Hop-i
f
CG5966
****
Gut>Yki
FB>Stat-i
g
schlank
*
*
Gut>Yki
FB>Hop-i
h
schlank
*
Gut>Yki
FB>Stat-i
i
Stat92E enrichment (ENCFF873KIF)
Chr X
5,988 kb
5,989 kb
5,990 kb
5,991 kb
5,992 kb
Peak1
CG5966
6,260 kb
6,262 kb
6,264 kb
6,266 kb
6,268 kb
Peak2
Peak1
schlank
j
Stat92E ChIP
Ctrl IgG
Anti-HA
Relative enrichment
Nag
CG5966.Peak1
schlank.Peak1
schlank.Peak3.
k
schlank
% of total lipid
***
*
**
Gut>Yki
FB>Hop-i
FB>Stat-i
l
Gut>+
FB>+
Gut>Yki-GFP
FB> +
FB>Hop-i1
FB>Stat-i
Autophagic vesicle
30um
Lysosome
Hoechst
m
Autophagic vesicle number
****
*
**
Gut>Yki
FB>Hop-i
FB>Stat-i
n
Autophagic vesicle size
Autophagic vesicle size (um²)
****
*
***
Gut>Yki
FB>Hop-i
FB>Stat-i
o
Lysosome number
****
**
***
Gut>Yki
FB>Hop-i
FB>Stat-i
p
Lysosome size
Lysosome size (um²)
****
**
****
Gut>Yki
FB>Hop-i
FB>Stat-i
q
Autolysosome number
****
****
****
Gut>Yki
FB>Hop-i
FB>Stat-i
r
CtsL
Pro-CtsL
Mature-CtsL
Rhodamine
Gut>Yki
FB>Hop-i
FB>Stat-i

893

894 **Figure 5. The JAK–STAT pathway regulates *CG5966* and *schlank* expression**

895 **in the fat body.**

896 **a**, **c**, qRT–PCR of *CG5966* (**a**) and *schlank* (**c**) mRNA in the fat body of flies with or without
897 ISC *Upd3* or *Pvf1* expression (*esg>Upd3* or *Pvf1*) at day 8 (n = 3). **b**, **d**, *CG5966* (**b**) and
898 *schlank* (**d**) mRNA in the fat body of flies with or without fat-body Stat92E-act (constitutive-
899 activated form of Stat92e) expression at day 8 (n = 3). **e**, **g**, *CG5966* (**e**) and *schlank* (**g**)
900 mRNA in the fat body of control, Yki flies, and Yki flies with fat-body *hop* depletion at day 6
901 (n = 3). **f**, **h**, *CG5966* (**f**) and *schlank* (**h**) mRNA in the fat body of Yki flies with or without fat-
902 body *Stat92e* depletion at day 6 (n = 3). **i**, Data from the ChIP-seq database indicating
903 enrichment of Stat92e binding at the *CG5966* and *schlank* promoter and gene regions. **j**,
904 ChIP revealed the enrichment of haemagglutinin (HA)-tagged Stat92E-act binding at the
905 *CG5966* and *schlank* gene regions, shown by fold changes relative to control IgG at day 8 (n
906 = 3 biological replicates). Neg, negative control. **k**, Relative levels of whole-body ceramide
907 levels of control, Yki flies, and Yki flies with fat-body *hop or Stat92E* depletion at day 6 (n =
908 3), data were retrieved from lipidomics analysis. **l**, Live imaging of lysosome and
909 autophagic vesicles in Yki flies with or without fat-body *hop* or *Stat92e* depletion at day 7.
910 **m**-**q**, Quantification of autophagic vesicle numbers (**m**) and sizes (**n**), lysosome numbers
911 (**o**) and sizes (**p**), and autolysosome numbers (**q**) in **l**. **r**, Western blot showing pro and
912 matured forms of CtsL in control flies, Yki flies with or without fat-body *hop* or *Stat92e*
913 depletion at day 7. *$p < 0.05$, **$p < 0.01$, ***$p < 0.001$, ****$p < 0.0001$, ns indicates not
914 significant. Error bars indicate SDs. n indicates the number of biological replicates in each
915 experiment.

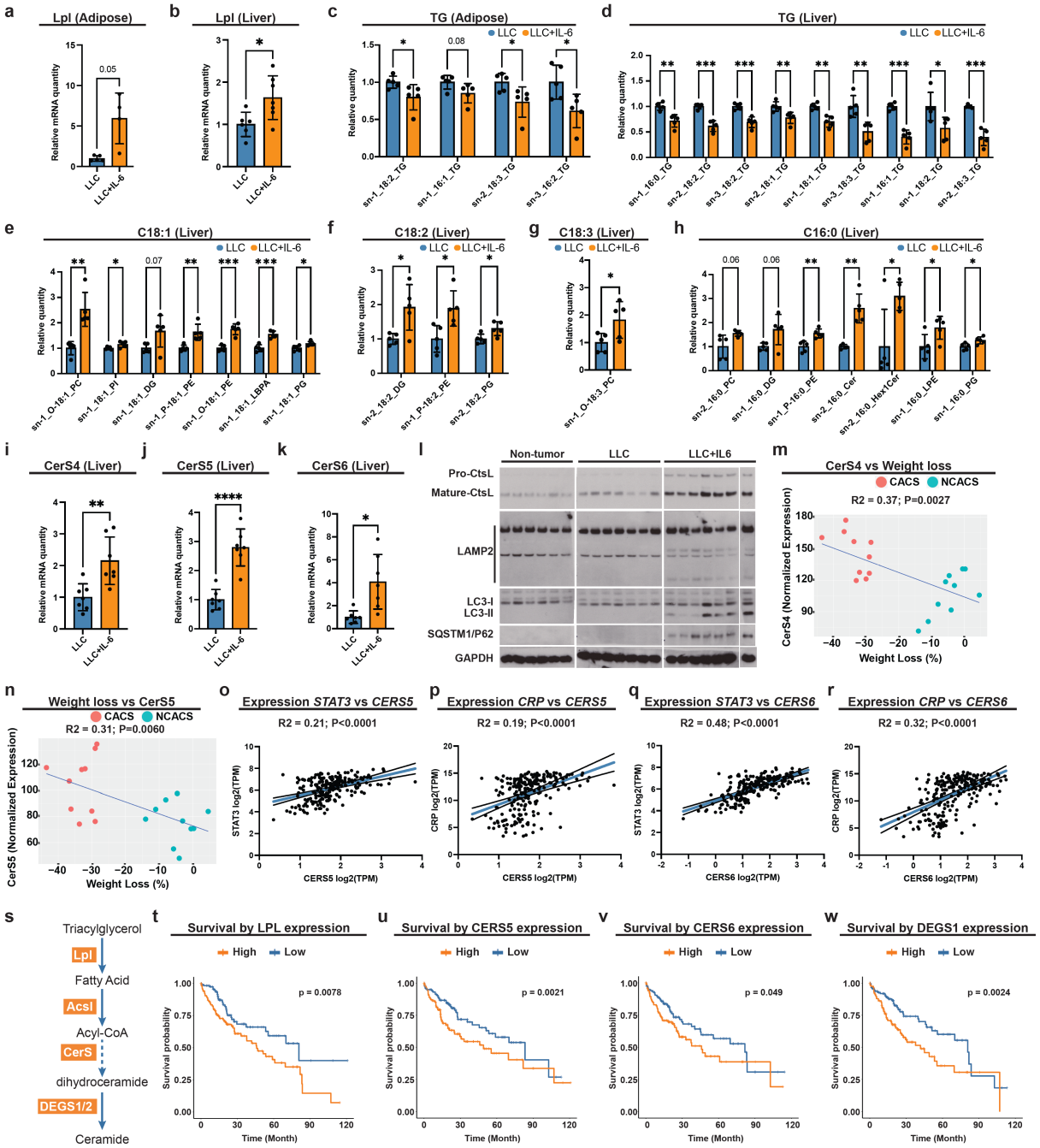
a
Lpl (Adipose)
Relative mRNA quantity
0.05
LLC
LLC+IL-6
b
Lpl (Liver)
c
TG (Adipose)
Relative quantity
0.08
sn-1_18:2_TG
sn-1_16:1_TG
sn-2_18:3_TG
sn-3_16:2_TG
d
TG (Liver)
sn-1_16:0_TG
sn-2_18:2_TG
sn-3_18:2_TG
sn-2_18:1_TG
sn-1_18:1_TG
sn-3_18:3_TG
sn-1_16:1_TG
sn-1_18:2_TG
sn-2_18:3_TG
e
C18:1 (Liver)
0.07
sn-1_O-18:1_PC
sn-1_18:1_PI
sn-1_18:1_DG
sn-1_P-18:1_PE
sn-1_O-18:1_PE
sn-1_18:1_LBPA
sn-1_18:1_PG
f
C18:2 (Liver)
sn-2_18:2_DG
sn-1_P-18:2_PE
sn-2_18:2_PG
g
C18:3 (Liver)
sn-1_O-18:3_PC
h
C16:0 (Liver)
0.06
0.06
sn-2_16:0_PC
sn-1_16:0_DG
sn-1_P-16:0_PE
sn-2_16:0_Cer
sn-2_16:0_HexCer
sn-1_16:0_LPE
sn-1_16:0_PG
i
CerS4 (Liver)
j
CerS5 (Liver)
k
CerS6 (Liver)
l
Non-tumor
LLC
LLC+IL6
Pro-CtsL
Mature-CtsL
LAMP2
LC3-I
LC3-II
SQSTM1/P62
GAPDH
m
CerS4 vs Weight loss
CACS
NCACS
R2 = 0.37; P=0.0027
CerS4 (Normalized Expression)
Weight Loss (%)
n
Weight loss vs CerS5
R2 = 0.31; P=0.0060
CerS5 (Normalized Expression)
o
Expression STAT3 vs CERS5
R2 = 0.21; P<0.0001
STAT3 log2(TPM)
CERS5 log2(TPM)
p
Expression CRP vs CERS5
R2 = 0.19; P<0.0001
CRP log2(TPM)
q
Expression STAT3 vs CERS6
R2 = 0.48; P<0.0001
CERS6 log2(TPM)
r
Expression CRP vs CERS6
R2 = 0.32; P<0.0001
s
Triacylglycerol
Lpl
Fatty Acid
AcsL
Acyl-CoA
CerS
dihydroceramide
DEGS1/2
Ceramide
t
Survival by LPL expression
High
Low
p = 0.0078
Survival probability
Time (Month)
u
Survival by CERS5 expression
p = 0.0021
v
Survival by CERS6 expression
p = 0.049
w
Survival by DEGS1 expression
p = 0.0024

Figure 6. Conserved pathogenic mechanism in mouse models and humans.

a, **b**, qRT–PCR of *Lpl* mRNA in adipose tissue (**a**) and liver (**b**) B6 mice injected with LLC cells with (n = 4) or without (n = 5) and IL-6 expression. **c**,**d**, Relative adipose (**c**) and liver (**d**) TG levels of B6 mice injected with LLC cells with or without IL-6 expression (n=5). **e**-**h**, Relative levels of liver C18:1 (**e**), C18:2 (**f**), C18:3 (**g**), and C16:0 (**h**) acyl chains levels of B6 mice injected with LLC cells with or without IL-6 expression (n=5). **i**-**k**, qRT–PCR of *CerS4* (**i**), *CerS5* (**j**), *CerS6* (**k**) mRNA in liver of B6 mice injected with LLC cells with or without IL-6 expression. **i**, Western blot showing forms of CtsL, LAMP2, LC3, and P62 in liver of B6 mice injected with LLC cells with or without IL-6 expression, with the loading control GAPDH. **m**,**n**, Correlation plots showing the positive relationship between liver CerS4 (**m**) and CerS5 (**n**) expression (n = 10) versus weight loss of KL mice. **o**-**r**, Correlation plots showing the positive relationship between expression of STAT3 and CerS5 (**o**), CPR and CerS5 (**p**), STAT3 and CerS6 (**q**), CPR and CerS6 (**r**) in non-diseased liver samples of 226 participants in the GTEx Project. TPM, transcript per million. **s**, Pathway map showing de novo ceramide synthesis pathway in human. **t**-**w**, Kaplan–Meier survival curves displaying the estimated survival probabilities of people with hepatocellular carcinoma with low (bottom third) and high (top third) hepatic expression of LPL (**t**), CERS5 (**u**), CERS6 (**v**), and DEGS1 (**w**). *$p < 0.05$, **$p < 0.01$, ***$p < 0.001$, ****$p < 0.0001$, ns indicates not significant. Error bars indicate SDs. n indicates the number of biological replicates in each experiment.

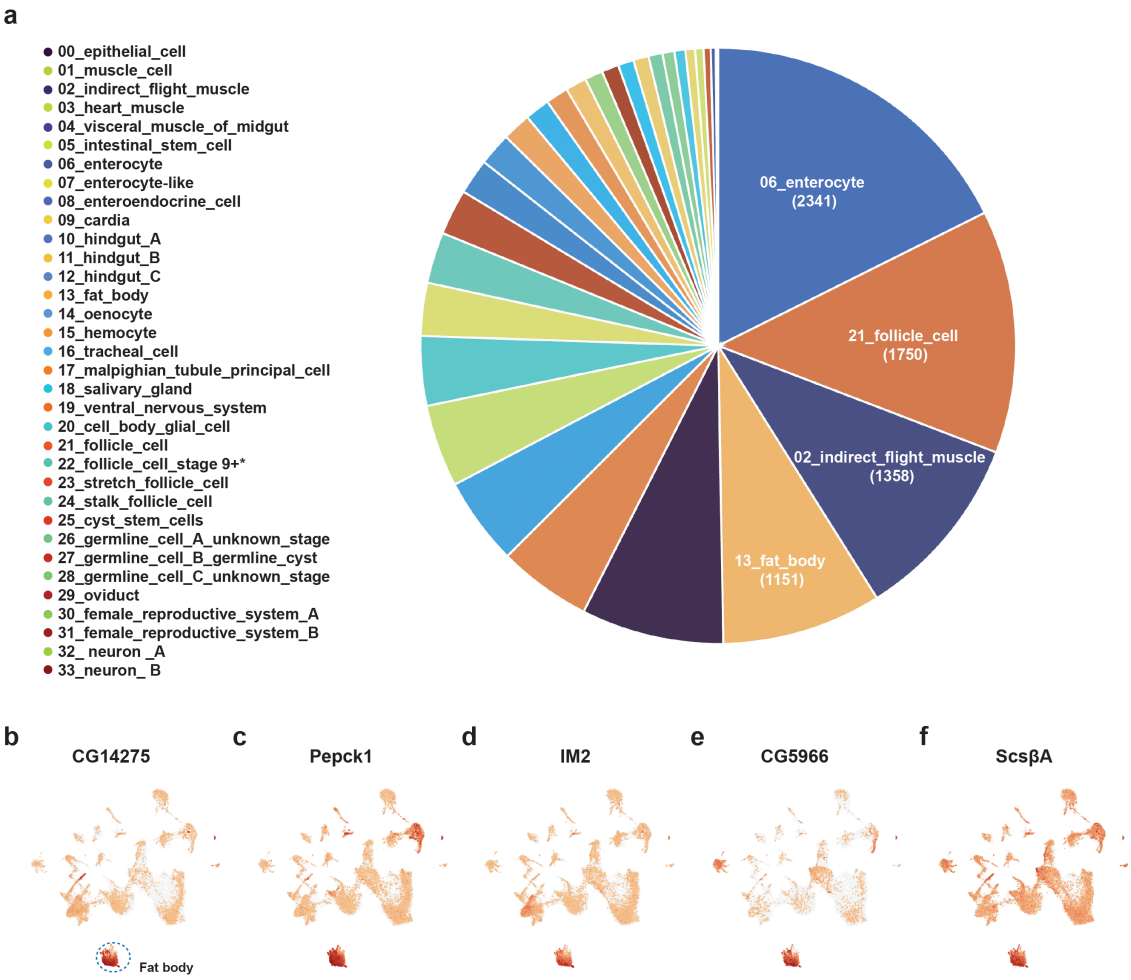
a
00_epithelial_cell
01_muscle_cell
02_indirect_flight_muscle
03_heart_muscle
04_visceral_muscle_of_midgut
05_intestinal_stem_cell
06_enterocyte
07_enterocyte-like
08_enteroendocrine_cell
09_cardia
10_hindgut_A
11_hindgut_B
12_hindgut_C
13_fat_body
14_oenocyte
15_hemocyte
16_tracheal_cell
17_malpighian_tubule_principal_cell
18_salivary_gland
19_ventral_nervous_system
20_cell_body_glial_cell
21_follicle_cell
22_follicle_cell_stage 9+*
23_stretch_follicle_cell
24_stalk_follicle_cell
25_cyst_stem_cells
26_germline_cell_A_unknown_stage
27_germline_cell_B_germline_cyst
28_germline_cell_C_unknown_stage
29_oviduct
30_female_reproductive_system_A
31_female_reproductive_system_B
32_ neuron _A
33_neuron_ B
06_enterocyte
(2341)
21_follicle_cell
(1750)
02_indirect_flight_muscle
(1358)
13_fat_body
(1151)
b
CG14275
Fat body
c
Pepck1
d
IM2
e
CG5966
f
ScsβA

936

937 **Figure S1, related to Figure 1.**

938 **a**, Distribution of progression associated genes across cell clusters. **b**-**f**, Expression of
939 CG14275 (**b**), Pepck1 (**c**), IM2 (**d**), CG5966 (**e**), ScsbetaA (**f**) across cell clusters, data retried
940 from snRNA-seq.

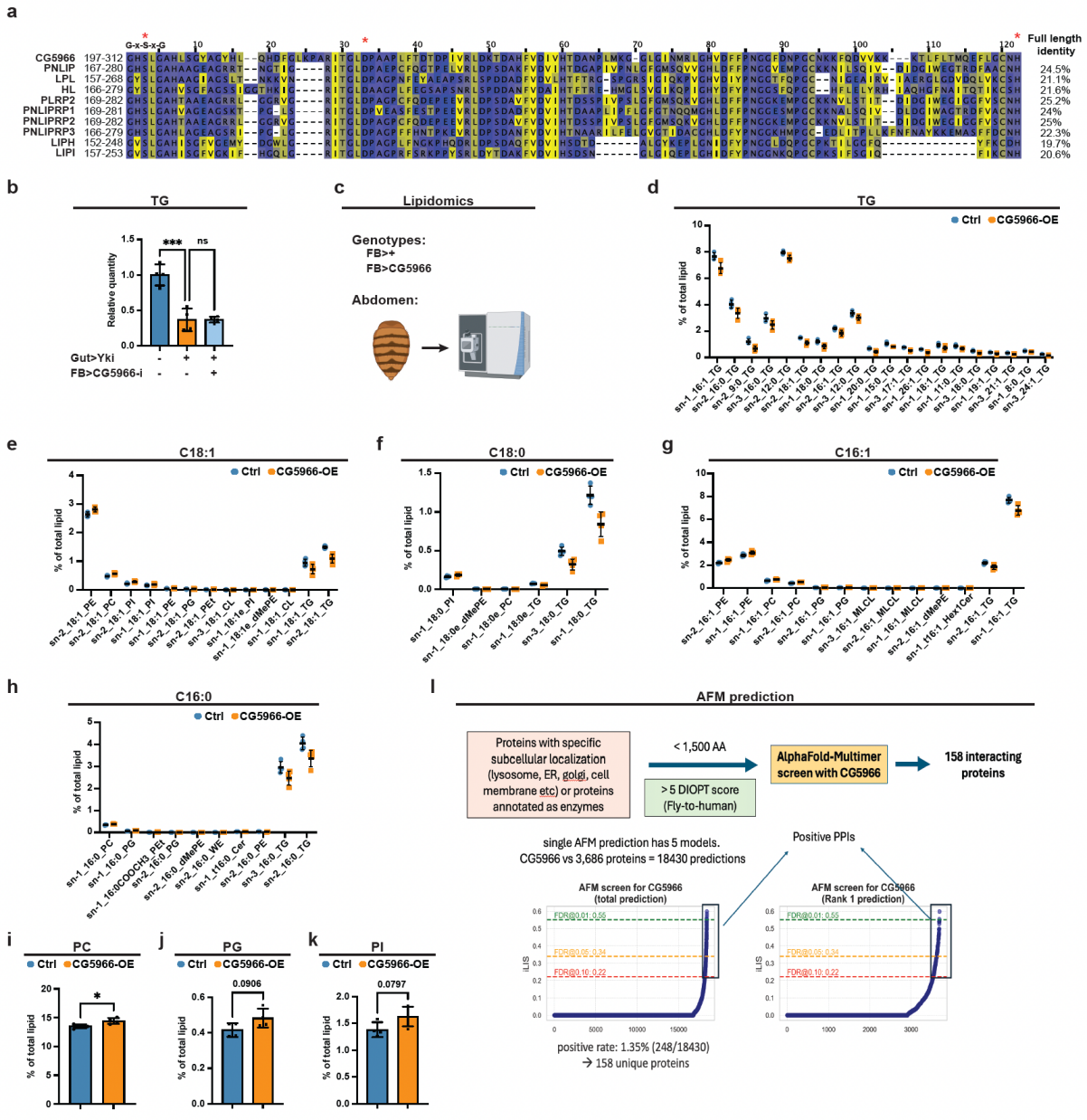
a
G-x-S-x-G
Full length identity
CG5966 197-312 24.5%
PNLIP 167-280 21.1%
LPL 157-268 21.6%
HL 166-279 25.2%
PLRP2 169-282 25%
PNLIPRP1 169-281 24%
PNLIPRP2 169-282 25%
PNLIPRP3 166-279 22.3%
LIPH 152-248 19.7%
LIPI 157-253 20.6%
b
TG
Relative quantity
***
ns
Gut>Yki
FB>CG5966-i
c
Lipidomics
Genotypes:
FB>+
FB>CG5966
Abdomen:
d
TG
Ctrl
CG5966-OE
% of total lipid
e
C18:1
f
C18:0
g
C16:1
h
C16:0
i
PC
j
PG
k
PI
0.0906
0.0797
l
AFM prediction
Proteins with specific subcellular localization (lysosome, ER, golgi, cell membrane etc) or proteins annotated as enzymes
< 1,500 AA
> 5 DIOPT score (Fly-to-human)
AlphaFold-Multimer screen with CG5966
158 interacting proteins
single AFM prediction has 5 models.
CG5966 vs 3,686 proteins = 18430 predictions
Positive PPIs
AFM screen for CG5966 (total prediction)
AFM screen for CG5966 (Rank 1 prediction)
FDR@0.01: 0.55
FDR@0.05: 0.34
FDR@0.10: 0.22
iLIS
positive rate: 1.35% (248/18430)
→ 158 unique proteins

941

942 **Figure S2, related to Figure 2.**

943 **a**, Amino acid sequence alignments showing similarity of human lipases to *CG5966*. **b**,
944 Whole-body TG levels of Yki flies with or without fat-body *CG5966* depletion at day 6 (n = 4).
945 **c**, Lipidomics analysis setting. **d**-**h**, Proportions of significantly changed abdomen TG (**d**),
946 and lipid species containing C18:1 (**e**), C18:0 (**f**), C16:1 (**g**), or C16:0 (**h**) Acyl chains in flies
947 with or without fat-body *CG5966* overexpression (n=4), data were retrieved from lipidomics
948 analysis. **i**-**k**, Proportions of abdomen PC (**i**), PG (**j**), PI (**k**) of flies with or without fat-body
949 CG5966 overexpression (n=4), data were retrieved from lipidomics analysis. **l**, AFM analysis
950 setting. *$p < 0.05$, **$p < 0.01$, ***$p < 0.001$, ****$p < 0.0001$, ns indicates not significant.
951 Error bars indicate SDs. n indicates the number of biological replicates in each experiment.

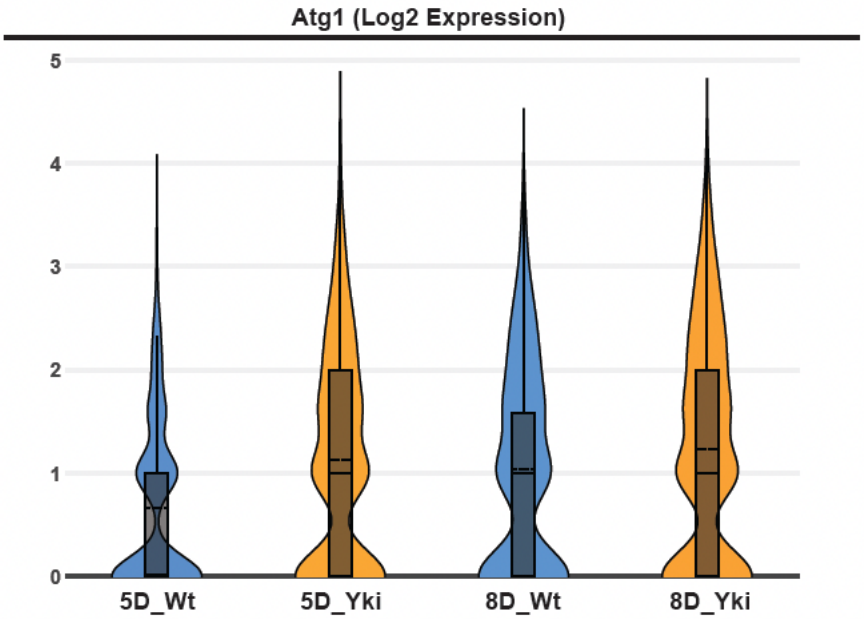

952

953 **Figure S3, related to Figure 3.**

954 Log2 expression of *Atg1* in day 5 and day 8 control and Yki flies, data were retrieved from
955 snRNAseq analysis.

956

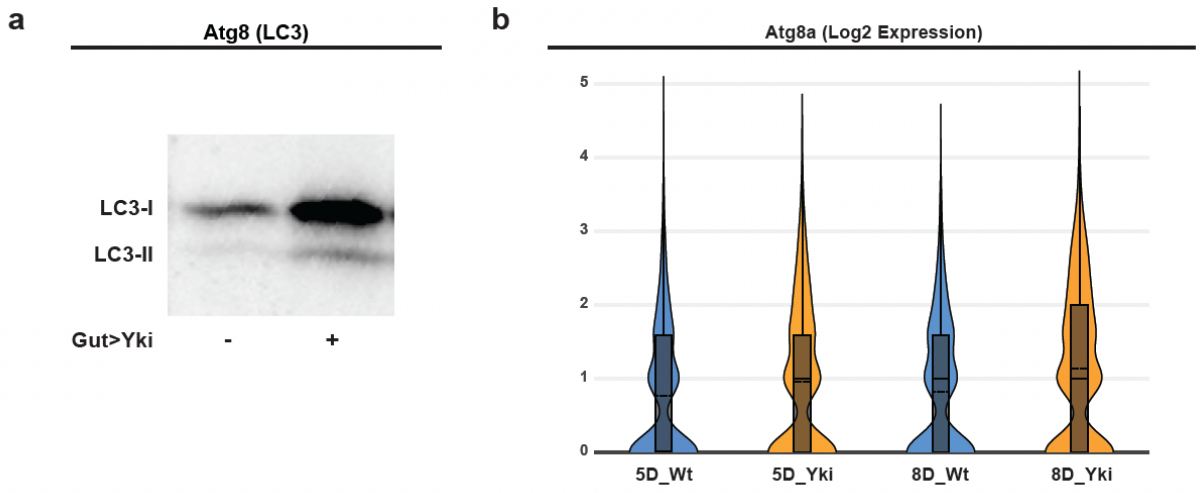
a
Atg8 (LC3)
LC3-I
LC3-II
Gut>Yki
-
+
b
Atg8a (Log2 Expression)
5
4
3
2
1
0
5D_Wt
5D_Yki
8D_Wt
8D_Yki

957

958 **Figure S4, related to Figure 4.**

959 **a**, Western blot of Atg8 (LC3) of abdomen samples from control and Yki flies. **b**, Log2
960 expression of *Atg8a* in day 5 and day 8 control and Yki flies, data were retrieved from
961 snRNAseq analysis.

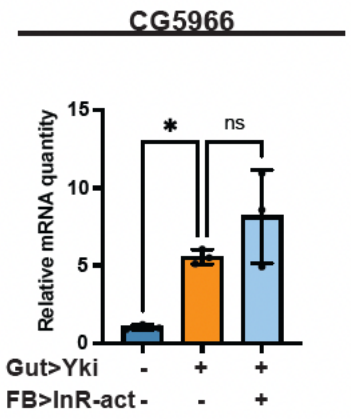

962

963 **Figure S5, related to Figure 5.**

964 *CG5966* mRNA expression in the fat body of control, Yki flies, and Yki flies with fat-body
965 *InR-act* (active form of InR) expression at day 6 (n = 3). *$p < 0.05$, **$p < 0.01$, ***$p < 0.001$,
966 ****$p < 0.0001$, ns indicates not significant. Error bars indicate SDs. n indicates biological
967 replicates.

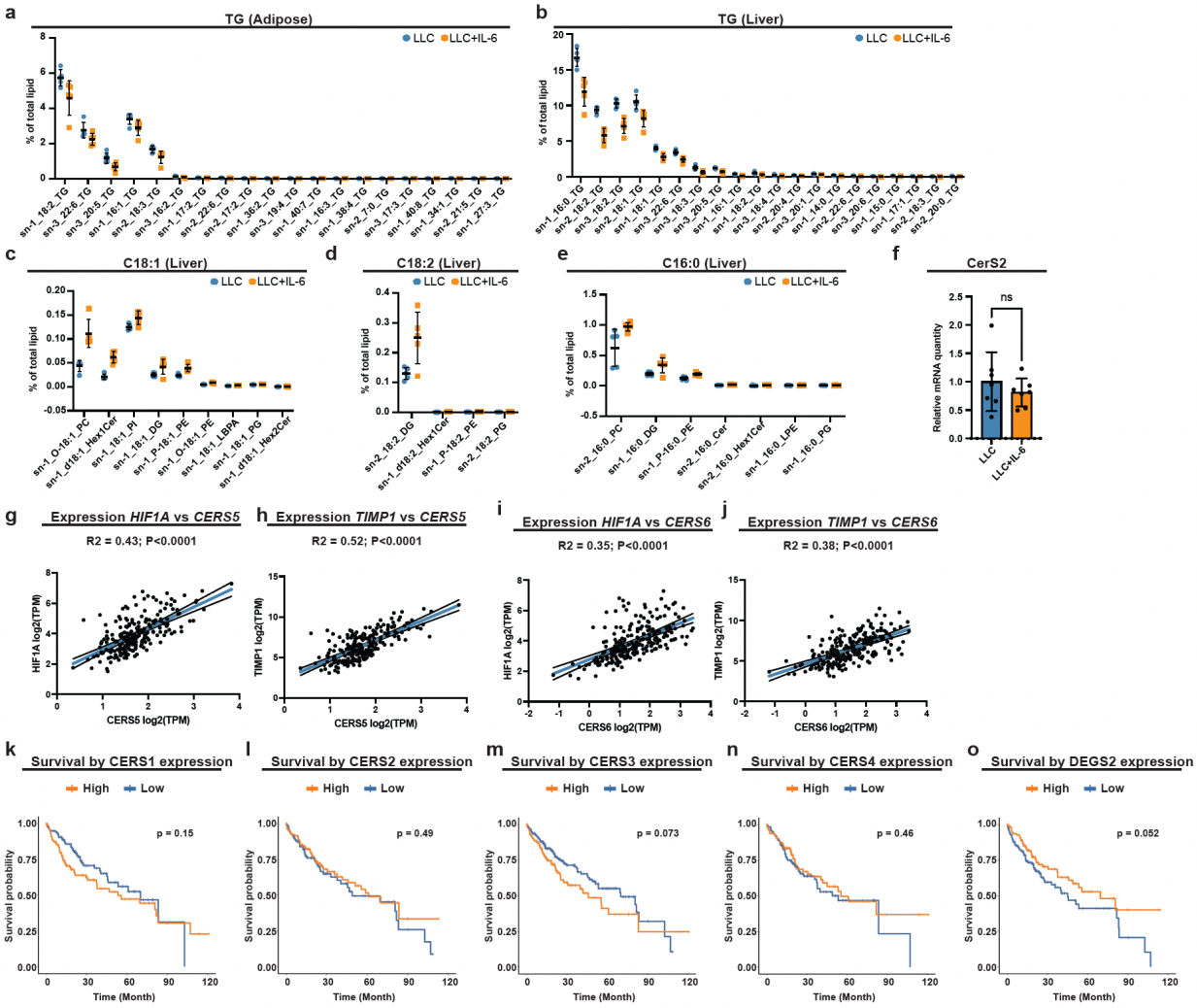
a
TG (Adipose)
LLC
LLC+IL-6
% of total lipid
sn-1_18:2_TG
sn-2_22:6_TG
sn-3_20:5_TG
sn-1_16:1_TG
sn-2_18:3_TG
sn-3_16:2_TG
sn-1_17:2_TG
sn-2_22:6_TG
sn-2_17:2_TG
sn-1_36:2_TG
sn-3_19:4_TG
sn-1_40:7_TG
sn-1_16:3_TG
sn-1_38:4_TG
sn-2_7:0_TG
sn-3_17:3_TG
sn-1_40:8_TG
sn-1_34:1_TG
sn-2_21:5_TG
sn-1_27:3_TG
b
TG (Liver)
LLC
LLC+IL-6
% of total lipid
sn-1_16:0_TG
sn-2_18:2_TG
sn-3_18:2_TG
sn-2_18:1_TG
sn-1_18:1_TG
sn-3_22:6_TG
sn-3_18:3_TG
sn-3_20:5_TG
sn-1_16:1_TG
sn-1_18:2_TG
sn-3_18:4_TG
sn-2_20:4_TG
sn-3_20:1_TG
sn-1_14:0_TG
sn-2_22:6_TG
sn-3_20:6_TG
sn-1_15:0_TG
sn-1_17:1_TG
sn-2_18:3_TG
sn-2_20:0_TG
c
C18:1 (Liver)
LLC
LLC+IL-6
% of total lipid
sn-1_O-18:1_PC
sn-1_d18:1_Hex1Cer
sn-1_18:1_PI
sn-1_18:1_DG
sn-1_18:1_PE
sn-1_P-18:1_PE
sn-1_O-18:1_PE
sn-1_18:1_LBPA
sn-1_18:1_PG
sn-1_d18:1_Hex2Cer
d
C18:2 (Liver)
LLC
LLC+IL-6
% of total lipid
sn-2_18:2_DG
sn-1_d18:2_Hex1Cer
sn-1_P-18:2_PE
sn-2_18:2_PG
e
C16:0 (Liver)
LLC
LLC+IL-6
% of total lipid
sn-2_16:0_PC
sn-1_16:0_DG
sn-1_P-16:0_PE
sn-2_16:0_Cer
sn-2_16:0_Hex1Cer
sn-1_16:0_LPE
sn-1_16:0_PG
f
CerS2
ns
Relative mRNA quantity
LLC
LLC+IL-6
g
Expression HIF1A vs CERS5
R2 = 0.43; P<0.0001
HIF1A log2(TPM)
CERS5 log2(TPM)
h
Expression TIMP1 vs CERS5
R2 = 0.52; P<0.0001
TIMP1 log2(TPM)
CERS5 log2(TPM)
i
Expression HIF1A vs CERS6
R2 = 0.35; P<0.0001
HIF1A log2(TPM)
CERS6 log2(TPM)
j
Expression TIMP1 vs CERS6
R2 = 0.38; P<0.0001
TIMP1 log2(TPM)
CERS6 log2(TPM)
k
Survival by CERS1 expression
High
Low
p = 0.15
Survival probability
Time (Month)
l
Survival by CERS2 expression
High
Low
p = 0.49
Survival probability
Time (Month)
m
Survival by CERS3 expression
High
Low
p = 0.073
Survival probability
Time (Month)
n
Survival by CERS4 expression
High
Low
p = 0.46
Survival probability
Time (Month)
o
Survival by DEGS2 expression
High
Low
p = 0.052
Survival probability
Time (Month)

968

969 **Figure S6. related to Figure 6.**

970 **a**,**b**, Proportions of significantly changed adipose (**a**) and liver (**b**) TG levels of B6 mice
971 injected with LLC cells with or without IL-6 expression (n=5). **c**-**e**, Proportions of
972 significantly changed lipid species containing C18:1 (**c**), C18:2 (**d**), or C16:0 (**e**) acyl chains
973 of B6 mice injected with LLC cells with or without IL-6 expression in liver (n=5). **f**, qRT–PCR
974 of *CerS2* mRNA in liver of B6 mice injected with LLC cells with or without IL-6 expression. **g**-
975 **j**, Correlation plots showing the positive relationship between expression of HIF1A and
976 CerS5 (**g**), TIMP1 and CerS5 (**h**), HIF1A and CerS6 (**i**), TIMP1 and CerS6 (**j**) in non-diseased
977 liver samples of 226 participants in the GTEx Project. TPM, transcript per million. **k**-**o**,
978 Kaplan–Meier survival curves displaying the estimated survival probabilities of people with
979 hepatocellular carcinoma with low (bottom third) and high (top third) hepatic expression of
980 CERS1 (**k**), CERS2 (**l**), CERS3 (**m**), CERS4 (**n**), and DEGS2 (**o**). *$p < 0.05$, **$p < 0.01$, ***$p <$
981 0.001, ****$p < 0.0001$, ns indicates not significant. Error bars indicate SDs. n indicates the
982 number of biological replicates in each experiment.

References

Agca, S., Kir, S., 2024. The role of interleukin-6 family cytokines in cancer cachexia. FEBS J. 291, 4009–4023. https://doi.org/10.1111/febs.17224

Barton, B.E., 2001. IL-6-like cytokines and cancer cachexia. Immunol. Res. 23, 41–58. https://doi.org/10.1385/IR:23:1:41

Bilder, D., Ong, K., Hsi, T.-C., Adiga, K., Kim, J., 2021. Tumour–host interactions through the lens of Drosophila. Nat. Rev. Cancer 1–14. https://doi.org/10.1038/s41568-021-00387-5

Castell, J.V., Gómez-Lechón, M.J., David, M., Fabra, R., Trullenque, R., Heinrich, P.C., 1990. Acute-phase response of human hepatocytes: regulation of acute-phase protein synthesis by interleukin-6. Hepatol. Baltim. Md 12, 1179–1186. https://doi.org/10.1002/hep.1840120517

Chavez, J.A., Summers, S.A., 2012. A ceramide-centric view of insulin resistance. Cell Metab. 15, 585–594. https://doi.org/10.1016/j.cmet.2012.04.002

Cheng, C., Liu, Y., Chen, Y., Li, J., Xu, W., Perrimon, N., Song, W., 2025. The Power of Drosophila in Modeling Cancer Cachexia, in: Deng, W.-M., Gonzaléz, C. (Eds.), The Drosophila Model in Cancer: Volume II. Springer Nature Switzerland, Cham, pp. 83–100. https://doi.org/10.1007/978-3-031-97035-1_5

Dien, J., Amin, H.M., Chiu, N., Wong, W., Frantz, C., Chiu, B., Mackey, J.R., Lai, R., 2006. Signal Transducers and Activators of Transcription-3 Up-Regulates Tissue Inhibitor of Metalloproteinase-1 Expression and Decreases Invasiveness of Breast Cancer. Am. J. Pathol. 169, 633–642. https://doi.org/10.2353/ajpath.2006.051109

Ding, G., Xiang, X., Hu, Y., Xiao, G., Chen, Y., Binari, R., Comjean, A., Li, J., Rushworth, E., Fu, Z., Mohr, S.E., Perrimon, N., Song, W., 2021. Coordination of tumor growth and host wasting by tumor-derived Upd3. Cell Rep. 36, 109553. https://doi.org/10.1016/j.celrep.2021.109553

Dong, W., He, B., Qian, H., Liu, Q., Wang, D., Li, J., Wei, Z., Wang, Z., Xu, Z., Wu, G., Qian, G., Wang, G., 2018. RAB26-dependent autophagy protects adherens junctional integrity in acute lung injury. Autophagy 14, 1677–1692. https://doi.org/10.1080/15548627.2018.1476811

Ekas, L.A., Cardozo, T.J., Flaherty, M.S., McMillan, E.A., Gonsalves, F.C., Bach, E.A., 2010. Characterization of a dominant-active STAT that promotes tumorigenesis in Drosophila. Dev. Biol. 344, 621–636. https://doi.org/10.1016/j.ydbio.2010.05.497

Evans, R., O'Neill, M., Pritzel, A., Antropova, N., Senior, A., Green, T., Žídek, A., Bates, R., Blackwell, S., Yim, J., Ronneberger, O., Bodenstein, S., Zielinski, M., Bridgland, A., Potapenko, A., Cowie, A., Tunyasuvunakool, K., Jain, R., Clancy, E., Kohli, P., Jumper, J., Hassabis, D., 2021. Protein complex prediction with AlphaFold-Multimer. https://doi.org/10.1101/2021.10.04.463034

Fearon, K.C.H., Glass, D.J., Guttridge, D.C., 2012. Cancer Cachexia: Mediators, Signaling, and Metabolic Pathways. Cell Metab. 16, 153–166. https://doi.org/10.1016/j.cmet.2012.06.011

Ferrer, M., Mourikis, N., Davidson, E.E., Kleeman, S.O., Zaccaria, M., Habel, J., Rubino, R., Gao, Q., Flint, T.R., Young, L., Connell, C.M., Lukey, M.J., Goncalves, M.D., White,

1026 E.P., Venkitaraman, A.R., Janowitz, T., 2023. Ketogenic diet promotes tumor
1027 ferroptosis but induces relative corticosterone deficiency that accelerates cachexia.
1028 Cell Metab. 35, 1147-1162.e7. https://doi.org/10.1016/j.cmet.2023.05.008
1029 Flint, T.R., Janowitz, T., Connell, C.M., Roberts, E.W., Denton, A.E., Coll, A.P., Jodrell, D.I.,
1030 Fearon, D.T., 2016. Tumor-Induced IL-6 Reprograms Host Metabolism to Suppress
1031 Anti-tumor Immunity. Cell Metab. 24, 672–684.
1032 https://doi.org/10.1016/j.cmet.2016.10.010
1033 Fresques, T., Niles, B., Aronova, S., Mogri, H., Rakhshandehroo, T., Powers, T., 2015.
1034 Regulation of Ceramide Synthase by Casein Kinase 2-dependent Phosphorylation in
1035 Saccharomyces cerevisiae. J. Biol. Chem. 290, 1395–1403.
1036 https://doi.org/10.1074/jbc.M114.621086
1037 Gabandé-Rodríguez, E., Boya, P., Labrador, V., Dotti, C.G., Ledesma, M.D., 2014. High
1038 sphingomyelin levels induce lysosomal damage and autophagy dysfunction in
1039 Niemann Pick disease type A. Cell Death Differ. 21, 864–875.
1040 https://doi.org/10.1038/cdd.2014.4
1041 Galluzzi, L., Baehrecke, E.H., Ballabio, A., Boya, P., Bravo-San Pedro, J.M., Cecconi, F.,
1042 Choi, A.M., Chu, C.T., Codogno, P., Colombo, M.I., Cuervo, A.M., Debnath, J.,
1043 Deretic, V., Dikic, I., Eskelinen, E.-L., Fimia, G.M., Fulda, S., Gewirtz, D.A., Green,
1044 D.R., Hansen, M., Harper, J.W., Jäättelä, M., Johansen, T., Juhasz, G., Kimmelman,
1045 A.C., Kraft, C., Ktistakis, N.T., Kumar, S., Levine, B., Lopez-Otin, C., Madeo, F.,
1046 Martens, S., Martinez, J., Melendez, A., Mizushima, N., Münz, C., Murphy, L.O.,
1047 Penninger, J.M., Piacentini, M., Reggiori, F., Rubinsztein, D.C., Ryan, K.M.,
1048 Santambrogio, L., Scorrano, L., Simon, A.K., Simon, H.-U., Simonsen, A.,
1049 Tavernarakis, N., Tooze, S.A., Yoshimori, T., Yuan, J., Yue, Z., Zhong, Q., Kroemer, G.,
1050 2017. Molecular definitions of autophagy and related processes. EMBO J. 36, 1811–
1051 1836. https://doi.org/10.15252/embj.201796697
1052 Gillingham, A.K., Sinka, R., Torres, I.L., Lilley, K.S., Munro, S., 2014. Toward a
1053 Comprehensive Map of the Effectors of Rab GTPases. Dev. Cell 31, 358–373.
1054 https://doi.org/10.1016/j.devcel.2014.10.007
1055 Goncalves, M.D., Hwang, S.-K., Pauli, C., Murphy, C.J., Cheng, Z., Hopkins, B.D., Wu, D.,
1056 Loughran, R.M., Emerling, B.M., Zhang, G., Fearon, D.T., Cantley, L.C., 2018.
1057 Fenofibrate prevents skeletal muscle loss in mice with lung cancer. Proc. Natl.
1058 Acad. Sci. 115, E743–E752. https://doi.org/10.1073/pnas.1714703115
1059 Hamel, S., Fantini, J., Schweisguth, F., 2010. Notch ligand activity is modulated by
1060 glycosphingolipid membrane composition in Drosophila melanogaster. J. Cell Biol.
1061 188, 581–594. https://doi.org/10.1083/jcb.200907116
1062 Hannun, Y.A., Obeid, L.M., 2018. Sphingolipids and their metabolism in physiology and
1063 disease. Nat. Rev. Mol. Cell Biol. 19, 175–191. https://doi.org/10.1038/nrm.2017.107
1064 Harayama, T., Riezman, H., 2018. Understanding the diversity of membrane lipid
1065 composition. Nat. Rev. Mol. Cell Biol. 19, 281–296.
1066 https://doi.org/10.1038/nrm.2017.138
1067 Hoadley, K.A., Yau, C., Hinoue, T., Wolf, D.M., Lazar, A.J., Drill, E., Shen, R., Taylor, A.M.,
1068 Cherniack, A.D., Thorsson, Vésteinn, Akbani, R., Bowlby, R., Wong, C.K.,
1069 Wiznerowicz, M., Sanchez-Vega, F., Robertson, A.G., Schneider, B.G., Lawrence,

M.S., Noushmehr, H., Malta, T.M., Caesar-Johnson, S.J., Demchok, J.A., Felau, I., Kasapi, M., Ferguson, M.L., Hutter, C.M., Sofia, H.J., Tarnuzzer, R., Wang, Z., Yang, L., Zenklusen, J.C., Zhang, J. (Julia), Chudamani, S., Liu, J., Lolla, L., Naresh, R., Pihl, T., Sun, Q., Wan, Y., Wu, Y., Cho, J., DeFreitas, T., Frazer, S., Gehlenborg, N., Getz, G., Heiman, D.I., Kim, J., Lawrence, M.S., Lin, P., Meier, S., Noble, M.S., Saksena, G., Voet, D., Zhang, Hailei, Bernard, B., Chambwe, N., Dhankani, V., Knijnenburg, T., Kramer, R., Leinonen, K., Liu, Y., Miller, M., Reynolds, S., Shmulevich, I., Thorsson, Vesteinn, Zhang, W., Akbani, R., Broom, B.M., Hegde, A.M., Ju, Z., Kanchi, R.S., Korkut, A., Li, J., Liang, H., Ling, S., Liu, W., Lu, Y., Mills, G.B., Ng, K.-S., Rao, A., Ryan, M., Wang, Jing, Weinstein, J.N., Zhang, J., Abeshouse, A., Armenia, J., Chakravarty, D., Chatila, W.K., Bruijn, I. de, Gao, J., Gross, B.E., Heins, Z.J., Kundra, R., La, K., Ladanyi, M., Luna, A., Nissan, M.G., Ochoa, A., Phillips, S.M., Reznik, E., Sanchez-Vega, F., Sander, C., Schultz, N., Sheridan, R., Sumer, S.O., Sun, Y., Taylor, B.S., Wang, Jioajiao, Zhang, Hongxin, Anur, P., Peto, M., Spellman, P., Benz, C., Stuart, J.M., Wong, C.K., Yau, C., Hayes, D.N., Parker, J.S., Wilkerson, M.D., Ally, A., Balasundaram, M., Bowlby, R., Brooks, D., Carlsen, R., Chuah, E., Dhalla, N., Holt, R., Jones, S.J.M., Kasaian, K., Lee, D., Ma, Y., Marra, M.A., Mayo, M., Moore, R.A., Mungall, A.J., Mungall, K., Robertson, A.G., Sadeghi, S., Schein, J.E., Sipahimalani, P., Tam, A., Thiessen, N., Tse, K., Wong, T., Berger, A.C., Beroukhim, R., Cherniack, A.D., Cibulskis, C., Gabriel, S.B., Gao, G.F., Ha, G., Meyerson, M., Schumacher, S.E., Shih, J., Kucherlapati, M.H., Kucherlapati, R.S., Baylin, S., Cope, L., Danilova, L., Bootwalla, M.S., Lai, P.H., Maglinte, D.T., Berg, D.J.V.D., Weisenberger, D.J., Auman, J.T., Balu, S., Bodenheimer, T., Fan, C., Hoadley, K.A., Hoyle, A.P., Jefferys, S.R., Jones, C.D., Meng, S., Mieczkowski, P.A., Mose, L.E., Perou, A.H., Perou, C.M., Roach, J., Shi, Y., Simons, J.V., Skelly, T., Soloway, M.G., Tan, D., Veluvolu, U., Fan, H., Hinoue, T., Laird, P.W., Shen, H., Zhou, W., Bellair, M., Chang, K., Covington, K., Creighton, C.J., Dinh, H., Doddapaneni, H., Donehower, L.A., Drummond, J., Gibbs, R.A., Glenn, R., Hale, W., Han, Y., Hu, J., Korchina, V., Lee, S., Lewis, L., Li, W., Liu, X., Morgan, M., Morton, D., Muzny, D., Santibanez, J., Sheth, M., Shinbrot, E., Wang, L., Wang, M., Wheeler, D.A., Xi, L., Zhao, F., Hess, J., Appelbaum, E.L., Bailey, M., Cordes, M.G., Ding, L., Fronick, C.C., Fulton, L.A., Fulton, R.S., Kandoth, C., Mardis, E.R., McLellan, M.D., Miller, C.A., Schmidt, H.K., Wilson, R.K., Crain, D., Curley, E., Gardner, J., Lau, K., Mallery, D., Morris, S., Paulauskis, J., Penny, R., Shelton, C., Shelton, T., Sherman, M., Thompson, E., Yena, P., Bowen, J., Gastier-Foster, J.M., Gerken, M., Leraas, K.M., Lichtenberg, T.M., Ramirez, N.C., Wise, L., Zmuda, E., Corcoran, N., Costello, T., Hovens, C., Carvalho, A.L., Carvalho, A.C. de, Fregnani, J.H., Longatto-Filho, A., Reis, R.M., Scapulatempo-Neto, C., Silveira, H.C.S., Vidal, D.O., Burnette, A., Eschbacher, J., Hermes, B., Noss, A., Singh, R., Anderson, M.L., Castro, P.D., Ittmann, M., Huntsman, D., Kohl, B., Le, X., Thorp, R., Andry, C., Duffy, E.R., Lyadov, V., Paklina, O., Setdikova, G., Shabunin, A., Tavobilov, M., McPherson, C., Warnick, R., Berkowitz, R., Cramer, D., Feltmate, C., Horowitz, N., Kibel, A., Muto, M., Raut, C.P., Malykh, A., Barnholtz-Sloan, J.S., Barrett, W., Devine, K., Fulop, J., Ostrom, Q.T., Shimmel, K., Wolinsky, Y., Sloan, A.E., Rose, A.D., Giuliante, F., Goodman, M., Karlan, B.Y., Hagedorn, C.H., Eckman, J., Harr, J., Myers, J., Tucker, K.,

Zach, L.A., Deyarmin, B., Hu, H., Kvecher, L., Larson, C., Mural, R.J., Somiari, S., Vicha, A., Zelinka, T., Bennett, J., Iacocca, M., Rabeno, B., Swanson, P., Latour, M., Lacombe, L., Têtu, B., Bergeron, A., McGraw, M., Staugaitis, S.M., Chabot, J., Hibshoosh, H., Sepulveda, A., Su, T., Wang, T., Potapova, O., Voronina, O., Desjardins, L., Mariani, O., Roman-Roman, S., Sastre, X., Stern, M.-H., Cheng, F., Signoretti, S., Berchuck, A., Bigner, D., Lipp, E., Marks, J., McCall, S., McLendon, R., Secord, A., Sharp, A., Behera, M., Brat, D.J., Chen, A., Delman, K., Force, S., Khuri, F., Magliocca, K., Maithel, S., Olson, J.J., Owonikoko, T., Pickens, A., Ramalingam, S., Shin, D.M., Sica, G., Meir, E.G.V., Zhang, Hongzheng, Eijckenboom, W., Gillis, A., Korpershoek, E., Looijenga, L., Oosterhuis, W., Stoop, H., Kessel, K.E. van, Zwarthoff, E.C., Calatozzolo, C., Cuppini, L., Cuzzubbo, S., DiMeco, F., Finocchiaro, G., Mattei, L., Perin, A., Pollo, B., Chen, C., Houck, J., Lohavanichbutr, P., Hartmann, A., Stoehr, C., Stoehr, R., Taubert, H., Wach, S., Wullich, B., Kycler, W., Murawa, D., Wiznerowicz, M., Chung, K., Edenfield, W.J., Martin, J., Baudin, E., Bubley, G., Bueno, R., Rienzo, A.D., Richards, W.G., Kalkanis, S., Mikkelsen, T., Noushmehr, H., Scarpace, L., Girard, N., Aymerich, M., Campo, E., Giné, E., Guillermo, A.L., Bang, N.V., Hanh, P.T., Phu, B.D., Tang, Y., Colman, H., Evason, K., Dottino, P.R., Martignetti, J.A., Gabra, H., Juhl, H., Akeredolu, T., Stepa, S., Hoon, D., Ahn, K., Kang, K.J., Beuschlein, F., Breggia, A., Birrer, M., Bell, D., Borad, M., Bryce, A.H., Castle, E., Chandan, V., Cheville, J., Copland, J.A., Farnell, M., Flotte, T., Giama, N., Ho, T., Kendrick, M., Kocher, J.-P., Kopp, K., Moser, C., Nagorney, D., O'Brien, D., O'Neill, B.P., Patel, T., Petersen, G., Que, F., Rivera, M., Roberts, L., Smallridge, R., Smyrk, T., Stanton, M., Thompson, R.H., Torbenson, M., Yang, J.D., Zhang, L., Brimo, F., Ajani, J.A., Gonzalez, A.M.A., Behrens, C., Bondaruk, O., Broaddus, R., Czerniak, B., Esmaeli, B., Fujimoto, J., Gershenwald, J., Guo, C., Lazar, A.J., Logothetis, C., Meric-Bernstam, F., Moran, C., Ramondetta, L., Rice, D., Sood, A., Tamboli, P., Thompson, T., Troncoso, P., Tsao, A., Wistuba, I., Carter, C., Haydu, L., Hersey, P., Jakrot, V., Kakavand, H., Kefford, R., Lee, K., Long, G., Mann, G., Quinn, M., Saw, R., Scolyer, R., Shannon, K., Spillane, A., Stretch, J., Synott, M., Thompson, J., Wilmott, J., Al-Ahmadie, H., Chan, T.A., Ghossein, R., Gopalan, A., Levine, D.A., Reuter, V., Singer, S., Singh, B., Tien, N.V., Broudy, T., Mirsaidi, C., Nair, P., Drwiega, P., Miller, J., Smith, J., Zaren, H., Park, J.-W., Hung, N.P., Kebebew, E., Linehan, W.M., Metwalli, A.R., Pacak, K., Pinto, P.A., Schiffman, M., Schmidt, L.S., Vocke, C.D., Wentzensen, N., Worrell, R., Yang, H., Moncrieff, M., Goparaju, C., Melamed, J., Pass, H., Botnariuc, N., Caraman, I., Cernat, M., Chemencedji, I., Clipca, A., Doruc, S., Gorincioi, G., Mura, S., Pirtac, M., Stancul, I., Tcaciuc, D., Albert, M., Alexopoulou, I., Arnaout, A., Bartlett, J., Engel, J., Gilbert, S., Parfitt, J., Sekhon, H., Thomas, G., Rassl, D.M., Rintoul, R.C., Bifulco, C., Tamakawa, R., Urba, W., Hayward, N., Timmers, H., Antenucci, A., Facciolo, F., Grazi, G., Marino, M., Merola, R., Krijger, R. de, Gimenez-Roqueplo, A.-P., Piché, A., Chevalier, S., McKercher, G., Birsoy, K., Barnett, G., Brewer, C., Farver, C., Naska, T., Pennell, N.A., Raymond, D., Schilero, C., Smolenski, K., Williams, F., Morrison, C., Borgia, J.A., Liptay, M.J., Pool, M., Seder, C.W., Junker, K., Omberg, L., Dinkin, M., Manikhas, G., Alvaro, D., Bragazzi, M.C., Cardinale, V., Carpino, G., Gaudio, E., Chesla, D., Cottingham, S., Dubina, M.,

Moiseenko, F., Dhanasekaran, R., Becker, K.-F., Janssen, K.-P., Slotta-Huspenina, J., Abdel-Rahman, M.H., Aziz, D., Bell, S., Cebulla, C.M., Davis, A., Duell, R., Elder, J.B., Hilty, J., Kumar, B., Lang, J., Lehman, N.L., Mandt, R., Nguyen, P., Pilarski, R., Rai, K., Schoenfield, L., Senecal, K., Wakely, P., Hansen, P., Lechan, R., Powers, J., Tischler, A., Grizzle, W.E., Sexton, K.C., Kastl, A., Henderson, J., Porten, S., Waldmann, J., Fassnacht, M., Asa, S.L., Schadendorf, D., Couce, M., Graefen, M., Huland, H., Sauter, G., Schlomm, T., Simon, R., Tennstedt, P., Olabode, O., Nelson, M., Bathe, O., Carroll, P.R., Chan, J.M., Disaia, P., Glenn, P., Kelley, R.K., Landen, C.N., Phillips, J., Prados, M., Simko, J., Smith-McCune, K., VandenBerg, S., Roggin, K., Fehrenbach, A., Kendler, A., Sifri, S., Steele, R., Jimeno, A., Carey, F., Forgie, I., Mannelli, M., Carney, M., Hernandez, B., Campos, B., Herold-Mende, C., Jungk, C., Unterberg, A., Deimling, A. von, Bossler, A., Galbraith, J., Jacobus, L., Knudson, M., Knutson, T., Ma, D., Milhem, M., Sigmund, R., Godwin, A.K., Madan, R., Rosenthal, H.G., Adebamowo, C., Adebamowo, S.N., Boussioutas, A., Beer, D., Giordano, T., Mes-Masson, A.-M., Saad, F., Bocklage, T., Landrum, L., Mannel, R., Moore, K., Moxley, K., Postier, R., Walker, J., Zuna, R., Feldman, M., Valdivieso, F., Dhir, R., Luketich, J., Pinero, E.M.M., Quintero-Aguilo, M., Carlotti, C.G., Santos, J.S.D., Kemp, R., Sankarankuty, A., Tirapelli, D., Catto, J., Agnew, K., Swisher, E., Creaney, J., Robinson, B., Shelley, C.S., Godwin, E.M., Kendall, S., Shipman, C., Bradford, C., Carey, T., Haddad, A., Moyer, J., Peterson, L., Prince, M., Rozek, L., Wolf, G., Bowman, R., Fong, K.M., Yang, I., Korst, R., Rathmell, W.K., Fantacone-Campbell, J.L., Hooke, J.A., Kovatich, A.J., Shriver, C.D., DiPersio, J., Drake, B., Govindan, R., Heath, S., Ley, T., Tine, B.V., Westervelt, P., Rubin, M.A., Lee, J.I., Aredes, N.D., Mariamidze, A., Stuart, J.M., Benz, C.C., Laird, P.W., 2018. Cell-of-Origin Patterns Dominate the Molecular Classification of 10,000 Tumors from 33 Types of Cancer. Cell 173, 291-304.e6. https://doi.org/10.1016/j.cell.2018.03.022

Ji, H., Ramsey, M.R., Hayes, D.N., Fan, C., McNamara, K., Kozlowski, P., Torrice, C., Wu, M.C., Shimamura, T., Perera, S.A., Liang, M.-C., Cai, D., Naumov, G.N., Bao, L., Contreras, C.M., Li, D., Chen, L., Krishnamurthy, J., Koivunen, J., Chirieac, L.R., Padera, R.F., Bronson, R.T., Lindeman, N.I., Christiani, D.C., Lin, X., Shapiro, G.I., Jänne, P.A., Johnson, B.E., Meyerson, M., Kwiatkowski, D.J., Castrillon, D.H., Bardeesy, N., Sharpless, N.E., Wong, K.-K., 2007. LKB1 modulates lung cancer differentiation and metastasis. Nature 448, 807–810. https://doi.org/10.1038/nature06030

Johnson, D.E., O'Keefe, R.A., Grandis, J.R., 2018. Targeting the IL-6/JAK/STAT3 signalling axis in cancer. Nat. Rev. Clin. Oncol. 15, 234–248. https://doi.org/10.1038/nrclinonc.2018.8

Kim, A.-R., Hu, Y., Comjean, A., Rodiger, J., Mohr, S.E., Perrimon, N., n.d. Enhanced Protein-Protein Interaction Discovery via AlphaFold-Multimer. bioRxiv 2024. https://doi.org/10.1101/2024.02.19.580970.

Kinoshita, E., Kinoshita-Kikuta, E., Takiyama, K., Koike, T., 2006. Phosphate-binding tag, a new tool to visualize phosphorylated proteins. Mol. Cell. Proteomics MCP 5, 749–757. https://doi.org/10.1074/mcp.T500024-MCP200

Kinoshita, T., 2020. Biosynthesis and biology of mammalian GPI-anchored proteins. Open Biol. 10, 190290. https://doi.org/10.1098/rsob.190290

Klionsky, D.J., Abdel-Aziz, A.K., Abdelfatah, S., Abdellatif, M., Abdoli, A., Abel, S., Abeliovich, H., Abildgaard, M.H., Abudu, Y.P., Acevedo-Arozena, A., Adamopoulos, I.E., Adeli, K., Adolph, T.E., Adornetto, A., Aflaki, E., Agam, G., Agarwal, A., Aggarwal, B.B., Agnello, M., Agostinis, P., Agrewala, J.N., Agrotis, A., Aguilar, P.V., Ahmad, S.T., Ahmed, Z.M., Ahumada-Castro, U., Aits, S., Aizawa, S., Akkoc, Y., Akoumianaki, T., Akpinar, H.A., Al-Abd, A.M., Al-Akra, L., Al-Gharaibeh, A., Alaoui-Jamali, M.A., Alberti, S., Alcocer-Gómez, E., Alessandri, C., Ali, M., Alim Al-Bari, M.A., Aliwaini, S., Alizadeh, J., Almacellas, E., Almasan, A., Alonso, A., Alonso, G.D., Altan-Bonnet, N., Altieri, D.C., Álvarez, É.M.C., Alves, S., Alves da Costa, C., Alzaharna, M.M., Amadio, M., Amantini, C., Amaral, C., Ambrosio, S., Amer, A.O., Ammanathan, V., An, Z., Andersen, S.U., Andrabi, S.A., Andrade-Silva, M., Andres, A.M., Angelini, S., Ann, D., Anozie, U.C., Ansari, M.Y., Antas, P., Antebi, A., Antón, Z., Anwar, T., Apetoh, L., Apostolova, N., Araki, T., Araki, Y., Arasaki, K., Araújo, W.L., Araya, J., Arden, C., Arévalo, M.-A., Arguelles, S., Arias, E., Arikkath, J., Arimoto, H., Ariosa, A.R., Armstrong-James, D., Arnauné-Pelloquin, L., Aroca, A., Arroyo, D.S., Arsov, I., Artero, R., Asaro, D.M.L., Aschner, M., Ashrafizadeh, M., Ashur-Fabian, O., Atanasov, A.G., Au, A.K., Auberger, P., Auner, H.W., Aurelian, L., Autelli, R., Avagliano, L., Ávalos, Y., Aveic, S., Aveleira, C.A., Avin-Wittenberg, T., Aydin, Y., Ayton, S., Ayyadevara, S., Azzopardi, M., Baba, M., Backer, J.M., Backues, S.K., Bae, D.-H., Bae, O.-N., Bae, S.H., Baehrecke, E.H., Baek, A., Baek, S.-H., Baek, S.H., Bagetta, G., Bagniewska-Zadworna, A., Bai, H., Bai, J., Bai, X., Bai, Y., Bairagi, N., Baksi, S., Balbi, T., Baldari, C.T., Balduini, W., Ballabio, A., Ballester, M., Balazadeh, S., Balzan, R., Bandopadhyay, R., Banerjee, Sreeparna, Banerjee, Sulagna, Bánréti, Á., Bao, Y., Baptista, M.S., Baracca, A., Barbati, C., Bargiela, A., Barilà, D., Barlow, P.G., Barmada, S.J., Barreiro, E., Barreto, G.E., Bartek, J., Bartel, B., Bartolome, A., Barve, G.R., Basagoudanavar, S.H., Bassham, D.C., Bast, R.C., Basu, A., Batoko, H., Batten, I., Baulieu, E.E., Baumgarner, B.L., Bayry, J., Beale, R., Beau, I., Beaumatin, F., Bechara, L.R.G., Beck, G.R., Beers, M.F., Begun, J., Behrends, C., Behrens, G.M.N., Bei, R., Bejarano, E., Bel, S., Behl, C., Belaid, A., Belgareh-Touzé, N., Bellarosa, C., Belleudi, F., Belló Pérez, M., Bello-Morales, R., Beltran, J.S. de O., Beltran, S., Benbrook, D.M., Bendorius, M., Benitez, B.A., Benito-Cuesta, I., Bensalem, J., Berchtold, M.W., Berezowska, S., Bergamaschi, D., Bergami, M., Bergmann, A., Berliocchi, L., Berlioz-Torrent, C., Bernard, A., Berthoux, L., Besirli, C.G., Besteiro, S., Betin, V.M., Beyaert, R., Bezbradica, J.S., Bhaskar, K., Bhatia-Kissova, I., Bhattacharya, R., Bhattacharya, S., Bhattacharyya, S., Bhuiyan, M.S., Bhutia, S.K., Bi, L., Bi, X., Biden, T.J., Bijian, K., Billes, V.A., Binart, N., Bincoletto, C., Birgisdottir, A.B., Bjorkoy, G., Blanco, G., Blas-Garcia, A., Blasiak, J., Blomgran, R., Blomgren, K., Blum, J.S., Boada-Romero, E., Boban, M., Boesze-Battaglia, K., Boeuf, P., Boland, B., Bomont, P., Bonaldo, P., Bonam, S.R., Bonfili, L., Bonifacino, J.S., Boone, B.A., Bootman, M.D., Bordi, M., Borner, C., Bornhauser, B.C., Borthakur, G., Bosch, J., Bose, S., Botana, L.M., Botas, J., Boulanger, C.M., Boulton, M.E., Bourdenx, M., Bourgeois, B., Bourke, N.M., Bousquet, G., Boya, P., Bozhkov, P.V., Bozi, L.H.M.,

Bozkurt, T.O., Brackney, D.E., Brandts, C.H., Braun, R.J., Braus, G.H., Bravo-Sagua, R., Bravo-San Pedro, J.M., Brest, P., Bringer, M.-A., Briones-Herrera, A., Broaddus, V.C., Brodersen, P., Brodsky, J.L., Brody, S.L., Bronson, P.G., Bronstein, J.M., Brown, C.N., Brown, R.E., Brum, P.C., Brumell, J.H., Brunetti-Pierri, N., Bruno, D., Bryson-Richardson, R.J., Bucci, C., Buchrieser, C., Bueno, M., Buitrago-Molina, L.E., Buraschi, S., Buch, S., Buchan, J.R., Buckingham, E.M., Budak, H., Budini, M., Bultynck, G., Burada, F., Burgoyne, J.R., Burón, M.I., Bustos, V., Büttner, S., Butturini, E., Byrd, A., Cabas, I., Cabrera-Benitez, S., Cadwell, K., Cai, J., Cai, L., Cai, Q., Cairó, M., Calbet, J.A., Caldwell, G.A., Caldwell, K.A., Call, J.A., Calvani, R., Calvo, A.C., Calvo-Rubio Barrera, M., Camara, N.O., Camonis, J.H., Camougrand, N., Campanella, M., Campbell, E.M., Campbell-Valois, F.-X., Campello, S., Campesi, I., Campos, J.C., Camuzard, O., Cancino, J., Candido de Almeida, D., Canesi, L., Caniggia, I., Canonico, B., Cantí, C., Cao, B., Caraglia, M., Caramés, B., Carchman, E.H., Cardenal-Muñoz, E., Cardenas, C., Cardenas, L., Cardoso, S.M., Carew, J.S., Carle, G.F., Carleton, G., Carloni, S., Carmona-Gutierrez, D., Carneiro, L.A., Carnevali, O., Carosi, J.M., Carra, S., Carrier, A., Carrier, L., Carroll, B., Carter, A.B., Carvalho, A.N., Casanova, M., Casas, C., Casas, J., Cassioli, C., Castillo, E.F., Castillo, K., Castillo-Lluva, S., Castoldi, F., Castori, M., Castro, A.F., Castro-Caldas, M., Castro-Hernandez, J., Castro-Obregon, S., Catz, S.D., Cavadas, C., Cavaliere, F., Cavallini, G., Cavinato, M., Cayuela, M.L., Cebollada Rica, P., Cecarini, V., Cecconi, F., Cechowska-Pasko, M., Cenci, S., Ceperuelo-Mallafré, V., Cerqueira, J.J., Cerutti, J.M., Cervia, D., Cetintas, V.B., Cetrullo, S., Chae, H.-J., Chagin, A.S., Chai, C.-Y., Chakrabarti, G., Chakrabarti, O., Chakraborty, Tapas, Chakraborty, Trinad, Chami, M., Chamilos, G., Chan, D.W., Chan, E.Y.W., Chan, E.D., Chan, H.Y.E., Chan, H.H., Chan, H., Chan, M.T.V., Chan, Y.S., Chandra, P.K., Chang, C.-P., Chang, C., Chang, H.-C., Chang, K., Chao, J., Chapman, T., Charlet-Berguerand, N., Chatterjee, S., Chaube, S.K., Chaudhary, A., Chauhan, S., Chaum, E., Checler, F., Cheetham, M.E., Chen, C.-S., Chen, G.-C., Chen, J.-F., Chen, L.L., Chen, Leilei, Chen, Lin, Chen, M., Chen, M.-K., Chen, N., Chen, Q., Chen, R.-H., Chen, S., Chen, Wei, Chen, Weiqiang, Chen, X.-M., Chen, X.-W., Chen, X., Chen, Yan, Chen, Y.-G., Chen, Yingyu, Chen, Yongqiang, Chen, Y.-J., Chen, Y.-Q., Chen, Z.S., Chen, Zhi, Chen, Z.-H., Chen, Z.J., Chen, Zhixiang, Cheng, H., Cheng, J., Cheng, S.-Y., Cheng, W., Cheng, X., Cheng, X.-T., Cheng, Y., Cheng, Z., Chen, Zhong, Cheong, H., Cheong, J.K., Chernyak, B.V., Cherry, S., Cheung, C.F.R., Cheung, C.H.A., Cheung, K.-H., Chevet, E., Chi, R.J., Chiang, A.K.S., Chiaradonna, F., Chiarelli, R., Chiariello, M., Chica, N., Chiocca, S., Chiong, M., Chiou, S.-H., Chiramel, A.I., Chiurchiù, V., Cho, D.-H., Choe, S.-K., Choi, A.M.K., Choi, M.E., Choudhury, K.R., Chow, N.S., Chu, C.T., Chua, J.P., Chua, J.J.E., Chung, H., Chung, K.P., Chung, S., Chung, S.-H., Chung, Y.-L., Cianfanelli, V., Ciechomska, I.A., Cifuentes, M., Cinque, L., Cirak, S., Cirone, M., Clague, M.J., Clarke, R., Clementi, E., Coccia, E.M., Codogno, P., Cohen, E., Cohen, M.M., Colasanti, T., Colasuonno, F., Colbert, R.A., Colell, A., Čolić, M., Coll, N.S., Collins, M.O., Colombo, M.I., Colón-Ramos, D.A., Combaret, L., Comincini, S., Cominetti, M.R., Consiglio, A., Conte, A., Conti, F., Contu, V.R., Cookson, M.R., Coombs, K.M., Coppens, I., Corasaniti, M.T., Corkery, D.P., Cordes, N., Cortese, K., Costa, M. do C.,

Costantino, S., Costelli, P., Coto-Montes, A., Crack, P.J., Crespo, J.L., Criollo, A., Crippa, V., Cristofani, R., Csizmadia, T., Cuadrado, A., Cui, B., Cui, J., Cui, Yixian, Cui, Yong, Culetto, E., Cumino, A.C., Cybulsky, A.V., Czaja, M.J., Czuczwar, S.J., D'Adamo, S., D'Amelio, M., D'Arcangelo, D., D'Lugos, A.C., D'Orazi, G., da Silva, J.A., Dafsari, H.S., Dagda, R.K., Dagdas, Y., Daglia, M., Dai, X., Dai, Yun, Dai, Yuyuan, Dal Col, J., Dalhaimer, P., Dalla Valle, L., Dallenga, T., Dalmasso, G., Damme, M., Dando, I., Dantuma, N.P., Darling, A.L., Das, H., Dasarathy, S., Dasari, S.K., Dash, S., Daumke, O., Dauphinee, A.N., Davies, J.S., Dávila, V.A., Davis, R.J., Davis, T., Dayalan Naidu, S., De Amicis, F., De Bosscher, K., De Felice, F., De Franceschi, L., De Leonibus, C., de Mattos Barbosa, M.G., De Meyer, G.R.Y., De Milito, A., De Nunzio, C., De Palma, C., De Santi, M., De Virgilio, C., De Zio, D., Debnath, J., DeBosch, B.J., Decuypere, J.-P., Deehan, M.A., Deflorian, G., DeGregori, J., Dehay, B., Del Rio, G., Delaney, J.R., Delbridge, L.M.D., Delorme-Axford, E., Delpino, M.V., Demarchi, F., Dembitz, V., Demers, N.D., Deng, H., Deng, Z., Dengjel, J., Dent, P., Denton, D., DePamphilis, M.L., Der, C.J., Deretic, V., Descoteaux, A., Devis, L., Devkota, S., Devuyst, O., Dewson, G., Dharmasivam, M., Dhiman, R., di Bernardo, D., Di Cristina, M., Di Domenico, F., Di Fazio, P., Di Fonzo, A., Di Guardo, G., Di Guglielmo, G.M., Di Leo, L., Di Malta, C., Di Nardo, A., Di Rienzo, M., Di Sano, F., Diallinas, G., Diao, J., Diaz-Araya, G., Díaz-Laviada, I., Dickinson, J.M., Diederich, M., Dieudé, M., Dikic, I., Ding, S., Ding, W.-X., Dini, L., Dinić, J., Dinic, M., Dinkova-Kostova, A.T., Dionne, M.S., Distler, J.H.W., Diwan, A., Dixon, I.M.C., Djavaheri-Mergny, M., Dobrinski, I., Dobrovinskaya, O., Dobrowolski, R., Dobson, R.C.J., Đokić, J., Dokmeci Emre, S., Donadelli, M., Dong, B., Dong, X., Dong, Z., Dorn Ii, G.W., Dotsch, V., Dou, H., Dou, J., Dowaidar, M., Dridi, S., Drucker, L., Du, A., Du, C., Du, G., Du, H.-N., Du, L.-L., du Toit, A., Duan, S.-B., Duan, X., Duarte, S.P., Dubrovska, A., Dunlop, E.A., Dupont, N., Durán, R.V., Dwarakanath, B.S., Dyshlovoy, S.A., Ebrahimi-Fakhari, D., Eckhart, L., Edelstein, C.L., Efferth, T., Eftekharpour, E., Eichinger, L., Eid, N., Eisenberg, T., Eissa, N.T., Eissa, S., Ejarque, M., El Andaloussi, A., El-Hage, N., El-Naggar, S., Eleuteri, A.M., El-Shafey, E.S., Elgendy, M., Eliopoulos, A.G., Elizalde, M.M., Elks, P.M., Elsasser, H.-P., Elsherbiny, E.S., Emerling, B.M., Emre, N.C.T., Eng, C.H., Engedal, N., Engelbrecht, A.-M., Engelsen, A.S.T., Enserink, J.M., Escalante, R., Esclatine, A., Escobar-Henriques, M., Eskelinen, E.-L., Espert, L., Eusebio, M.-O., Fabrias, G., Fabrizi, C., Facchiano, A., Facchiano, F., Fadeel, B., Fader, C., Faesen, A.C., Fairlie, W.D., Falcó, A., Falkenburger, B.H., Fan, D., Fan, J., Fan, Y., Fang, E.F., Fang, Yanshan, Fang, Yognqi, Fanto, M., Farfel-Becker, T., Faure, M., Fazeli, G., Fedele, A.O., Feldman, A.M., Feng, D., Feng, J., Feng, L., Feng, Yibin, Feng, Yuchen, Feng, W., Fenz Araujo, T., Ferguson, T.A., Fernández, Á.F., Fernandez-Checa, J.C., Fernández-Veledo, S., Fernie, A.R., Ferrante, A.W., Ferraresi, A., Ferrari, M.F., Ferreira, J.C.B., Ferro-Novick, S., Figueras, A., Filadi, R., Filigheddu, N., Filippi-Chiela, E., Filomeni, G., Fimia, G.M., Fineschi, V., Finetti, F., Finkbeiner, S., Fisher, E.A., Fisher, P.B., Flamigni, F., Fliesler, S.J., Flo, T.H., Florance, I., Florey, O., Florio, T., Fodor, E., Follo, C., Fon, E.A., Forlino, A., Fornai, F., Fortini, P., Fracassi, A., Fraldi, A., Franco, B., Franco, R., Franconi, F., Frankel, L.B., Friedman, S.L., Fröhlich, L.F., Frühbeck, G., Fuentes, J.M., Fujiki, Y., Fujita, N., Fujiwara, Y., Fukuda, M., Fulda, S.,

Furic, L., Furuya, N., Fusco, C., Gack, M.U., Gaffke, L., Galadari, S., Galasso, A., Galindo, M.F., Gallolu Kankanamalage, S., Galluzzi, L., Galy, V., Gammoh, N., Gan, B., Ganley, I.G., Gao, F., Gao, H., Gao, M., Gao, P., Gao, S.-J., Gao, W., Gao, X., Garcera, A., Garcia, M.N., Garcia, V.E., García-Del Portillo, F., Garcia-Escudero, V., Garcia-Garcia, A., Garcia-Macia, M., García-Moreno, D., Garcia-Ruiz, C., García-Sanz, P., Garg, A.D., Gargini, R., Garofalo, T., Garry, R.F., Gassen, N.C., Gatica, D., Ge, L., Ge, W., Geiss-Friedlander, R., Gelfi, C., Genschik, P., Gentle, I.E., Gerbino, V., Gerhardt, C., Germain, K., Germain, M., Gewirtz, D.A., Ghasemipour Afshar, E., Ghavami, S., Ghigo, A., Ghosh, M., Giamas, G., Giampietri, C., Giatromanolaki, A., Gibson, G.E., Gibson, S.B., Ginet, V., Giniger, E., Giorgi, C., Girao, H., Girardin, S.E., Giridharan, M., Giuliano, S., Giulivi, C., Giuriato, S., Giustiniani, J., Gluschko, A., Goder, V., Goginashvili, A., Golab, J., Goldstone, D.C., Golebiewska, A., Gomes, L.R., Gomez, R., Gómez-Sánchez, R., Gomez-Puerto, M.C., Gomez-Sintes, R., Gong, Q., Goni, F.M., González-Gallego, J., Gonzalez-Hernandez, T., Gonzalez-Polo, R.A., Gonzalez-Reyes, J.A., González-Rodríguez, P., Goping, I.S., Gorbatyuk, M.S., Gorbunov, N.V., Görgülü, K., Gorojod, R.M., Gorski, S.M., Goruppi, S., Gotor, C., Gottlieb, R.A., Gozes, I., Gozuacik, D., Graef, M., Gräler, M.H., Granatiero, V., Grasso, D., Gray, J.P., Green, D.R., Greenhough, A., Gregory, S.L., Griffin, E.F., Grinstaff, M.W., Gros, F., Grose, C., Gross, A.S., Gruber, F., Grumati, P., Grune, T., Gu, X., Guan, J.-L., Guardia, C.M., Guda, K., Guerra, F., Guerri, C., Guha, P., Guillén, C., Gujar, S., Gukovskaya, A., Gukovsky, I., Gunst, J., Günther, A., Guntur, A.R., Guo, Chuanyong, Guo, Chun, Guo, H., Guo, L.-W., Guo, M., Gupta, P., Gupta, S.K., Gupta, S., Gupta, V.B., Gupta, V., Gustafsson, A.B., Gutterman, D.D., H B, R., Haapasalo, A., Haber, J.E., Hać, A., Hadano, S., Hafrén, A.J., Haidar, M., Hall, B.S., Halldén, G., Hamacher-Brady, A., Hamann, A., Hamasaki, M., Han, W., Hansen, M., Hanson, P.I., Hao, Z., Harada, M., Harhaji-Trajkovic, L., Hariharan, N., Haroon, N., Harris, J., Hasegawa, T., Hasima Nagoor, N., Haspel, J.A., Haucke, V., Hawkins, W.D., Hay, B.A., Haynes, C.M., Hayrabedyan, S.B., Hays, T.S., He, C., He, Q., He, R.-R., He, Y.-W., He, Y.-Y., Heakal, Y., Heberle, A.M., Hejtmancik, J.F., Helgason, G.V., Henkel, V., Herb, M., Hergovich, A., Herman-Antosiewicz, A., Hernández, A., Hernandez, C., Hernandez-Diaz, S., Hernandez-Gea, V., Herpin, A., Herreros, J., Hervás, J.H., Hesselson, D., Hetz, C., Heussler, V.T., Higuchi, Y., Hilfiker, S., Hill, J.A., Hlavacek, W.S., Ho, E.A., Ho, I.H.T., Ho, P.W.-L., Ho, S.-L., Ho, W.Y., Hobbs, G.A., Hochstrasser, M., Hoet, P.H.M., Hofius, D., Hofman, P., Höhn, A., Holmberg, C.I., Hombrebueno, J.R., Yi-Ren Hong, C.-W.H., Hooper, L.V., Hoppe, T., Horos, R., Hoshida, Y., Hsin, I.-L., Hsu, H.-Y., Hu, B., Hu, D., Hu, L.-F., Hu, M.C., Hu, R., Hu, W., Hu, Y.-C., Hu, Z.-W., Hua, F., Hua, J., Hua, Y., Huan, C., Huang, Canhua, Huang, Chuanshu, Huang, Chuanxin, Huang, Chunling, Huang, H., Huang, K., Huang, M.L.H., Huang, R., Huang, S., Huang, T., Huang, X., Huang, Y.J., Huber, T.B., Hubert, V., Hubner, C.A., Hughes, S.M., Hughes, W.E., Humbert, M., Hummer, G., Hurley, J.H., Hussain, Sabah, Hussain, Salik, Hussey, P.J., Hutabarat, M., Hwang, H.-Y., Hwang, S., Ieni, A., Ikeda, F., Imagawa, Y., Imai, Y., Imbriano, C., Imoto, M., Inman, D.M., Inoki, K., Iovanna, J., Iozzo, R.V., Ippolito, G., Irazoqui, J.E., Iribarren, P., Ishaq, M., Ishikawa, M., Ishimwe, N., Isidoro, C., Ismail, N., Issazadeh-Navikas, S., Itakura, E., Ito, D., Ivankovic, D., Ivanova, S.,

Iyer, A.K.V., Izquierdo, J.M., Izumi, M., Jäättelä, M., Jabir, M.S., Jackson, W.T., Jacobo-Herrera, N., Jacomin, A.-C., Jacquin, E., Jadiya, P., Jaeschke, H., Jagannath, C., Jakobi, A.J., Jakobsson, J., Janji, B., Jansen-Dürr, P., Jansson, P.J., Jantsch, J., Januszewski, S., Jassey, A., Jean, S., Jeltsch-David, H., Jendelova, P., Jenny, A., Jensen, T.E., Jessen, N., Jewell, J.L., Ji, J., Jia, L., Jia, R., Jiang, L., Jiang, Q., Jiang, R., Jiang, T., Jiang, X., Jiang, Y., Jimenez-Sanchez, M., Jin, E.-J., Jin, F., Jin, H., Jin, Li, Jin, Luqi, Jin, M., Jin, S., Jo, E.-K., Joffre, C., Johansen, T., Johnson, G.V.W., Johnston, S.A., Jokitalo, E., Jolly, M.K., Joosten, L.A.B., Jordan, J., Joseph, B., Ju, D., Ju, J.-S., Ju, J., Juárez, E., Judith, D., Juhász, G., Jun, Y., Jung, C.H., Jung, S.-C., Jung, Y.K., Jungbluth, H., Jungverdorben, J., Just, S., Kaarniranta, K., Kaasik, A., Kabuta, T., Kaganovich, D., Kahana, A., Kain, R., Kajimura, S., Kalamvoki, M., Kalia, M., Kalinowski, D.S., Kaludercic, N., Kalvari, I., Kaminska, J., Kaminskyy, V.O., Kanamori, H., Kanasaki, K., Kang, C., Kang, R., Kang, S.S., Kaniyappan, S., Kanki, T., Kanneganti, T.-D., Kanthasamy, A.G., Kanthasamy, A., Kantorow, M., Kapuy, O., Karamouzis, M.V., Karim, M.R., Karmakar, P., Katare, R.G., Kato, M., Kaufmann, S.H.E., Kauppinen, A., Kaushal, G.P., Kaushik, S., Kawasaki, K., Kazan, K., Ke, P.-Y., Keating, D.J., Keber, U., Kehrl, J.H., Keller, K.E., Keller, C.W., Kemper, J.K., Kenific, C.M., Kepp, O., Kermorgant, S., Kern, A., Ketteler, R., Keulers, T.G., Khalfin, B., Khalil, H., Khambu, B., Khan, S.Y., Khandelwal, V.K.M., Khandia, R., Kho, W., Khobrekar, N.V., Khuansuwan, S., Khundadze, M., Killackey, S.A., Kim, D., Kim, D.R., Kim, D.-H., Kim, D.-E., Kim, E.Y., Kim, E.-K., Kim, H.-R., Kim, H.-S., Hyung-Ryong Kim, null, Kim, Jeong Hun, Kim, J.K., Kim, J.-H., Kim, J., Kim, Ju Hwan, Kim, K.I., Kim, P.K., Kim, S.-J., Kimball, S.R., Kimchi, A., Kimmelman, A.C., Kimura, T., King, M.A., Kinghorn, K.J., Kinsey, C.G., Kirkin, V., Kirshenbaum, L.A., Kiselev, S.L., Kishi, S., Kitamoto, K., Kitaoka, Y., Kitazato, K., Kitsis, R.N., Kittler, J.T., Kjaerulff, O., Klein, P.S., Klopstock, T., Klucken, J., Knævelsrud, H., Knorr, R.L., Ko, B.C.B., Ko, F., Ko, J.-L., Kobayashi, H., Kobayashi, S., Koch, I., Koch, J.C., Koenig, U., Kögel, D., Koh, Y.H., Koike, M., Kohlwein, S.D., Kocaturk, N.M., Komatsu, M., König, J., Kono, T., Kopp, B.T., Korcsmaros, T., Korkmaz, G., Korolchuk, V.I., Korsnes, M.S., Koskela, A., Kota, J., Kotake, Y., Kotler, M.L., Kou, Y., Koukourakis, M.I., Koustas, E., Kovacs, A.L., Kovács, T., Koya, D., Kozako, T., Kraft, C., Krainc, D., Krämer, H., Krasnodembskaya, A.D., Kretz-Remy, C., Kroemer, G., Ktistakis, N.T., Kuchitsu, K., Kuenen, S., Kuerschner, L., Kukar, T., Kumar, Ajay, Kumar, Ashok, Kumar, Deepak, Kumar, Dhiraj, Kumar, S., Kume, S., Kumsta, C., Kundu, C.N., Kundu, M., Kunnumakkara, A.B., Kurgan, L., Kutateladze, T.G., Kutlu, O., Kwak, S., Kwon, H.J., Kwon, T.K., Kwon, Y.T., Kyrmizi, I., La Spada, A., Labonté, P., Ladoire, S., Laface, I., Lafont, F., Lagace, D.C., Lahiri, V., Lai, Z., Laird, A.S., Lakkaraju, A., Lamark, T., Lan, S.-H., Landajuela, A., Lane, D.J.R., Lane, J.D., Lang, C.H., Lange, C., Langel, Ü., Langer, R., Lapaquette, P., Laporte, J., LaRusso, N.F., Lastres-Becker, I., Lau, W.C.Y., Laurie, G.W., Lavandero, S., Law, B.Y.K., Law, H.K.-W., Layfield, R., Le, W., Le Stunff, H., Leary, A.Y., Lebrun, J.-J., Leck, L.Y.W., Leduc-Gaudet, J.-P., Lee, C., Lee, C.-P., Lee, D.-H., Lee, E.B., Lee, E.F., Lee, G.M., Lee, H.-J., Lee, H.K., Lee, J.M., Lee, J.S., Lee, J.-A., Lee, J.-Y., Lee, J.H., Lee, M., Lee, M.G., Lee, M.J., Lee, M.-S., Lee, Sang Yoon, Lee, S.-J., Lee, Stella Y., Lee, S.B., Lee, W.H., Lee, Y.-R., Lee, Y.-H., Lee, Y., Lefebvre, C., Legouis, R., Lei, Y.L., Lei, Y.,

Leikin, S., Leitinger, G., Lemus, L., Leng, S., Lenoir, O., Lenz, G., Lenz, H.J., Lenzi, P., León, Y., Leopoldino, A.M., Leschczyk, C., Leskelä, S., Letellier, E., Leung, C.-T., Leung, P.S., Leventhal, J.S., Levine, B., Lewis, P.A., Ley, K., Li, B., Li, D.-Q., Li, Jianming, Li, Jing, Li, Jiong, Li, K., Li, L., Li, Mei, Li, Min, Li, Min, Li, Ming, Li, Mingchuan, Li, P.-L., Li, M.-Q., Li, Q., Li, S., Li, T., Li, Wei, Li, Wenming, Li, X., Li, Y.-P., Li, Y., Li, Zhiqiang, Li, Zhiyong, Li, Zhiyuan, Lian, J., Liang, C., Liang, Q., Liang, W., Liang, Yongheng, Liang, YongTian, Liao, G., Liao, L., Liao, M., Liao, Y.-F., Librizzi, M., Lie, P.P.Y., Lilly, M.A., Lim, H.J., Lima, T.R.R., Limana, F., Lin, C., Lin, C.-W., Lin, D.-S., Lin, F.-C., Lin, J.D., Lin, K.M., Lin, K.-H., Lin, L.-T., Lin, P.-H., Lin, Q., Lin, S., Lin, S.-J., Lin, W., Lin, X., Lin, Y.-X., Lin, Y.-S., Linden, R., Lindner, P., Ling, S.-C., Lingor, P., Linnemann, A.K., Liou, Y.-C., Lipinski, M.M., Lipovšek, S., Lira, V.A., Lisiak, N., Liton, P.B., Liu, C., Liu, C.-H., Liu, C.-F., Liu, C.H., Liu, F., Liu, Hao, Liu, H.-S., Liu, H.-F., Liu, Huifang, Liu, Jia, Liu, Jing, Liu, Julia, Liu, Leyuan, Liu, Longhua, Liu, M., Liu, Q., Liu, Wei, Liu, Wende, Liu, X.-H., Liu, Xiaodong, Liu, Xingguo, Liu, Xu, Liu, Xuedong, Liu, Yanfen, Liu, Yang, Liu, Yang, Liu, Yueyang, Liu, Yule, Livingston, J.A., Lizard, G., Lizcano, J.M., Ljubojevic-Holzer, S., LLeonart, M.E., Llobet-Navàs, D., Llorente, A., Lo, C.H., Lobato-Márquez, D., Long, Q., Long, Y.C., Loos, B., Loos, J.A., López, M.G., López-Doménech, G., López-Guerrero, J.A., López-Jiménez, A.T., López-Pérez, Ó., López-Valero, I., Lorenowicz, M.J., Lorente, M., Lorincz, P., Lossi, L., Lotersztajn, S., Lovat, P.E., Lovell, J.F., Lovy, A., Lőw, P., Lu, G., Lu, H., Lu, J.-H., Lu, J.-J., Lu, M., Lu, S., Luciani, A., Lucocq, J.M., Ludovico, P., Luftig, M.A., Luhr, M., Luis-Ravelo, D., Lum, J.J., Luna-Dulcey, L., Lund, A.H., Lund, V.K., Lünemann, J.D., Lüningschrör, P., Luo, H., Luo, R., Luo, S., Luo, Z., Luparello, C., Lüscher, B., Luu, L., Lyakhovich, A., Lyamzaev, K.G., Lystad, A.H., Lytvynchuk, L., Ma, A.C., Ma, C., Ma, M., Ma, N.-F., Ma, Q.-H., Ma, X., Ma, Y., Ma, Z., MacDougald, O.A., Macian, F., MacIntosh, G.C., MacKeigan, J.P., Macleod, K.F., Maday, S., Madeo, F., Madesh, M., Madl, T., Madrigal-Matute, J., Maeda, A., Maejima, Y., Magarinos, M., Mahavadi, P., Maiani, E., Maiese, K., Maiti, P., Maiuri, M.C., Majello, B., Major, M.B., Makareeva, E., Malik, F., Mallilankaraman, K., Malorni, W., Maloyan, A., Mammadova, N., Man, G.C.W., Manai, F., Mancias, J.D., Mandelkow, E.-M., Mandell, M.A., Manfredi, A.A., Manjili, M.H., Manjithaya, R., Manque, P., Manshian, B.B., Manzano, R., Manzoni, C., Mao, K., Marchese, C., Marchetti, S., Marconi, A.M., Marcucci, F., Mardente, S., Mareninova, O.A., Margeta, M., Mari, M., Marinelli, S., Marinelli, O., Mariño, G., Mariotto, S., Marshall, R.S., Marten, M.R., Martens, S., Martin, A.P.J., Martin, K.R., Martin, Sara, Martin, Shaun, Martín-Segura, A., Martín-Acebes, M.A., Martin-Burriel, I., Martin-Rincon, M., Martin-Sanz, P., Martina, J.A., Martinet, W., Martinez, Aitor, Martinez, Ana, Martinez, J., Martinez Velazquez, M., Martinez-Lopez, N., Martinez-Vicente, M., Martins, D.O., Martins, J.O., Martins, W.K., Martins-Marques, T., Marzetti, E., Masaldan, S., Masclaux-Daubresse, C., Mashek, D.G., Massa, V., Massieu, L., Masson, G.R., Masuelli, L., Masyuk, A.I., Masyuk, T.V., Matarrese, P., Matheu, A., Matoba, S., Matsuzaki, S., Mattar, P., Matte, A., Mattoscio, D., Mauriz, J.L., Mauthe, M., Mauvezin, C., Maverakis, E., Maycotte, P., Mayer, J., Mazzoccoli, G., Mazzoni, C., Mazzulli, J.R., McCarty, N., McDonald, C., McGill, M.R., McKenna, S.L., McLaughlin, B., McLoughlin, F., McNiven, M.A., McWilliams, T.G., Mechta-Grigoriou,

F., Medeiros, T.C., Medina, D.L., Megeney, L.A., Megyeri, K., Mehrpour, M., Mehta, J.L., Meijer, A.J., Meijer, A.H., Mejlvang, J., Meléndez, A., Melk, A., Memisoglu, G., Mendes, A.F., Meng, D., Meng, F., Meng, T., Menna-Barreto, R., Menon, M.B., Mercer, C., Mercier, A.E., Mergny, J.-L., Merighi, A., Merkley, S.D., Merla, G., Meske, V., Mestre, A.C., Metur, S.P., Meyer, C., Meyer, H., Mi, W., Mialet-Perez, J., Miao, J., Micale, L., Miki, Y., Milan, E., Milczarek, M., Miller, D.L., Miller, S.I., Miller, S., Millward, S.W., Milosevic, I., Minina, E.A., Mirzaei, H., Mirzaei, H.R., Mirzaei, M., Mishra, A., Mishra, N., Mishra, P.K., Misirkic Marjanovic, M., Misasi, R., Misra, A., Misso, G., Mitchell, C., Mitou, G., Miura, T., Miyamoto, S., Miyazaki, Makoto, Miyazaki, Mitsunori, Miyazaki, T., Miyazawa, K., Mizushima, N., Mogensen, T.H., Mograbi, B., Mohammadinejad, R., Mohamud, Y., Mohanty, A., Mohapatra, S., Möhlmann, T., Mohmmed, A., Moles, A., Moley, K.H., Molinari, M., Mollace, V., Møller, A.B., Mollereau, B., Mollinedo, F., Montagna, C., Monteiro, M.J., Montella, A., Montes, L.R., Montico, B., Mony, V.K., Monzio Compagnoni, G., Moore, M.N., Moosavi, M.A., Mora, A.L., Mora, M., Morales-Alamo, D., Moratalla, R., Moreira, P.I., Morelli, E., Moreno, S., Moreno-Blas, D., Moresi, V., Morga, B., Morgan, A.H., Morin, F., Morishita, H., Moritz, O.L., Moriyama, M., Moriyasu, Y., Morleo, M., Morselli, E., Moruno-Manchon, J.F., Moscat, J., Mostowy, S., Motori, E., Moura, A.F., Moustaid-Moussa, N., Mrakovcic, M., Muciño-Hernández, G., Mukherjee, A., Mukhopadhyay, S., Mulcahy Levy, J.M., Mulero, V., Muller, S., Münch, C., Munjal, A., Munoz-Canoves, P., Muñoz-Galdeano, T., Münz, C., Murakawa, T., Muratori, C., Murphy, B.M., Murphy, J.P., Murthy, A., Myöhänen, T.T., Mysorekar, I.U., Mytych, J., Nabavi, S.M., Nabissi, M., Nagy, P., Nah, J., Nahimana, A., Nakagawa, I., Nakamura, K., Nakatogawa, H., Nandi, S.S., Nanjundan, M., Nanni, M., Napolitano, G., Nardacci, R., Narita, M., Nassif, M., Nathan, I., Natsumeda, M., Naude, R.J., Naumann, C., Naveiras, O., Navid, F., Nawrocki, S.T., Nazarko, T.Y., Nazio, F., Negoita, F., Neill, T., Neisch, A.L., Neri, L.M., Netea, M.G., Neubert, P., Neufeld, T.P., Neumann, D., Neutzner, A., Newton, P.T., Ney, P.A., Nezis, I.P., Ng, C.C.W., Ng, T.B., Nguyen, H.T.T., Nguyen, L.T., Ni, H.-M., Ní Cheallaigh, C., Ni, Z., Nicolao, M.C., Nicoli, F., Nieto-Diaz, M., Nilsson, P., Ning, S., Niranjan, R., Nishimune, H., Niso-Santano, M., Nixon, R.A., Nobili, A., Nobrega, C., Noda, T., Nogueira-Recalde, U., Nolan, T.M., Nombela, I., Novak, I., Novoa, B., Nozawa, T., Nukina, N., Nussbaum-Krammer, C., Nylandsted, J., O'Donovan, T.R., O'Leary, S.M., O'Rourke, E.J., O'Sullivan, M.P., O'Sullivan, T.E., Oddo, S., Oehme, I., Ogawa, M., Ogier-Denis, E., Ogmundsdottir, M.H., Ogretmen, B., Oh, G.T., Oh, S.-H., Oh, Y.J., Ohama, T., Ohashi, Y., Ohmuraya, M., Oikonomou, V., Ojha, R., Okamoto, K., Okazawa, H., Oku, M., Oliván, S., Oliveira, J.M.A., Ollmann, M., Olzmann, J.A., Omari, S., Omary, M.B., Önal, G., Ondrej, M., Ong, S.-B., Ong, S.-G., Onnis, A., Orellana, J.A., Orellana-Muñoz, S., Ortega-Villaizan, M.D.M., Ortiz-Gonzalez, X.R., Ortona, E., Osiewacz, H.D., Osman, A.-H.K., Osta, R., Otegui, M.S., Otsu, K., Ott, C., Ottobrini, L., Ou, J.-H.J., Outeiro, T.F., Oynebraten, I., Ozturk, M., Pagès, G., Pahari, S., Pajares, M., Pajvani, U.B., Pal, R., Paladino, S., Pallet, N., Palmieri, M., Palmisano, G., Palumbo, C., Pampaloni, F., Pan, L., Pan, Q., Pan, W., Pan, X., Panasyuk, G., Pandey, R., Pandey, U.B., Pandya, V., Paneni, F., Pang, S.Y., Panzarini, E., Papademetrio, D.L., Papaleo, E., Papinski, D., Papp, D., Park, E.C.,

Park, H.T., Park, J.-M., Park, J.-I., Park, J.T., Park, J., Park, S.C., Park, S.-Y., Parola, A.H., Parys, J.B., Pasquier, A., Pasquier, B., Passos, J.F., Pastore, N., Patel, H.H., Patschan, D., Pattingre, S., Pedraza-Alva, G., Pedraza-Chaverri, J., Pedrozo, Z., Pei, G., Pei, J., Peled-Zehavi, H., Pellegrini, J.M., Pelletier, J., Peñalva, M.A., Peng, D., Peng, Y., Penna, F., Pennuto, M., Pentimalli, F., Pereira, C.M., Pereira, G.J.S., Pereira, L.C., Pereira de Almeida, L., Perera, N.D., Pérez-Lara, Á., Perez-Oliva, A.B., Pérez-Pérez, M.E., Periyasamy, P., Perl, A., Perrotta, C., Perrotta, I., Pestell, R.G., Petersen, M., Petrache, I., Petrovski, G., Pfirrmann, T., Pfister, A.S., Philips, J.A., Pi, H., Picca, A., Pickrell, A.M., Picot, S., Pierantoni, G.M., Pierdominici, M., Pierre, P., Pierrefite-Carle, V., Pierzynowska, K., Pietrocola, F., Pietruczuk, M., Pignata, C., Pimentel-Muiños, F.X., Pinar, M., Pinheiro, R.O., Pinkas-Kramarski, R., Pinton, P., Pircs, K., Piya, S., Pizzo, P., Plantinga, T.S., Platta, H.W., Plaza-Zabala, A., Plomann, M., Plotnikov, E.Y., Plun-Favreau, H., Pluta, R., Pocock, R., Pöggeler, S., Pohl, C., Poirot, M., Poletti, A., Ponpuak, M., Popelka, H., Popova, B., Porta, H., Porte Alcon, S., Portilla-Fernandez, E., Post, M., Potts, M.B., Poulton, J., Powers, T., Prahlad, V., Prajsnar, T.K., Praticò, D., Prencipe, R., Priault, M., Proikas-Cezanne, T., Promponas, V.J., Proud, C.G., Puertollano, R., Puglielli, L., Pulinilkunnil, T., Puri, D., Puri, R., Puyal, J., Qi, X., Qi, Y., Qian, W., Qiang, L., Qiu, Y., Quadrilatero, J., Quarleri, J., Raben, N., Rabinowich, H., Ragona, D., Ragusa, M.J., Rahimi, N., Rahmati, M., Raia, V., Raimundo, N., Rajasekaran, N.-S., Ramachandra Rao, S., Rami, A., Ramírez-Pardo, I., Ramsden, D.B., Randow, F., Rangarajan, P.N., Ranieri, D., Rao, H., Rao, L., Rao, R., Rathore, S., Ratnayaka, J.A., Ratovitski, E.A., Ravanan, P., Ravegnini, G., Ray, S.K., Razani, B., Rebecca, V., Reggiori, F., Régnier-Vigouroux, A., Reichert, A.S., Reigada, D., Reiling, J.H., Rein, T., Reipert, S., Rekha, R.S., Ren, H., Ren, J., Ren, W., Renault, T., Renga, G., Reue, K., Rewitz, K., Ribeiro de Andrade Ramos, B., Riazuddin, S.A., Ribeiro-Rodrigues, T.M., Ricci, J.-E., Ricci, R., Riccio, V., Richardson, D.R., Rikihisa, Y., Risbud, M.V., Risueño, R.M., Ritis, K., Rizza, S., Rizzuto, R., Roberts, H.C., Roberts, L.D., Robinson, K.J., Roccheri, M.C., Rocchi, S., Rodney, G.G., Rodrigues, T., Rodrigues Silva, V.R., Rodriguez, A., Rodriguez-Barrueco, R., Rodriguez-Henche, N., Rodriguez-Rocha, H., Roelofs, J., Rogers, R.S., Rogov, V.V., Rojo, A.I., Rolka, K., Romanello, V., Romani, L., Romano, A., Romano, P.S., Romeo-Guitart, D., Romero, L.C., Romero, M., Roney, J.C., Rongo, C., Roperto, S., Rosenfeldt, M.T., Rosenstiel, P., Rosenwald, A.G., Roth, K.A., Roth, L., Roth, S., Rouschop, K.M.A., Roussel, B.D., Roux, S., Rovere-Querini, P., Roy, A., Rozieres, A., Ruano, D., Rubinsztein, D.C., Rubtsova, M.P., Ruckdeschel, K., Ruckenstuhl, C., Rudolf, E., Rudolf, R., Ruggieri, A., Ruparelia, A.A., Rusmini, P., Russell, R.R., Russo, G.L., Russo, M., Russo, R., Ryabaya, O.O., Ryan, K.M., Ryu, K.-Y., Sabater-Arcis, M., Sachdev, U., Sacher, M., Sachse, C., Sadhu, A., Sadoshima, J., Safren, N., Saftig, P., Sagona, A.P., Sahay, G., Sahebkar, A., Sahin, M., Sahin, O., Sahni, S., Saito, N., Saito, S., Saito, T., Sakai, R., Sakai, Y., Sakamaki, J.-I., Saksela, K., Salazar, G., Salazar-Degracia, A., Salekdeh, G.H., Saluja, A.K., Sampaio-Marques, B., Sanchez, M.C., Sanchez-Alcazar, J.A., Sanchez-Vera, V., Sancho-Shimizu, V., Sanderson, J.T., Sandri, M., Santaguida, S., Santambrogio, L., Santana, M.M., Santoni, G., Sanz, A., Sanz, P., Saran, S., Sardiello, M., Sargeant, T.J., Sarin, A., Sarkar, C., Sarkar, Sovan, Sarrias, M.-R., Sarkar, Surajit,

Sarmah, D.T., Sarparanta, J., Sathyanarayan, A., Sathyanarayanan, R., Scaglione, K.M., Scatozza, F., Schaefer, L., Schafer, Z.T., Schaible, U.E., Schapira, A.H.V., Scharl, M., Schatzl, H.M., Schein, C.H., Scheper, W., Scheuring, D., Schiaffino, M.V., Schiappacassi, M., Schindl, R., Schlattner, U., Schmidt, O., Schmitt, R., Schmidt, S.D., Schmitz, I., Schmukler, E., Schneider, A., Schneider, B.E., Schober, R., Schoijet, A.C., Schott, M.B., Schramm, M., Schröder, B., Schuh, K., Schüller, C., Schulze, R.J., Schürmanns, L., Schwamborn, J.C., Schwarten, M., Scialo, F., Sciarretta, S., Scott, M.J., Scotto, K.W., Scovassi, A.I., Scrima, A., Scrivo, A., Sebastian, D., Sebti, S., Sedej, S., Segatori, L., Segev, N., Seglen, P.O., Seiliez, I., Seki, E., Selleck, S.B., Sellke, F.W., Selsby, J.T., Sendtner, M., Senturk, S., Seranova, E., Sergi, C., Serra-Moreno, R., Sesaki, H., Settembre, C., Setty, S.R.G., Sgarbi, G., Sha, O., Shacka, J.J., Shah, J.A., Shang, D., Shao, C., Shao, F., Sharbati, S., Sharkey, L.M., Sharma, D., Sharma, G., Sharma, K., Sharma, P., Sharma, S., Shen, H.-M., Shen, H., Shen, J., Shen, M., Shen, W., Shen, Z., Sheng, R., Sheng, Z., Sheng, Z.-H., Shi, J., Shi, X., Shi, Y.-H., Shiba-Fukushima, K., Shieh, J.-J., Shimada, Y., Shimizu, S., Shimozawa, M., Shintani, T., Shoemaker, C.J., Shojaei, S., Shoji, I., Shravage, B.V., Shridhar, V., Shu, C.-W., Shu, H.-B., Shui, K., Shukla, A.K., Shutt, T.E., Sica, V., Siddiqui, A., Sierra, A., Sierra-Torre, V., Signorelli, S., Sil, P., Silva, B.J. de A., Silva, J.D., Silva-Pavez, E., Silvente-Poirot, S., Simmonds, R.E., Simon, A.K., Simon, H.-U., Simons, M., Singh, A., Singh, L.P., Singh, R., Singh, S.V., Singh, S.K., Singh, S.B., Singh, S., Singh, S.P., Sinha, D., Sinha, R.A., Sinha, S., Sirko, A., Sirohi, K., Sivridis, E.L., Skendros, P., Skirycz, A., Slaninová, I., Smaili, S.S., Smertenko, A., Smith, M.D., Soenen, S.J., Sohn, E.J., Sok, S.P.M., Solaini, G., Soldati, T., Soleimanpour, S.A., Soler, R.M., Solovchenko, A., Somarelli, J.A., Sonawane, A., Song, F., Song, H.K., Song, J.-X., Song, K., Song, Z., Soria, L.R., Sorice, M., Soukas, A.A., Soukup, S.-F., Sousa, D., Sousa, N., Spagnuolo, P.A., Spector, S.A., Srinivas Bharath, M.M., St Clair, D., Stagni, V., Staiano, L., Stalnecker, C.A., Stankov, M.V., Stathopulos, P.B., Stefan, K., Stefan, S.M., Stefanis, L., Steffan, J.S., Steinkasserer, A., Stenmark, H., Sterneckert, J., Stevens, C., Stoka, V., Storch, S., Stork, B., Strappazzon, F., Strohecker, A.M., Stupack, D.G., Su, H., Su, L.-Y., Su, L., Suarez-Fontes, A.M., Subauste, C.S., Subbian, S., Subirada, P.V., Sudhandiran, G., Sue, C.M., Sui, X., Summers, C., Sun, G., Sun, J., Sun, K., Sun, M.-X., Sun, Q., Sun, Y., Sun, Z., Sunahara, K.K.S., Sundberg, E., Susztak, K., Sutovsky, P., Suzuki, H., Sweeney, G., Symons, J.D., Sze, S.C.W., Szewczyk, N.J., Tabęcka-Łonczynska, A., Tabolacci, C., Tacke, F., Taegtmeyer, H., Tafani, M., Tagaya, M., Tai, H., Tait, S.W.G., Takahashi, Y., Takats, S., Talwar, P., Tam, C., Tam, S.Y., Tampellini, D., Tamura, A., Tan, C.T., Tan, E.-K., Tan, Y.-Q., Tanaka, Masaki, Tanaka, Motomasa, Tang, D., Tang, J., Tang, T.-S., Tanida, I., Tao, Z., Taouis, M., Tatenhorst, L., Tavernarakis, N., Taylor, A., Taylor, G.A., Taylor, J.M., Tchetina, E., Tee, A.R., Tegeder, I., Teis, D., Teixeira, N., Teixeira-Clerc, F., Tekirdag, K.A., Tencomnao, T., Tenreiro, S., Tepikin, A.V., Testillano, P.S., Tettamanti, G., Tharaux, P.-L., Thedieck, K., Thekkinghat, A.A., Thellung, S., Thinwa, J.W., Thirumalaikumar, V.P., Thomas, S.M., Thomes, P.G., Thorburn, A., Thukral, L., Thum, T., Thumm, M., Tian, L., Tichy, A., Till, A., Timmerman, V., Titorenko, V.I., Todi, S.V., Todorova, K., Toivonen, J.M., Tomaipitinca, L., Tomar, D., Tomas-Zapico, C., Tomić,

S., Tong, B.C.-K., Tong, C., Tong, X., Tooze, S.A., Torgersen, M.L., Torii, S., Torres-López, L., Torriglia, A., Towers, C.G., Towns, R., Toyokuni, S., Trajkovic, V., Tramontano, D., Tran, Q.-G., Travassos, L.H., Trelford, C.B., Tremel, S., Trougakos, I.P., Tsao, B.P., Tschan, M.P., Tse, H.-F., Tse, T.F., Tsugawa, H., Tsvetkov, A.S., Tumbarello, D.A., Tumtas, Y., Tuñón, M.J., Turcotte, S., Turk, B., Turk, V., Turner, B.J., Tuxworth, R.I., Tyler, J.K., Tyutereva, E.V., Uchiyama, Y., Ugun-Klusek, A., Uhlig, H.H., Ułamek-Kozioł, M., Ulasov, I.V., Umekawa, M., Ungermann, C., Unno, R., Urbe, S., Uribe-Carretero, E., Üstün, S., Uversky, V.N., Vaccari, T., Vaccaro, M.I., Vahsen, B.F., Vakifahmetoglu-Norberg, H., Valdor, R., Valente, M.J., Valko, A., Vallee, R.B., Valverde, A.M., Van den Berghe, G., van der Veen, S., Van Kaer, L., van Loosdregt, J., van Wijk, S.J.L., Vandenberghe, W., Vanhorebeek, I., Vannier-Santos, M.A., Vannini, N., Vanrell, M.C., Vantaggiato, C., Varano, G., Varela-Nieto, I., Varga, M., Vasconcelos, M.H., Vats, S., Vavvas, D.G., Vega-Naredo, I., Vega-Rubin-de-Celis, S., Velasco, G., Velázquez, A.P., Vellai, T., Vellenga, E., Velotti, F., Verdier, M., Verginis, P., Vergne, I., Verkade, P., Verma, M., Verstreken, P., Vervliet, T., Vervoorts, J., Vessoni, A.T., Victor, V.M., Vidal, M., Vidoni, C., Vieira, O.V., Vierstra, R.D., Viganó, S., Vihinen, H., Vijayan, V., Vila, M., Vilar, M., Villalba, J.M., Villalobo, A., Villarejo-Zori, B., Villarroya, F., Villarroya, J., Vincent, O., Vindis, C., Viret, C., Viscomi, M.T., Visnjic, D., Vitale, I., Vocadlo, D.J., Voitsekhovskaja, O.V., Volonté, C., Volta, M., Vomero, M., Von Haefen, C., Vooijs, M.A., Voos, W., Vucicevic, L., Wade-Martins, R., Waguri, S., Waite, K.A., Wakatsuki, S., Walker, D.W., Walker, M.J., Walker, S.A., Walter, J., Wandosell, F.G., Wang, B., Wang, Chao-Yung, Wang, Chen, Wang, Chenran, Wang, Chenwei, Wang, Cun-Yu, Wang, D., Wang, Fangyang, Wang, Feng, Wang, Fengming, Wang, G., Wang, Han, Wang, Hao, Wang, Hexiang, Wang, H.-G., Wang, Jianrong, Wang, Jigang, Wang, Jiou, Wang, Jundong, Wang, K., Wang, Lianrong, Wang, Liming, Wang, M.H., Wang, M., Wang, N., Wang, Pengwei, Wang, Peipei, Wang, Ping, Wang, Ping, Wang, Q.J., Wang, Q., Wang, Q.K., Wang, Q.A., Wang, W.-T., Wang, W., Wang, Xinnan, Wang, Xuejun, Wang, Yan, Wang, Yanchang, Wang, Yanzhuang, Wang, Y.-Y., Wang, Yihua, Wang, Yipeng, Wang, Yu, Wang, Yuqi, Wang, Zhe, Wang, Zhenyu, Wang, Zhouguang, Warnes, G., Warnsmann, V., Watada, H., Watanabe, E., Watchon, M., Wawrzyńska, A., Weaver, T.E., Wegrzyn, G., Wehman, A.M., Wei, H., Wei, L., Wei, T., Wei, Y., Weiergräber, O.H., Weihl, C.C., Weindl, G., Weiskirchen, R., Wells, A., Wen, R.H., Wen, X., Werner, A., Weykopf, B., Wheatley, S.P., Whitton, J.L., Whitworth, A.J., Wiktorska, K., Wildenberg, M.E., Wileman, T., Wilkinson, S., Willbold, D., Williams, B., Williams, R.S.B., Williams, R.L., Williamson, P.R., Wilson, R.A., Winner, B., Winsor, N.J., Witkin, S.S., Wodrich, H., Woehlbier, U., Wollert, T., Wong, E., Wong, J.H., Wong, R.W., Wong, V.K.W., Wong, W.W.-L., Wu, A.-G., Wu, C., Wu, Jian, Wu, Junfang, Wu, K.K., Wu, M., Wu, Shan-Ying, Wu, Shengzhou, Wu, Shu-Yan, Wu, Shufang, Wu, W.K.K., Wu, Xiaohong, Wu, Xiaoqing, Wu, Y.-W., Wu, Y., Xavier, R.J., Xia, H., Xia, L., Xia, Z., Xiang, G., Xiang, J., Xiang, M., Xiang, W., Xiao, B., Xiao, G., Xiao, H., Xiao, H.-T., Xiao, J., Xiao, L., Xiao, S., Xiao, Y., Xie, B., Xie, C.-M., Xie, M., Xie, Y., Xie, Zhiping, Xie, Zhonglin, Xilouri, M., Xu, C., Xu, E., Xu, H., Xu, Jing, Xu, JinRong, Xu, L., Xu, W.W., Xu, X., Xue, Y., Yakhine-Diop, S.M.S., Yamaguchi, M., Yamaguchi, O., Yamamoto, A., Yamashina, S., Yan, S., Yan, S.-J., Yan, Z., Yanagi, Y.,

Yang, C., Yang, D.-S., Yang, Huan, Yang, H.-T., Yang, Hui, Yang, J.-M., Yang, Jing, Yang, Jingyu, Yang, Ling, Yang, Liu, Yang, M., Yang, P.-M., Yang, Q., Yang, Seungwon, Yang, Shu, Yang, S.-F., Yang, W., Yang, W.Y., Yang, Xiaoyong, Yang, Xuesong, Yang, Yi, Yang, Ying, Yao, H., Yao, S., Yao, X., Yao, Y.-G., Yao, Y.-M., Yasui, T., Yazdankhah, M., Yen, P.M., Yi, C., Yin, X.-M., Yin, Y., Yin, Zhangyuan, Yin, Ziyi, Ying, M., Ying, Z., Yip, C.K., Yiu, S.P.T., Yoo, Y.H., Yoshida, K., Yoshii, S.R., Yoshimori, T., Yousefi, B., Yu, B., Yu, H., Yu, J., Yu, J., Yu, L., Yu, M.-L., Yu, S.-W., Yu, V.C., Yu, W.H., Yu, Zhengping, Yu, Zhou, Yuan, J., Yuan, L.-Q., Yuan, S., Yuan, S.-S.F., Yuan, Y., Yuan, Z., Yue, J., Yue, Z., Yun, J., Yung, R.L., Zacks, D.N., Zaffagnini, G., Zambelli, V.O., Zanella, I., Zang, Q.S., Zanivan, S., Zappavigna, S., Zaragoza, P., Zarbalis, K.S., Zarebkohan, A., Zarrouk, A., Zeitlin, S.O., Zeng, J., Zeng, J.-D., Žerovnik, E., Zhan, L., Zhang, B., Zhang, D.D., Zhang, Hanlin, Zhang, Hong, Zhang, Hong, Zhang, Honghe, Zhang, Huafeng, Zhang, Huaye, Zhang, Hui, Zhang, H.-L., Zhang, Jianbin, Zhang, Jianhua, Zhang, J.-P., Zhang, K.Y.B., Zhang, L.W., Zhang, Lin, Zhang, Lisheng, Zhang, Lu, Zhang, Luoying, Zhang, M., Zhang, P., Zhang, S., Zhang, W., Zhang, Xiangnan, Zhang, X.-W., Zhang, Xiaolei, Zhang, Xiaoyan, Zhang, Xin, Zhang, Xinxin, Zhang, X.D., Zhang, Yang, Zhang, Yanjin, Zhang, Yi, Zhang, Y.-D., Zhang, Yingmei, Zhang, Y.-Y., Zhang, Yuchen, Zhang, Zhe, Zhang, Zhengguang, Zhang, Zhibing, Zhang, Zhihai, Zhang, Zhiyong, Zhang, Zili, Zhao, H., Zhao, L., Zhao, S., Zhao, T., Zhao, X.-F., Zhao, Ying, Zhao, Yongchao, Zhao, Yongliang, Zhao, Yuting, Zheng, G., Zheng, K., Zheng, L., Zheng, S., Zheng, X.-L., Zheng, Y., Zheng, Z.-G., Zhivotovsky, B., Zhong, Q., Zhou, A., Zhou, B., Zhou, C., Zhou, G., Zhou, Hao, Zhou, Hong, Zhou, Hongbo, Zhou, Jie, Zhou, Jing, Zhou, Jing, Zhou, Jiyong, Zhou, K., Zhou, R., Zhou, X.-J., Zhou, Yanshuang, Zhou, Yinghong, Zhou, Yubin, Zhou, Z.-Y., Zhou, Z., Zhu, B., Zhu, C., Zhu, G.-Q., Zhu, Haining, Zhu, Hongxin, Zhu, Hua, Zhu, W.-G., Zhu, Yanping, Zhu, Yushan, Zhuang, H., Zhuang, X., Zientara-Rytter, K., Zimmermann, C.M., Ziviani, E., Zoladek, T., Zong, W.-X., Zorov, D.B., Zorzano, A., Zou, W., Zou, Zhen, Zou, Zhengzhi, Zuryn, S., Zwerschke, W., Brand-Saberi, B., Dong, X.C., Kenchappa, C.S., Li, Zuguo, Lin, Y., Oshima, S., Rong, Y., Sluimer, J.C., Stallings, C.L., Tong, C.-K., 2021. Guidelines for the use and interpretation of assays for monitoring autophagy (4th edition)1. Autophagy 17, 1–382. https://doi.org/10.1080/15548627.2020.1797280

Komatsu, M., Waguri, S., Koike, M., Sou, Y.-S., Ueno, T., Hara, T., Mizushima, N., Iwata, J.-I., Ezaki, J., Murata, S., Hamazaki, J., Nishito, Y., Iemura, S.-I., Natsume, T., Yanagawa, T., Uwayama, J., Warabi, E., Yoshida, H., Ishii, T., Kobayashi, A., Yamamoto, M., Yue, Z., Uchiyama, Y., Kominami, E., Tanaka, K., 2007. Homeostatic levels of p62 control cytoplasmic inclusion body formation in autophagy-deficient mice. Cell 131, 1149–1163. https://doi.org/10.1016/j.cell.2007.10.035

Komatsu, M., Waguri, S., Ueno, T., Iwata, J., Murata, S., Tanida, I., Ezaki, J., Mizushima, N., Ohsumi, Y., Uchiyama, Y., Kominami, E., Tanaka, K., Chiba, T., 2005. Impairment of starvation-induced and constitutive autophagy in Atg7-deficient mice. J. Cell Biol. 169, 425–434. https://doi.org/10.1083/jcb.200412022

Kongton, K., McCall, K., Phongdara, A., 2014. Identification of gamma-interferon-inducible lysosomal thiol reductase (GILT) homologues in the fruit fly *Drosophila*

melanogaster. Dev. Comp. Immunol. 44, 389–396. https://doi.org/10.1016/j.dci.2014.01.007

Kwon, Y., Song, W., Droujinine, I.A., Hu, Y., Asara, J.M., Perrimon, N., 2015. Systemic Organ Wasting Induced by Localized Expression of the Secreted Insulin/IGF Antagonist ImpL2. Dev. Cell 33, 36–46. https://doi.org/10.1016/j.devcel.2015.02.012

Liu, F., Li, X., Lu, C., Bai, A., Bielawski, J., Bielawska, A., Marshall, B., Schoenlein, P.V., Lebedyeva, I.O., Liu, K., 2016. Ceramide activates lysosomal cathepsin B and cathepsin D to attenuate autophagy and induces ER stress to suppress myeloid-derived suppressor cells. Oncotarget 7, 83907–83925. https://doi.org/10.18632/oncotarget.13438

Liu, Jianfang, Lichtenberg, T., Hoadley, K.A., Poisson, L.M., Lazar, A.J., Cherniack, A.D., Kovatich, A.J., Benz, C.C., Levine, D.A., Lee, A.V., Omberg, L., Wolf, D.M., Shriver, C.D., Thorsson, V., Caesar-Johnson, S.J., Demchok, J.A., Felau, I., Kasapi, M., Ferguson, M.L., Hutter, C.M., Sofia, H.J., Tarnuzzer, R., Wang, Z., Yang, L., Zenklusen, J.C., Zhang, J. (Julia), Chudamani, S., Liu, Jia, Lolla, L., Naresh, R., Pihl, T., Sun, Q., Wan, Y., Wu, Y., Cho, J., DeFreitas, T., Frazer, S., Gehlenborg, N., Getz, G., Heiman, D.I., Kim, J., Lawrence, M.S., Lin, P., Meier, S., Noble, M.S., Saksena, G., Voet, D., Zhang, Hailei, Bernard, B., Chambwe, N., Dhankani, V., Knijnenburg, T., Kramer, R., Leinonen, K., Liu, Y., Miller, M., Reynolds, S., Shmulevich, I., Thorsson, V., Zhang, W., Akbani, R., Broom, B.M., Hegde, A.M., Ju, Z., Kanchi, R.S., Korkut, A., Li, J., Liang, H., Ling, S., Liu, W., Lu, Y., Mills, G.B., Ng, K.-S., Rao, A., Ryan, M., Wang, Jing, Weinstein, J.N., Zhang, J., Abeshouse, A., Armenia, J., Chakravarty, D., Chatila, W.K., Bruijn, I. de, Gao, J., Gross, B.E., Heins, Z.J., Kundra, R., La, K., Ladanyi, M., Luna, A., Nissan, M.G., Ochoa, A., Phillips, S.M., Reznik, E., Sanchez-Vega, F., Sander, C., Schultz, N., Sheridan, R., Sumer, S.O., Sun, Y., Taylor, B.S., Wang, Jioajiao, Zhang, Hongxin, Anur, P., Peto, M., Spellman, P., Benz, C., Stuart, J.M., Wong, C.K., Yau, C., Hayes, D.N., Parker, J.S., Wilkerson, M.D., Ally, A., Balasundaram, M., Bowlby, R., Brooks, D., Carlsen, R., Chuah, E., Dhalla, N., Holt, R., Jones, S.J.M., Kasaian, K., Lee, D., Ma, Y., Marra, M.A., Mayo, M., Moore, R.A., Mungall, A.J., Mungall, K., Robertson, A.G., Sadeghi, S., Schein, J.E., Sipahimalani, P., Tam, A., Thiessen, N., Tse, K., Wong, T., Berger, A.C., Beroukhim, R., Cherniack, A.D., Cibulskis, C., Gabriel, S.B., Gao, G.F., Ha, G., Meyerson, M., Schumacher, S.E., Shih, J., Kucherlapati, M.H., Kucherlapati, R.S., Baylin, S., Cope, L., Danilova, L., Bootwalla, M.S., Lai, P.H., Maglinte, D.T., Berg, D.J.V.D., Weisenberger, D.J., Auman, J.T., Balu, S., Bodenheimer, T., Fan, C., Hoadley, K.A., Hoyle, A.P., Jefferys, S.R., Jones, C.D., Meng, S., Mieczkowski, P.A., Mose, L.E., Perou, A.H., Perou, C.M., Roach, J., Shi, Y., Simons, J.V., Skelly, T., Soloway, M.G., Tan, D., Veluvolu, U., Fan, H., Hinoue, T., Laird, P.W., Shen, H., Zhou, W., Bellair, M., Chang, K., Covington, K., Creighton, C.J., Dinh, H., Doddapaneni, H., Donehower, L.A., Drummond, J., Gibbs, R.A., Glenn, R., Hale, W., Han, Y., Hu, J., Korchina, V., Lee, S., Lewis, L., Li, W., Liu, X., Morgan, M., Morton, D., Muzny, D., Santibanez, J., Sheth, M., Shinbro, E., Wang, L., Wang, M., Wheeler, D.A., Xi, L., Zhao, F., Hess, J., Appelbaum, E.L., Bailey, M., Cordes, M.G., Ding, L., Fronick, C.C., Fulton, L.A., Fulton, R.S., Kandoth, C., Mardis, E.R., McLellan, M.D., Miller, C.A., Schmidt, H.K., Wilson, R.K., Crain, D., Curley, E., Gardner, J., Lau, K., Mallery,

D., Morris, S., Paulauskis, J., Penny, R., Shelton, C., Shelton, T., Sherman, M., Thompson, E., Yena, P., Bowen, J., Gastier-Foster, J.M., Gerken, M., Leraas, K.M., Lichtenberg, T.M., Ramirez, N.C., Wise, L., Zmuda, E., Corcoran, N., Costello, T., Hovens, C., Carvalho, A.L., Carvalho, A.C. de, Fregnani, J.H., Longatto-Filho, A., Reis, R.M., Scapulatempo-Neto, C., Silveira, H.C.S., Vidal, D.O., Burnette, A., Eschbacher, J., Hermes, B., Noss, A., Singh, R., Anderson, M.L., Castro, P.D., Ittmann, M., Huntsman, D., Kohl, B., Le, X., Thorp, R., Andry, C., Duffy, E.R., Lyadov, V., Paklina, O., Setdikova, G., Shabunin, A., Tavobilov, M., McPherson, C., Warnick, R., Berkowitz, R., Cramer, D., Feltmate, C., Horowitz, N., Kibel, A., Muto, M., Raut, C.P., Malykh, A., Barnholtz-Sloan, J.S., Barrett, W., Devine, K., Fulop, J., Ostrom, Q.T., Shimmel, K., Wolinsky, Y., Sloan, A.E., Rose, A.D., Giuliante, F., Goodman, M., Karlan, B.Y., Hagedorn, C.H., Eckman, J., Harr, J., Myers, J., Tucker, K., Zach, L.A., Deyarmin, B., Hu, H., Kvecher, L., Larson, C., Mural, R.J., Somiari, S., Vicha, A., Zelinka, T., Bennett, J., Iacocca, M., Rabeno, B., Swanson, P., Latour, M., Lacombe, L., Têtu, B., Bergeron, A., McGraw, M., Staugaitis, S.M., Chabot, J., Hibshoosh, H., Sepulveda, A., Su, T., Wang, T., Potapova, O., Voronina, O., Desjardins, L., Mariani, O., Roman-Roman, S., Sastre, X., Stern, M.-H., Cheng, F., Signoretti, S., Berchuck, A., Bigner, D., Lipp, E., Marks, J., McCall, S., McLendon, R., Secord, A., Sharp, A., Behera, M., Brat, D.J., Chen, A., Delman, K., Force, S., Khuri, F., Magliocca, K., Maithel, S., Olson, J.J., Owonikoko, T., Pickens, A., Ramalingam, S., Shin, D.M., Sica, G., Meir, E.G.V., Zhang, Hongzheng, Eijckenboom, W., Gillis, A., Korpershoek, E., Looijenga, L., Oosterhuis, W., Stoop, H., Kessel, K.E. van, Zwarthoff, E.C., Calatozzolo, C., Cuppini, L., Cuzzubbo, S., DiMeco, F., Finocchiaro, G., Mattei, L., Perin, A., Pollo, B., Chen, C., Houck, J., Lohavanichbutr, P., Hartmann, A., Stoehr, C., Stoehr, R., Taubert, H., Wach, S., Wullich, B., Kycler, W., Murawa, D., Wiznerowicz, M., Chung, K., Edenfield, W.J., Martin, J., Baudin, E., Bubley, G., Bueno, R., Rienzo, A.D., Richards, W.G., Kalkanis, S., Mikkelsen, T., Noushmehr, H., Scarpace, L., Girard, N., Aymerich, M., Campo, E., Giné, E., Guillermo, A.L., Bang, N.V., Hanh, P.T., Phu, B.D., Tang, Y., Colman, H., Evason, K., Dottino, P.R., Martignetti, J.A., Gabra, H., Juhl, H., Akeredolu, T., Stepa, S., Hoon, D., Ahn, K., Kang, K.J., Beuschlein, F., Breggia, A., Birrer, M., Bell, D., Borad, M., Bryce, A.H., Castle, E., Chandan, V., Cheville, J., Copland, J.A., Farnell, M., Flotte, T., Giama, N., Ho, T., Kendrick, M., Kocher, J.-P., Kopp, K., Moser, C., Nagorney, D., O'Brien, D., O'Neill, B.P., Patel, T., Petersen, G., Que, F., Rivera, M., Roberts, L., Smallridge, R., Smyrk, T., Stanton, M., Thompson, R.H., Torbenson, M., Yang, J.D., Zhang, L., Brimo, F., Ajani, J.A., Gonzalez, A.M.A., Behrens, C., Bondaruk, J., Broaddus, R., Czerniak, B., Esmaeli, B., Fujimoto, J., Gershenwald, J., Guo, C., Lazar, A.J., Logothetis, C., Meric-Bernstam, F., Moran, C., Ramondetta, L., Rice, D., Sood, A., Tamboli, P., Thompson, T., Troncoso, P., Tsao, A., Wistuba, I., Carter, C., Haydu, L., Hersey, P., Jakrot, V., Kakavand, H., Kefford, R., Lee, K., Long, G., Mann, G., Quinn, M., Saw, R., Scolyer, R., Shannon, K., Spillane, A., Stretch, J., Synott, M., Thompson, J., Wilmott, J., Al-Ahmadie, H., Chan, T.A., Ghossein, R., Gopalan, A., Levine, D.A., Reuter, V., Singer, S., Singh, B., Tien, N.V., Broudy, T., Mirsaidi, C., Nair, P., Drwiega, P., Miller, J., Smith, J., Zaren, H., Park, J.-W., Hung, N.P., Kebebew, E., Linehan, W.M., Metwalli, A.R., Pacak, K., Pinto, P.A.,

Schiffman, M., Schmidt, L.S., Vocke, C.D., Wentzensen, N., Worrell, R., Yang, H., Moncrieff, M., Goparaju, C., Melamed, J., Pass, H., Botnariuc, N., Caraman, I., Cernat, M., Chemencedji, I., Clipca, A., Doruc, S., Gorincioi, G., Mura, S., Pirtac, M., Stancul, I., Tcaciuc, D., Albert, M., Alexopoulou, I., Arnaout, A., Bartlett, J., Engel, J., Gilbert, S., Parfitt, J., Sekhon, H., Thomas, G., Rassl, D.M., Rintoul, R.C., Bifulco, C., Tamakawa, R., Urba, W., Hayward, N., Timmers, H., Antenucci, A., Facciolo, F., Grazi, G., Marino, M., Merola, R., Krijger, R. de, Gimenez-Roqueplo, A.-P., Piché, A., Chevalier, S., McKercher, G., Birsoy, K., Barnett, G., Brewer, C., Farver, C., Naska, T., Pennell, N.A., Raymond, D., Schilero, C., Smolenski, K., Williams, F., Morrison, C., Borgia, J.A., Liptay, M.J., Pool, M., Seder, C.W., Junker, K., Omberg, L., Dinkin, M., Manikhas, G., Alvaro, D., Bragazzi, M.C., Cardinale, V., Carpino, G., Gaudio, E., Chesla, D., Cottingham, S., Dubina, M., Moiseenko, F., Dhanasekaran, R., Becker, K.-F., Janssen, K.-P., Slotta-Huspenina, J., Abdel-Rahman, M.H., Aziz, D., Bell, S., Cebulla, C.M., Davis, A., Duell, R., Elder, J.B., Hilty, J., Kumar, B., Lang, J., Lehman, N.L., Mandt, R., Nguyen, P., Pilarski, R., Rai, K., Schoenfield, L., Senecal, K., Wakely, P., Hansen, P., Lechan, R., Powers, J., Tischler, A., Grizzle, W.E., Sexton, K.C., Kastl, A., Henderson, J., Porten, S., Waldmann, J., Fassnacht, M., Asa, S.L., Schadendorf, D., Couce, M., Graefen, M., Huland, H., Sauter, G., Schlomm, T., Simon, R., Tennstedt, P., Olabode, O., Nelson, M., Bathe, O., Carroll, P.R., Chan, J.M., Disaia, P., Glenn, P., Kelley, R.K., Landen, C.N., Phillips, J., Prados, M., Simko, J., Smith-McCune, K., VandenBerg, S., Roggin, K., Fehrenbach, A., Kendler, A., Sifri, S., Steele, R., Jimeno, A., Carey, F., Forgie, I., Mannelli, M., Carney, M., Hernandez, B., Campos, B., Herold-Mende, C., Jungk, C., Unterberg, A., Deimling, A. von, Bossler, A., Galbraith, J., Jacobus, L., Knudson, M., Knutson, T., Ma, D., Milhem, M., Sigmund, R., Godwin, A.K., Madan, R., Rosenthal, H.G., Adebamowo, C., Adebamowo, S.N., Boussioutas, A., Beer, D., Giordano, T., Mes-Masson, A.-M., Saad, F., Bocklage, T., Landrum, L., Mannel, R., Moore, K., Moxley, K., Postier, R., Walker, J., Zuna, R., Feldman, M., Valdivieso, F., Dhir, R., Luketich, J., Pinero, E.M.M., Quintero-Aguilo, M., Carlos Gilberto Carlotti, J., Santos, J.S.D., Kemp, R., Sankarankuty, A., Tirapelli, D., Catto, J., Agnew, K., Swisher, E., Creaney, J., Robinson, B., Shelley, C.S., Godwin, E.M., Kendall, S., Shipman, C., Bradford, C., Carey, T., Haddad, A., Moyer, J., Peterson, L., Prince, M., Rozek, L., Wolf, G., Bowman, R., Fong, K.M., Yang, I., Korst, R., Rathmell, W.K., Fantacone-Campbell, J.L., Hooke, J.A., Kovatich, A.J., Shriver, C.D., DiPersio, J., Drake, B., Govindan, R., Heath, S., Ley, T., Tine, B.V., Westervelt, P., Rubin, M.A., Lee, J.I., Aredes, N.D., Mariamidze, A., Hu, H., 2018. An Integrated TCGA Pan-Cancer Clinical Data Resource to Drive High-Quality Survival Outcome Analytics. Cell 173, 400-416.e11. https://doi.org/10.1016/j.cell.2018.02.052

Liu, Y., Saavedra, P., Perrimon, N., 2022. Cancer cachexia: lessons from Drosophila. Dis. Model. Mech. 15, dmm049298. https://doi.org/10.1242/dmm.049298

Liu, Ying, Dantas, E., Ferrer, M., Miao, T., Qadiri, M., Liu, Yifang, Comjean, A., Davidson, E.E., Perrier, T., Ahmed, T., Hu, Y., Goncalves, M.D., Janowitz, T., Perrimon, N., 2025. Hepatic gluconeogenesis and PDK3 upregulation drive cancer cachexia in flies and mice. Nat. Metab. 7, 823–841. https://doi.org/10.1038/s42255-025-01265-2

Luzio, J.P., Pryor, P.R., Bright, N.A., 2007. Lysosomes: fusion and function. Nat. Rev. Mol. Cell Biol. 8, 622–632. https://doi.org/10.1038/nrm2217

Mirdita, M., Schütze, K., Moriwaki, Y., Heo, L., Ovchinnikov, S., Steinegger, M., 2022. ColabFold: making protein folding accessible to all. Nat. Methods 19, 679–682. https://doi.org/10.1038/s41592-022-01488-1

Mizutani, Y., Kihara, A., Igarashi, Y., 2005. Mammalian Lass6 and its related family members regulate synthesis of specific ceramides. Biochem. J. 390, 263–271. https://doi.org/10.1042/BJ20050291

Mulakkal, N.C., Nagy, P., Takats, S., Tusco, R., Juhász, G., Nezis, I.P., 2014. Autophagy in Drosophila: From Historical Studies to Current Knowledge. BioMed Res. Int. 2014, 273473. https://doi.org/10.1155/2014/273473

Mullen, T.D., Hannun, Y.A., Obeid, L.M., 2012. Ceramide synthases at the centre of sphingolipid metabolism and biology. Biochem. J. 441, 789–802. https://doi.org/10.1042/BJ20111626

Ni, H.-M., Woolbright, B.L., Williams, J., Copple, B., Cui, W., Luyendyk, J.P., Jaeschke, H., Ding, W.-X., 2014. Nrf2 promotes the development of fibrosis and tumorigenesis in mice with defective hepatic autophagy. J. Hepatol. 61, 617–625. https://doi.org/10.1016/j.jhep.2014.04.043

Passaro, S., Corso, G., Wohlwend, J., Reveiz, M., Thaler, S., Somnath, V.R., Getz, N., Portnoi, T., Roy, J., Stark, H., Kwabi-Addo, D., Beaini, D., Jaakkola, T., Barzilay, R., 2025. Boltz-2: Towards Accurate and Efficient Binding Affinity Prediction. BioRxiv Prepr. Serv. Biol. 2025.06.14.659707. https://doi.org/10.1101/2025.06.14.659707

Pelosof, L.C., Gerber, D.E., 2010. Paraneoplastic Syndromes: An Approach to Diagnosis and Treatment. Mayo Clin. Proc. 85, 838–854. https://doi.org/10.4065/mcp.2010.0099

Pewzner-Jung, Y., Park, H., Laviad, E.L., Silva, L.C., Lahiri, S., Stiban, J., Erez-Roman, R., Brügger, B., Sachsenheimer, T., Wieland, F., Prieto, M., Merrill, A.H., Futerman, A.H., 2010. A Critical Role for Ceramide Synthase 2 in Liver Homeostasis: I. ALTERATIONS IN LIPID METABOLIC PATHWAYS*. J. Biol. Chem. 285, 10902–10910. https://doi.org/10.1074/jbc.M109.077594

Qi, D., Song, X., Xue, C., Yao, W., Shen, P., Yu, H., Zhang, Z., 2021. AKT1/FOXP3 axis-mediated expression of CerS6 promotes p53 mutant pancreatic tumorigenesis. Cancer Lett. 522, 105–118. https://doi.org/10.1016/j.canlet.2021.06.024

Qian, H., Chao, X., Williams, J., Fulte, S., Li, T., Yang, L., Ding, W.-X., 2021. Autophagy in liver diseases: A review. Mol. Aspects Med. 82, 100973. https://doi.org/10.1016/j.mam.2021.100973

Queiroz, A.L., Dantas, E., Ramsamooj, S., Murthy, A., Ahmed, M., Zunica, E.R.M., Liang, R.J., Murphy, J., Holman, C.D., Bare, C.J., Ghahramani, G., Wu, Z., Cohen, D.E., Kirwan, J.P., Cantley, L.C., Axelrod, C.L., Goncalves, M.D., 2022. Blocking ActRIIB and restoring appetite reverses cachexia and improves survival in mice with lung cancer. Nat. Commun. 13, 4633. https://doi.org/10.1038/s41467-022-32135-0

Riebeling, C., Allegood, J.C., Wang, E., Merrill, A.H., Futerman, A.H., 2003. Two Mammalian Longevity Assurance Gene (LAG1) Family Members, *trh1* and *trh4*, Regulate

Dihydroceramide Synthesis Using Different Fatty Acyl-CoA Donors*. J. Biol. Chem. 278, 43452–43459. https://doi.org/10.1074/jbc.M307104200

Rowland, L.A., Guilherme, A., Henriques, F., DiMarzio, C., Munroe, S., Wetoska, N., Kelly, M., Reddig, K., Hendricks, G., Pan, M., Han, X., Ilkayeva, O.R., Newgard, C.B., Czech, M.P., 2023. De novo lipogenesis fuels adipocyte autophagosome and lysosome membrane dynamics. Nat. Commun. 14, 1362. https://doi.org/10.1038/s41467-023-37016-8

Ryter, S.W., Cloonan, S.M., Choi, A.M.K., 2013. Autophagy: A Critical Regulator of Cellular Metabolism and Homeostasis. Mol. Cells 36, 7–16. https://doi.org/10.1007/s10059-013-0140-8

Saavedra, P., Dumesic, P.A., Hu, Y., Jouandin, P., Binari, R., Wilensky, S.E., Filine, E., Rodiger, J., Wang, H., Spiegelman, B.M., Perrimon, N., 2021. REPTOR/CREBRF encode key regulators of muscle energy metabolism. https://doi.org/10.1101/2021.12.17.473012

Schütter, M., Graef, M., 2020. Localized de novo phospholipid synthesis drives autophagosome biogenesis. Autophagy 16, 770–771. https://doi.org/10.1080/15548627.2020.1725379

Song, W., Kir, S., Hong, S., Hu, Y., Wang, X., Binari, R., Tang, H.-W., Chung, V., Banks, A.S., Spiegelman, B., Perrimon, N., 2019. Tumor-Derived Ligands Trigger Tumor Growth and Host Wasting via Differential MEK Activation. Dev. Cell 48, 277-286.e6. https://doi.org/10.1016/j.devcel.2018.12.003

Song, W., Owusu-Ansah, E., Hu, Y., Cheng, D., Ni, X., Zirin, J., Perrimon, N., 2017. Activin signaling mediates muscle-to-adipose communication in a mitochondria dysfunction-associated obesity model. Proc. Natl. Acad. Sci. 114, 8596–8601. https://doi.org/10.1073/pnas.1708037114

Stone, R.L., Nick, A.M., McNeish, I.A., Balkwill, F., Han, H.D., Bottsford-Miller, J., Rupaimoole, R., Armaiz-Pena, G.N., Pecot, C.V., Coward, J., Deavers, M.T., Vasquez, H.G., Urbauer, D., Landen, C.N., Hu, W., Gershenson, H., Matsuo, K., Shahzad, M.M.K., King, E.R., Tekedereli, I., Ozpolat, B., Ahn, E.H., Bond, V.K., Wang, R., Drew, A.F., Gushiken, F., Lamkin, D., Collins, K., DeGeest, K., Lutgendorf, S.K., Chiu, W., Lopez-Berestein, G., Afshar-Kharghan, V., Sood, A.K., 2012. Paraneoplastic Thrombocytosis in Ovarian Cancer [WWW Document]. N. Engl. J. Med. https://doi.org/10.1056/NEJMoa1110352

Taniguchi, M., Kitatani, K., Kondo, T., Hashimoto-Nishimura, M., Asano, S., Hayashi, A., Mitsutake, S., Igarashi, Y., Umehara, H., Takeya, H., Kigawa, J., Okazaki, T., 2012. Regulation of Autophagy and Its Associated Cell Death by “Sphingolipid Rheostat.” J. Biol. Chem. 287, 39898–39910. https://doi.org/10.1074/jbc.M112.416552

Tiede, A., Nischan, C., Schubert, J., Schmidt, R.E., 2000. Characterisation of the enzymatic complex for the first step in glycosylphosphatidylinositol biosynthesis. Int. J. Biochem. Cell Biol. 32, 339–350. https://doi.org/10.1016/S1357-2725(99)00122-3

Turk, V., Turk, B., Turk, D., 2001. Lysosomal cysteine proteases: facts and opportunities. EMBO J. 20, 4629–4633. https://doi.org/10.1093/emboj/20.17.4629

Ueno, T., Komatsu, M., 2017. Autophagy in the liver: functions in health and disease. Nat. Rev. Gastroenterol. Hepatol. 14, 170–184. https://doi.org/10.1038/nrgastro.2016.185

Wang, B., Moya, N., Niessen, S., Hoover, H., Mihaylova, M.M., Shaw, R.J., Yates, J.R., Fischer, W.H., Thomas, J.B., Montminy, M., 2011. A hormone-dependent module regulating energy balance. Cell 145, 596–606. https://doi.org/10.1016/j.cell.2011.04.013

Wegner, M.-S., Wanger, R.A., Oertel, S., Brachtendorf, S., Hartmann, D., Schiffmann, S., Marschalek, R., Schreiber, Y., Ferreirós, N., Geisslinger, G., Grösch, S., 2014. Ceramide synthases CerS4 and CerS5 are upregulated by 17β-estradiol and GPER1 via AP-1 in human breast cancer cells. Biochem. Pharmacol. 92, 577–589. https://doi.org/10.1016/j.bcp.2014.10.007

Weidberg, H., Shvets, E., Elazar, Z., 2011. Biogenesis and Cargo Selectivity of Autophagosomes. Annu. Rev. Biochem. 80, 125–156. https://doi.org/10.1146/annurev-biochem-052709-094552

Woodcock, K.J., Kierdorf, K., Pouchelon, C.A., Vivancos, V., Dionne, M.S., Geissmann, F., 2015. Macrophage-derived upd3 cytokine causes impaired glucose homeostasis and reduced lifespan in Drosophila fed a lipid-rich diet. Immunity 42, 133–144. https://doi.org/10.1016/j.immuni.2014.12.023

Wu, X., Tao, P., Zhou, Q., Li, Jie, Yu, Z., Wang, X., Li, Jiaanfang, Li, C., Yan, M., Zhu, Z., Liu, B., Su, L., 2017. IL-6 secreted by cancer-associated fibroblasts promotes epithelial-mesenchymal transition and metastasis of gastric cancer via JAK2/STAT3 signaling pathway. Oncotarget 8, 20741–20750. https://doi.org/10.18632/oncotarget.15119

Xie, Z., Nair, U., Klionsky, D.J., 2008. Atg8 controls phagophore expansion during autophagosome formation. Mol. Biol. Cell 19, 3290–3298. https://doi.org/10.1091/mbc.e07-12-1292

Xu, J., Kim, A.-R., Cheloha, R.W., Fischer, F.A., Li, J.S.S., Feng, Y., Stoneburner, E., Binari, R., Mohr, S.E., Zirin, J., Ploegh, H.L., Perrimon, N., 2022. Protein visualization and manipulation in Drosophila through the use of epitope tags recognized by nanobodies. eLife 11, e74326. https://doi.org/10.7554/eLife.74326

Xu, J., Liu, Y., Yang, F., Cao, Y., Chen, W., Li, J.S.S., Zhang, S., Comjean, A., Hu, Y., Perrimon, N., 2024. Mechanistic characterization of a Drosophila model of paraneoplastic nephrotic syndrome. Nat. Commun. 15, 1241. https://doi.org/10.1038/s41467-024-45493-8

Yu, H., Kortylewski, M., Pardoll, D., 2007. Crosstalk between cancer and immune cells: role of STAT3 in the tumour microenvironment. Nat. Rev. Immunol. 7, 41–51. https://doi.org/10.1038/nri1995